VALVE REGULATED LEAD ACID BATTERY BANK FAILURE

A Dissertation

by

YIQI WANG

Submitted to the Office of Graduate and Professional Studies of

Texas A&M University

in partial fulfillment of the requirements for the degree of

DOCTOR OF PHILOSOPHY

Chair of Committee,	Mehrdad Ehsani
Committee Members,	Chanan Singh
	Shankar P.Bhattacharyya
	Won-Jong Kim
Head of Department,	Miroslav M.Begovic

December 2019

Major Subject: Electrical Engineering

ABSTRACT

Battery banks play a vital role in many applications, including and not limited to: serve as energy buffer for renewable energy integration, provide high value service for grid support, and function as energy storage for electrical and hybrid vehicles. Albeit their wide usage and great potentials, little research has been conducted into investigating the failure of battery banks.

The motivation of this research is to model the failure of battery bank for failure prediction.

Most literature focuses on the failure of single battery. When considered in a battery bank setup, individual batteries are assumed identical, and interactions between them are simply neglected. In reality, minor differences between individual batteries lead to them behaving differently in a connected bank from the case of standalone batteries. The accumulating effects of the behavior differences will lead batteries to age and deteriorate at different rates, and eventually lead to unpredicted failures of battery bank.

A modified model of lead acid battery with failure mechanisms and aging effects considered has been proposed. This model is then thoroughly investigated to study the failure of individual battery. Failure modes of single battery is defined based on the well-defined failure mechanism found in literature.

This model is then used for studying battery bank failure. Failure modes of battery banks are defined based on single battery failure modes. To simulate the interaction between batteries in a battery bank, parameters of individual batteries within the bank are randomly chosen assuming normal distribution.

Different topologies of the battery bank has been investigated and compared. A meshed topology has been proposed for its ability to balance batteries and increased reliability.

A model based battery bank failure prediction methodology is proposed. Method for battery bank failure prediction based on parameter estimation and classification has been studied. Parameter estimation is carried out using filtering method to extract battery initial

parameters based on measurements and imperfect model. Different classification approaches have been tested.

Machine learning algorithms are compared when applied to classify battery banks of a specific topology into normal and abnormal failure groups. Their performance are compared using statistic tests.

DEDICATION

To my wife, Jianing, and our son, Ethan.

ACKNOWLEDGEMENTS

I would like to thank my committee chair, Dr. Ehsani, and my committee members, Dr. Bhattcharyya, Dr. Kim, and Dr. Singh, for their guidance and support throughout the course of this research.

Thanks also go to my friends and colleagues and the department faculty and staff for making my time at Texas A&M University a great experience.

Finally, thanks to my parents for their encouragement and to my wife for her patience and love. Thanks to my son, Ethan, for bring joy to me and the whole family in this whole process.

CONTRIBUTORS AND FUNDING SOURCES

Contributors

This work was supervised by a dissertation committee consisting of Professors Dr. Ehsani, Dr. Bhattacharyya and Dr. Singh of the Department of Electrical and Computer Engineering and Professor Dr. Kim of the Department of Mechanical Engineering.

All work conducted for the dissertation was completed by the student independently.

Funding Sources

Graduate study was supported by a fellowship from Texas A&M University.

Its contents are solely the responsibility of the author and do not necessarily represent the official views of Texas A&M University.

NOMENCLATURE

VLRA	Valve Regulated Lead Acid Battery
SOC	State of Charge
DOD	Depth of Discharge
SOH	State of Health

TABLE OF CONTENTS

Page

LIST OF FIGURES

Page

LIST OF TABLES

Page

1. INTRODUCTION: LEAD ACID BATTERY

Lead acid battery has been widely adopted for different applications for over a century. Its widely usage has led to extensive development for its improvement. To this day, new designs, additives and technologies are still being introduced to lead acid battery at a rapid rate. Lead acid battery is almost certainly always the least expensive energy storage device of choice in most applications while still offering respectable performance and satisfactory characteristics.

In this chapter, the basic concepts in lead acid battery are introduced, with detailed discussion on chemical reactions involved. Thermodynamics of lead acid battery is also presented. These contents serve as the basis for lead acid battery modeling.

Table 1.1 summarizes the advantages and disadvantages of lead acid battery.

1.1. Different Categories of Lead Acid Battery

There are two well-known categories of lead acid battery: flooded lead acid battery and valve regulated lead acid (VRLA) battery. They differ in two major different aspects: state of electrolyte and internal gas management. Liquid (aqueous) electrolyte is used in flooded lead acid battery, immobilized electrolyte is used in VRLA battery; gas generated is directly vented in flooded lead acid battery, oxygen generated in VRLA battery is recombined in the so-called oxygen cycle until gas pressure reached the regulated value then oxygen is directly released.

1.1.1. Flooded Lead Acid Battery

Flooded lead acid battery is the first technology employed in lead acid battery. Its name refers to its plates which are submerged in aqueous solution of sulfuric acid. Flooded

lead acid battery is sometimes referred to as vented battery, as gas by-products generated in battery are directly vented into atmosphere. Since gas generated in water electrolysis is directly vented, water loss has long been a major issue in flooded battery, distilled water can be added to battery to maintain proper amount of electrolyte.

Table 1.1 Major advantages and Disadvantages of Lead-Acid Batteries[1]

Advantages	Disadvantages
Popular low-cost secondary battery-capable of manufacture on a local basis, worldwide, from low to high scale of production	Relatively low cycle life(50-500 cycles, up to 2000 cycles in special designs)
Available in large quantities and in a variety of sizes and designs, manufactured in sizes from smaller than 1Ah to thousands of Ampere-hours	Limited energy density-typically 30-40 Wh/kg
Good high-rate performance, suitable for engine starting (but outperformed by some nickel-cadmium and nickel-metal – hydride batteries)	Long-term storage in a discharged condition can lead to irreversible polarization of electrodes
Moderately good low and high temperature performance	Difficult to manufacture in very small sizes
Electrically efficient, turnaround efficiency of over 70%, comparing discharge energy out with charge energy in	Hydrogen evolution in some designs can be an explosion hazard
	Stibine and arsine evolution in designs with antimony and arsenic in grid alloys can be health hazard
	Positive post blister corrosion with some designs
	Thermal runaway in improperly designed batteries or charging equipment
	Relatively low cycle life(50-500 cycles, up to 2000 cycles in special designs)
	Limited energy density-typically 30-40 Wh/kg

Table 1.1 Continued

Advantages	Disadvantages
High cell voltage-open circuit voltage of >2.0 V is the highest of all aqueous-electrolyte batteries	Long-term storage in a discharged condition can lead to irreversible polarization of electrodes
Good float service	Difficult to manufacture in very small sizes
Easy state-of-charge indication	Hydrogen evolution in some designs can be an explosion hazard
Good charge retention for intermittent charge applications (if grids are made with high-overvoltage alloys)	Stibine and arsine evolution in designs with antimony and arsenic in grid alloys can be health hazard
Available in maintenance-free designs	Thermal runaway in improperly designed batteries or charging equipment
Low cost compared with other secondary batteries	Positive post blister corrosion with some designs
Cell components are easily recycled	

Effort to reduce water loss in flooded lead acid has made great progress, different grid alloys are developed that help to increases the polarization voltage required for oxygen and hydrogen evolution. This effort eventually leads to the introduction of valve regulated lead acid battery.

1.1.2. Valve Regulated Lead Acid Battery

The first valve regulated lead acid battery was introduced in early 1950s. Battery of this technology is given different names, ‘sealed battery’ as opposed to vented flooded battery, ’maintenance free battery’ as no extra electrolyte can be added to it any time in

its service life. Battery of this technology is equipped with pressure regulated valves which only vent when pressure accumulated in battery case reaches pre-set threshold. VRLA battery was first introduced to counter the problem of water loss in flooded battery thus greatly reduces maintenance requirements. Oxygen and hydrogen are generated in the overcharging process in VRLA battery. Oxygen travels through unfilled micro-pores in separators to be recombined on the other electrode, hydrogen is accumulated in battery case until the pressure threshold is reached and released into atmosphere. As high concentration of hydrogen can be hazardous, flame arrestor is usually added to VRLA battery.

Table 1.2 summarizes the differences of flooded and valve regulated lead acid batteries.

1.2. Lead Acid Battery Constitutions

A typical lead acid battery consists of five major parts: positive electrode, negative electrode, grid, separator and electrolyte. These five parts are briefly discussed. The basic construction of a typical lead acid battery is shown in Figure 1.1 below.

Table 1.2 Summary of Comparison between Flooded and Valve Regulated Lead Acid Battery[2]

Battery Type	Flooded Battery	VRLA Battery
Electrolyte	Free liquid	Gelled or AGM
Positive grid material	Different type with antimony	Antimony Free
Advantage	Lower cost Better float service	Low maintenance Low tolerance to abuse
Disadvantage	Water loss Safety Issue (Gas evolution)	Shorter service Thermal issue (runaway)

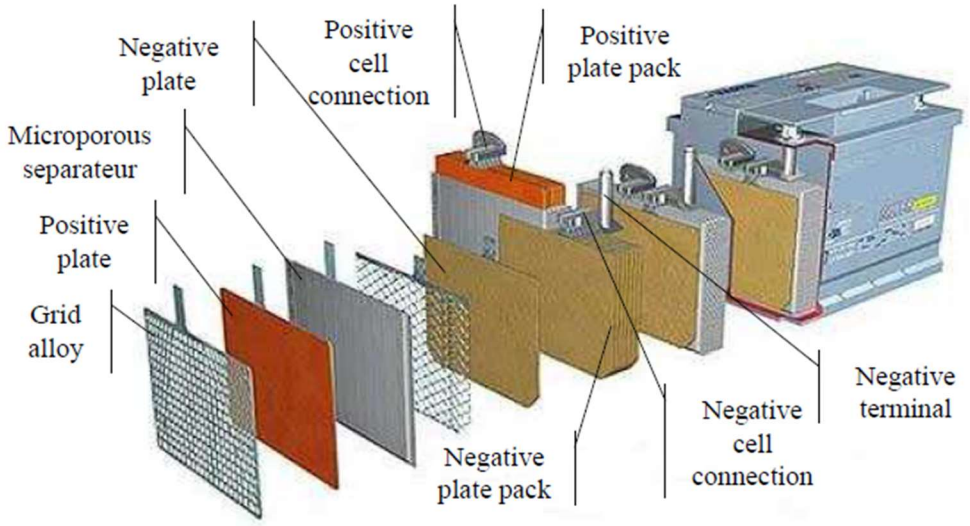

Figure 1.1 Typical construction of a Lead Acid Battery[3]

1.2.1. Positive Electrode

Active chemical material in the cathode of lead acid battery is lead dioxide (PbO_2). Two major forms of positive electrodes are used in lead acid battery: flat plate and tubular plate. In flat plate, active material is directly pasted onto grid; in tubular plate, active material is packed into porous sleeves, called gauntlet, with a casted spine in the center. Both grid and spine serve as mechanical support and current collector.

Flat plate is the easier to construct of the two type, but suffers for its deep cycling performance due to active material softening and shedding in cycling process. Where as in tubular plate, the existence of sleeves limit the dilatation and contraction of active material thus improve life span of positive electrode. The differences are shown in Figure 1.2.

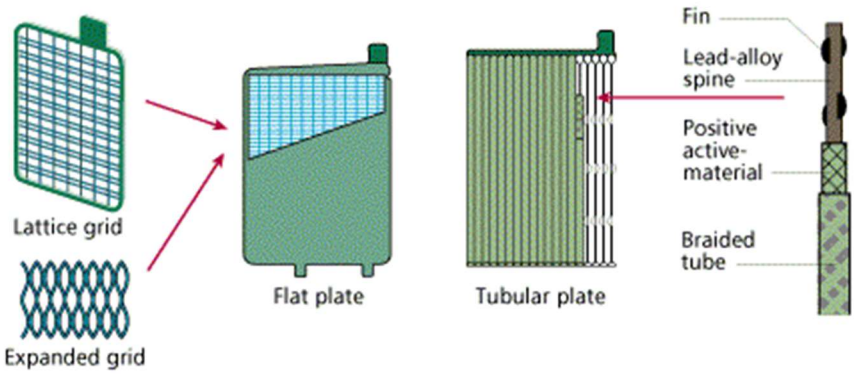

Figure 1.2 Flat Plate and Tubular Plate in Lead Acid Battery. Reprinted from[4]**.**

1.2.2. Negative Electrode

Active chemical material in lead acid battery negative electrode is metallic lead.

Negative electrodes are all of flat plate type.

Spongy lead is formed onto grid to ensure large active surface on negative electrode. As lead tend to agglomerate in cycling process, additives called expander are add to negative active material to maintain its porosity. Typical expanders used are barium sulfate and carbon. The added carbon has also been claimed to improve battery performance in high rate discharge at partial state of charge[5].

1.2.3. Grid

Grid in lead acid battery serves multiple purpose: as mechanical support for active material on both electrodes and current collector in battery operation.

Grid is first casted using pure lead in early lead acid battery. Pure metallic lead grid is quickly deemed too soft to handle the mechanical stress accumulated in battery cycling process. Different grid alloys are thus developed to meet different performance requirement.

Common grid alloys are compared in Table 1.3 below.

Table 1.3 Grid Alloys for Lead Acid Batteries, Characteristics and Fields of Applications. Reprinted from [6]**.**

Alloy Type	Advantage	Disadvantage
Standard antimony 4-11% Sb As, Sn, Cu(Ag)	High mechanical strength, stability for active material in positive electrode, improvement of cycle performance	Higher rate of water decomposition in service
Low antimony 0.5-3.5% Sb Se, Te, S, Cu, As, Sn, (Al)	Decrease Sb contamination on negative electrode, lower water decomposition rate	Stability of capacity during float charge, extend cycle life
Standard calcium 0.06-0.12% Ca 0 to 3% Sn, (Al)	No Sb contamination on negative electrode	Grid growth, lower capacity
Pure lead	Better deep cycling performance	Poor mechanical strength
Antimony/cadmium	Low antimony contamination	Toxic material used (Cadmium)

Different geometries are employed in lead acid battery grid. These geometries are introduced for different performance improvements including higher mechanical strength, even active material utilization and corrosion resistance in positive electrode. Figure 1.3 below shows examples of conventional flat grid and radial grid. More exotic grid geometries can also be find in literature, but they are seldom used in commercial products.

A metal contact, called lug, is located on top of grid. It is used for connecting different grids together to form plate groups. They are designed to add minimum resistance to grid. Exact location of lug varies per design and is usually chosen accord to grid geometry.

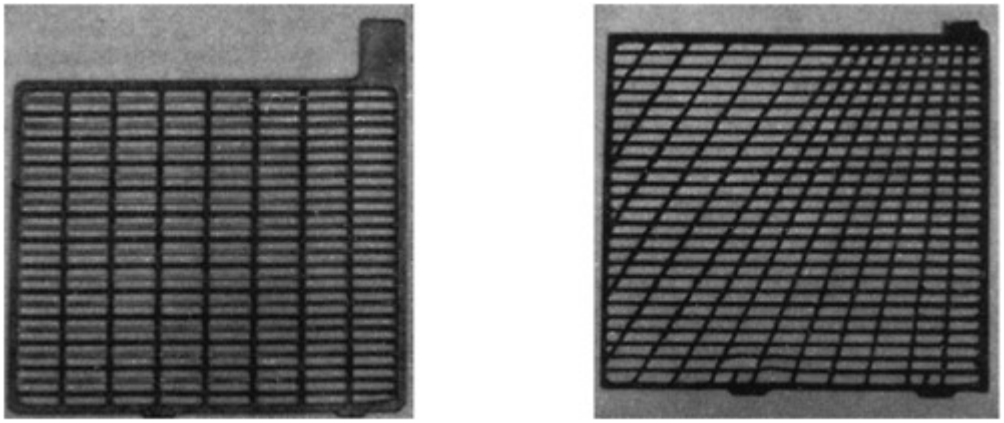

Figure 1.3 Flat Grid and Radical Grid Example in Lead Acid Battery. Reprinted from [7]**.**

1.2.4. Separator

Separator is inserted between positive and negative in lead acid battery to ensure proper electrical insulation.

Separators in flooded lead acid battery and valve regulated lead acid battery have their distinctive characteristics. Separators in flooded lead acid battery needs to maintain high ion conductivity and low resistivity. The same requirements also apply to separators in valve regulated battery, but they also need to serve as mechanical support for immobilized electrolyte as well having a certain percentage of unfilled micro-pores as channels for oxygen recombination.

Separators made of polyvinyl chloride, polyethylene, phenolic resins and natural rubber are used in flooded lead acid battery. In valve regulated battery, glass absorbent mat is also used.

Some specific properties are desired of in all separators, they are listed below[8]:

Low acid solubility, good oxidation resistance, low electrical resistance, low acid displacement, high tensile strength, good flexibility, high porosity good wettability and low level of leachable impurities.

1.2.5. Electrolyte

Electrolyte plays two major roles in battery: it serves as path for ionic conductivity, this differs from electrical conductivity as electrical conductivity of electrolyte will cause direct short circuit within battery; it participates in the reversible charge discharge as reactant.

Solution of sulfuric acid with additives to enhance ion conductivity is adopted as electrolyte in lead acid battery. It come in either liquid or immobilized form. Immobilized electrolyte can be in absorbent form or gel form.

Liquid electrolyte is aqueous solution of sulfuric acid of concentration between 1.10 g cm^{-3} to 1.28 cm^{-3} given different ambient temperatures and different state of charge of the battery. Density of liquid electrolyte can be chosen as a measurable indicator for state of charge in lead acid battery. Distilled water is often added when higher density is observed to replenish water loss, sulfuric acid can also be added in some cases. The most prominent ions in the solution are H^+ and HSO_4^-, the products of sulfuric acid disassociation, there are also sulfate ions SO_4^{2-} at a much lower concentration.

Absorbent electrolyte is immobilized by being absorbed into glass fiber mat. Battery using this type of electrolyte is also referred to as AGM battery. Absorbent glass mat is used to grant higher oxygen transportation speed between electrodes in battery, as oxygen transportation speed is greatly limited in water. A percentage of pores in AGM are designed to be not filled to facilitate faster oxygen transportation. Studies have been carried out on the percentage of electrolyte filling to battery to optimize oxygen recombination efficiency while avoiding battery thermal runaway.

Gel electrolyte is formed by adding 6% of silicon oxide to electrolyte. Battery with gel electrolyte has been reported having better performance in deep cycle application[9]. Gel electrolyte can help suppress gas evolution in battery. There are no fix pores in gel electrolyte, cracks are formed through shrinkage in charging process to facilitate faster oxygen transportation.

1.3. Typical Lead Acid Battery Manufacturing Process

The manufacturing process of lead acid battery are usually divided the several different stages, they are listed here in the order as in manufacturing: oxide and grid production, pasting and curing, plate formation, assembly, electrolyte filling, charge-discharge process, finished product inspection, packing and distribution[10][11][12].

1.3.1. Oxide and Grid production

Lead ore inlet is first converted to lead oxide in this process through two different methods: Barton pot or milling.

In Barton pot, air is blown over a pool of molten lead to produce a stream of micro lead droplet. Outer surface of these droplets react with oxygen in the air flow to form different lead oxides.

In milling process, pig lead is tumbled in a rotating mill. Heat generated by the tumbling motion accelerates the speed of lead oxidizing in air. Oxidized lead on the surface layer is removed in the due process to expose clean metallic lead surface for reaction. Fine lead oxide particles are blow out of the mill to be collected.

Grid is casted using the proper lead alloy. In some rare examples, grid can also be made using die cut process.

1.3.2. Plate Formation

Plate formation is the most important procedure in lead acid battery manufacturing. As plates are the active components in the battery that go through charge and discharge. Lead oxide produced is usually further grinded into finer grains for larger active surface area. Different additives are added to lead oxide designated for positive and negative plate. The two mixtures are mixed with water and sulfuric acid to form different pastes. They are then pasted to corresponding grid to form plates.

Filled plates are collected and soaked into aqueous solution for prolonged charging which usually last from 16 to 24 hours to form active material on each plate. This process is named plate curing, before curing the mixture on both electrode are the same besides differences in additives.

The cured plated are then washed and dried to be assembled. This is the core of lead acid battery manufacturing process.

1.3.3. Assemble and Filling

In this procedure, groups of positive and negative electrodes are wielded together with separators placed in between to form the basic structure of a cell. Multiple cells are then bridge wield together to form a battery. These components are then place into battery

case, other components such terminal connectors are installed. Battery is also filled with fresh electrolyte in this procedure.

1.3.4. Charging, Inspection and Packing

Finished battery then go through another charging process, get inspected and then either stored or shipped to customer.

Figure 1.4 below illustrates the basic manufacture process of lead acid battery.

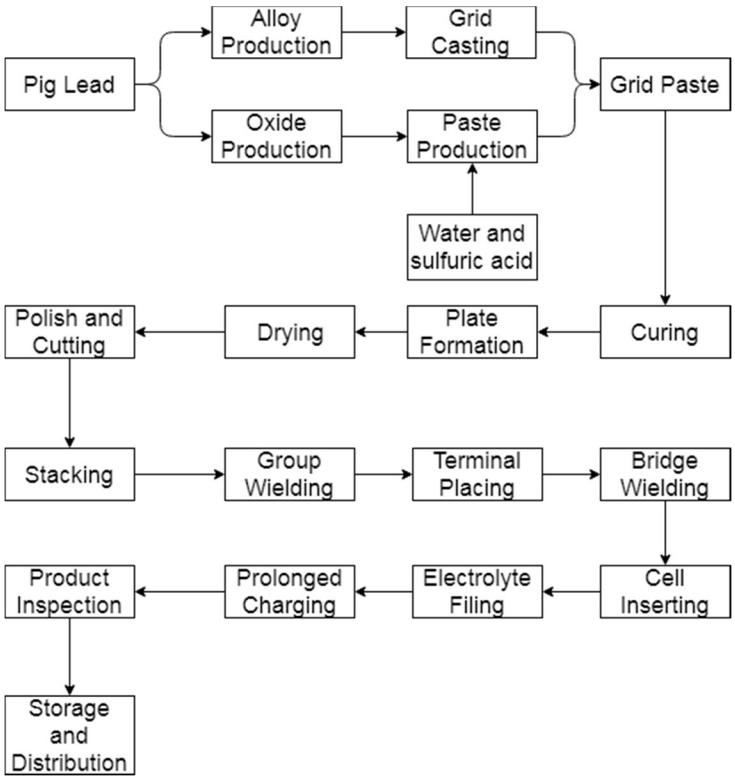

Figure 1.4 Lead Acid Battery Principal Manufacturing Process[13]

1.4. Principal and Secondary Reactions in Lead Acid Battery

An electrochemical cell consists of an electrode pair of different active materials submerged in electrolyte, electrochemical systems of different potentials are formed at

the surfaces of anode and cathode. Electrochemical reactions proceed at the surfaces of contact involve transfer of electrons between the active material surfaces and ions from electrolyte.

When a pair of electrodes are connected to external load through conductors to supply power, electric current flow between the electrodes forming a close loop doing work through the difference in potentials. Chemical energy is thus converted to other forms through the media of electrical energy. The maximum amount of energy available in the due process depends on the potential difference as well the amount of electrons transferred in the valence of active material on each electrode. The possible amount of energy an electrochemical cell can deliver is:

$$Q = nF(E_1 - E_2) \qquad \text{Eq 1.1}$$

Where *n* is the number of valence electrons that have been transferred in the electrochemical reactions. *F* is Faraday constant, it depicts the amount of charges carried by one mole of electrons. It takes the value of 96,487 C and is usually rounded to 96,500 C. E_1 and E_2 are the electrical potentials of the corresponding electrodes involved in the reactions respectively. *n* is a constant depends on the given electrochemical system, meaning the electrode materials used and the electrolyte they are immersed in. *F* is a constant for all electrochemical reactions. The electrical potentials of electrodes depends on many different factors including and not limited to reactants concentration, temperature and interface conditions.

In lead acid cell, the pair of electrodes in question are lead metal (Pb) electrode and lead dioxide (PbO_2) electrode. Both electrodes are formed as paste onto lead metal grid. The

two electrodes are immersed in sulfuric acid solution in aqueous liquid form (in flooded lead acid battery) or in gel and absorbent form (in AGM lead acid battery).

Lead acid cell utilizes the reaction pair of metallic lead oxidation ($Pb \rightarrow Pb^{2+}+2e^-$) and lead dioxide reduction ($Pb^{4+}+2e^- \rightarrow Pb^{2+}$). The end product of both reactions then reaction with sulfuric acid aqueous solution to form lead sulfate ($PbSO_4$). Lead sulfate is not soluble in water and its solubility increase slightly with the change of concentration of sulfuric acid. It thus forms a porous film on the surface of both electrodes and the structure of both electrodes stays relatively intact in the process. This characteristic of lead makes it suitable for building battery with long cycle life. Figure 1.5 below shows the difference in solubility of material affecting integrity of electrodes in electrochemical cell.

Two concepts are often used in describing electrochemical cells: galvanic cell and electrolytic cell. The main different being the site where reduction reaction taking place and whether an external power source is involved. In galvanic cell, reduction reaction processes at the electrode with higher potential thus energy is released from the electrochemical cell and can be utilized by external load. In electrolytic cell, reduction reaction proceeds at the electrode with lower potential thus the electrochemical cell is absorbing energy from external source. As can be seen from the above explanation, these concepts are overlapping with the conventional concepts of discharge and charge reaction in an electrochemical cell. They will not be used through this work.

1.4.1. Principle Reaction

The overall reaction in lead acid battery is:

$$Pb + PbO_2 + 2H_2SO_4 \rightleftharpoons 2PbSO_4 + 2H_2O \quad \text{Eq 1.2}$$

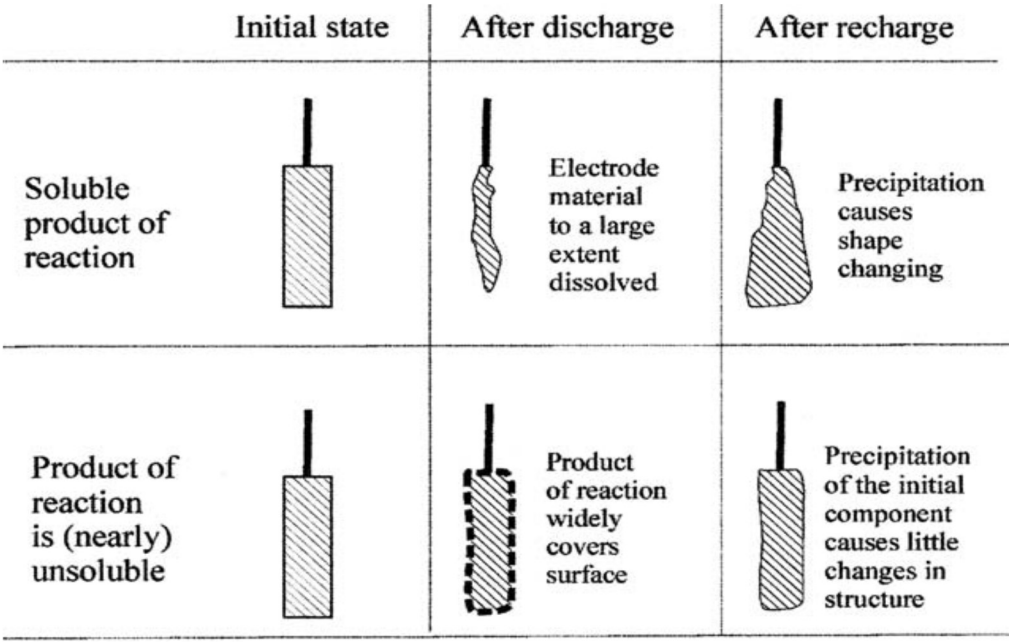

Figure 1.5 Effect of Solubility of Reaction Products on Electrode Structure. Reprinted from [14]**.**

Where following reactions proceed at each electrode:

$Pb/PbSO_4$ electrode:

$$Pb + SO_4^{2-} \rightleftharpoons PbSO_4 + 2e^- \quad \text{Eq 1.3}$$

$PbO_2/PbSO_4$ electrode:

$$PbO_2 + SO_4^{2-} + 4H^+ + 2e^- \rightleftharpoons PbSO_4 + 2H_2O \quad \text{Eq 1.4}$$

The direction of reaction is charging from right to left, discharging from left to right. Figure 1.6 shows the electrochemical operation of a lead acid cell in both charge and discharge.

Note, anode and cathode are equivalent to positive and negative electrode per the direction of reaction.

1.4.2. Side Reaction

Multiple side reactions co-exist with the main discharge-charge reaction with lead acid cell. A brief introduction of the major side reactions is presented here.

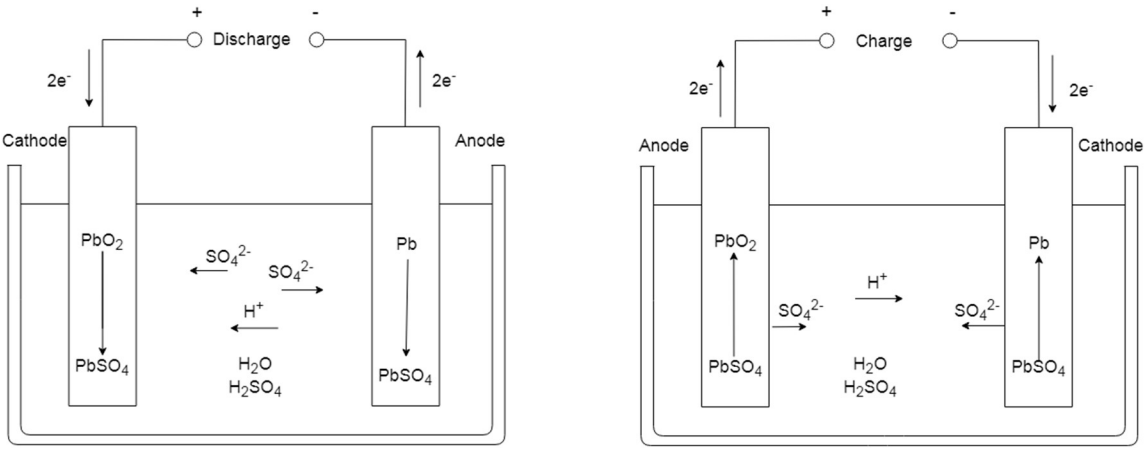

Figure 1.6 Discharge and Charge Reaction in Lead Acid Battery/Cell

1.4.2.1. Water Electrolysis

Water electrolysis always exists in lead acid cell, as the potential required of water electrolysis (1.23V) is lower than the cell voltage. Without proper additive, this is a major issue in lead acid battery. The corresponding reactions proceeds:

Positive electrode:

$$3H_2O \rightarrow \frac{1}{2}O_2 + 2e^- + 2H_3O^+ \qquad \text{Eq 1.4}$$

Negative electrode:

$$2H_3O^+ + 2e^- \rightarrow H_2 + 2H_2O \qquad \text{Eq 1.5}$$

The overall reaction is:

$$2H_2O \rightarrow 2H_2 + O_2 \qquad \text{Eq 1.6}$$

1.4.2.2. Corrosion

Positive electrode in lead acid cell consists of lead dioxide (PbO_2) and lead grid. Lead dioxide and metallic lead react to form intermediate oxides of lead (PbO_X). A layer of intermediate product forms between active material and grid. Grid is consumed in this process and cannot be recovered. Corrosion is considered the ultimate life limiting factor in lead acid battery.

1.4.2.3. Gas Recombination

The end products of water electrolysis in lead acid cell is hydrogen and oxygen. Gases can be recombined or consumed within the cell.

Oxygen is generated at positive electrode and recombined at negative electrode, the following reaction proceeds at negative electrode:

$$2Pb + O_2 + 2H_2SO_4 \rightarrow 2PbSO_4 + 2H_2O \qquad \text{Eq 1.7}$$

Hydrogen is generated at negative electrode and recombined at positive electrode, the following reaction proceeds at positive electrode:

$$H_2 + 2H_2O \rightarrow 2H_3O^+ + 2e^- \qquad \text{Eq 1.8}$$

$$PbO_2 + 2e^- + H_2SO_4 + 2H_3O^+ \rightarrow PbSO_4 + 4H_2O \qquad \text{Eq 1.9}$$

1.5. Thermodynamics of Lead Acid Cell

In this section, the following topics are covered. First, the basic thermodynamic laws are discussed. Then the equivalent potential of lead acid cell is calculated. Factors causing cell voltage to differentiate from equivalent voltage are listed and briefly introduced.

Some of these factors are covered more detailed in later chapters and included in the model of lead acid battery.

Note this is only a brief introduction for more details please refer to literature.

1.5.1. Thermodynamics Law

A chemical reaction will only proceed when the thermodynamic conditions are prevalent. Thermodynamics parameters of an electrochemical cell are state functions that only depends on the equilibrium state of the system not on the reaction path. The three quantities or functions that depict energy exchange in any electrochemical cells are listed below.

Enthalpy of reaction:

The total amount of energy released or absorbed by the reaction, notated as ΔH.

Gibbs free energy:

The amount of chemical energy available to be converted to electrical energy, notated as ΔG.

Entropy of reaction:

The amount of energy dissipated or gained with the reaction, which can be viewed as heat exchanged with external environment, notated as $\boldsymbol{T\Delta S}$, where T is the temperature.

The relation of these three quantities is:

$$\Delta H = \Delta G + T\Delta S \qquad \text{Eq 1.10}$$

1.5.2. Equivalent Potential of Lead Acid Cell

The equivalent potential of an electrochemical cell is the potential of the cell at zero current and balanced reversible reaction rates that is all reactions are stopped

macroscopically. As there is no current going through the cell no potential drop is present, the amount of electrical energy possible for utilization is:

$$Q = nF(E_1 - E_2) \qquad \text{Eq 1.11}$$

Thermal dynamic data can be used to calculate the equilibrium potential on both electrodes in a lead acid cell.

Nernst equation is the equation that relates the equilibrium potential of a reversible electrochemical reaction to standard electrode potential, temperature and activities of the reactants involved in reduction and oxidation. Nernst equation is derived from the standard changes in the Gibbs free energy associate with the corresponding electrochemical reactions. The nominal free energy change ΔG is related the free energy change under standard condition by the following relation:

$$\Delta G = \Delta G^0 + RTInQ \qquad \text{Eq 1.12}$$

Where $\Delta G^0$the free energy change under standard condition, T is temperature and R is the ideal gas constant and Q is the reaction quotient.

Q is a function of the activities of the reactants involved. In practice, concentration of the corresponding reactant is usually used to substitute its activity. Given the reaction below:

$$\alpha A + \beta B \leftrightarrow \rho R + \sigma S \qquad \text{Eq 1.13}$$

The quotient in equilibrium state can be given as:

$$Q_r = \frac{R^\rho S^\sigma}{A^\alpha B^\beta} \qquad \text{Eq 1.14}$$

Where the activities of each corresponding reactant is expressed using the letter representation as in the reaction equation.

The aforementioned procedure is then used for the two electrodes in lead acid battery.

The Gibbs free energy of each reactants can be found in Table 1.4.

For the $Pb/PbSO_4$ electrode, the change in Gibbs free energy is given in:

$$Pb + SO_4^{2-} \rightleftharpoons PbSO_4 + 2e^- \quad \text{Eq 1.14}$$

$$\Delta G^0 = -\Delta G^0_{PbSO_4} - (\Delta G^0_{SO_4^{2-}} + \Delta G^0_{Pb}) \quad \text{Eq 1.15}$$

The potential of the corresponding electrode under standard condition is thus:

$$E^0_{Pb/PbSO_4} = \left[-\Delta G^0_{PbSO_4} - \left(\Delta G^0_{SO_4^{2-}} + \Delta G^0_{Pb}\right)\right]/nF \quad \text{Eq 1.16}$$

By substituting the corresponding Gibbs free energy from the table above, the following value is obtained:

$$E^0_{Pb/PbSO_4} = -0.358V \quad \text{Eq 1.17}$$

Note, this is only the standard electrode potential, to relate it to the actual electrode potential, Nernst equation is used:

$$E_{Pb/PbSO_4} = E^0_{Pb/PbSO_4} + (RT/nF)In\frac{a_{PbSO_4}}{a_{Pb}a_{SO_4^{2-}}} \quad \text{Eq 1.18}$$

The activities of the corresponding reactants can be found in literature.

The same procedure can be carried out for PbO_2/ $PbSO_4$ electrode. The change in Gibbs free energy:

$$PbO_2 + SO_4^{2-} + 4H^+ + 2e^- \rightleftharpoons PbSO_4 + 2H_2O \quad \text{Eq 1.19}$$

$$\Delta G^0 = -\Delta G^0_{PbO_2} - \Delta G^0_{SO_4^{2-}} - 4\Delta G^0_{H^+} + \Delta G^0_{PbSO_4} + 2\Delta G_{H_2O} \quad \text{Eq 1.20}$$

The potential of the electrode under standard condition is thus:

$$E^0_{PbO_2/PbSO_4} = 1.683V \quad \text{Eq 1.21}$$

Relating the standard potential to equilibrium potential:

$$E_{PbO_2/PbSO_4} = E^0_{PbO_2/PbSO_4} + (RT/2F)In(a_{PbO_2} \cdot a_{SO_4^{2-}} \cdot a^4_{H^+}/a_{PbSO_4} \cdot a^2_{H_2O}) \quad \text{Eq 1.22}$$

Where $a_{PbO_2,} a_{SO_4^{2-}}$ are the activities of corresponding reactants which can be substituted by concentration in dilute solution. The equation above can be rearranged by substituting the correspondent constants in Table 1.4.

Table 1.4 Thermodynamic Characteristics of Compounds in Lead Acid Battery[15]

	ΔG^0	
Compound	kcal mol^{-1}	kJ mol^{-1}
Pb(crystal)	0.0	0.0
Pb^{2+}(aq.)	-5.73	-23.98
Pb^{4+}(aq.)	-72.3	-302.57
PbO(red)	-45.25	-189.37
PbO(yellow)	-45.05	-188.53
α-PbO_2	-51.94	-217.37
β-PbO_2	-52.34	-219.04
$PbSO_4$	-193.89	-811.43
H^+(aq.)	0.0	0.0
SO_4^{2-}(aq.)	-177.34	-742.17
HSO_4^{2-}	-179.94	-753.05
H_2SO_4	-177.34	-743.17
H_2O	-56.69	-237.25

The overall cell equilibrium potential is:

$$E_{cell} = E_{PbO_2/PbSO_4} - E_{Pb/PbSO_4} \quad \text{Eq 1.23}$$

$$E_{cell} = 2.041 + (1.98 * 10^{-4}) * T * \lg(a_{H_2SO_4}/a_{H_2O}) \quad \text{Eq 1.24}$$

Table 1.5 summarizing the correlation between concentration of water and sulfuric acid within the cell and their corresponding activity is shown below. The last column of the table shows the corresponding cell equilibrium potential at each different state. Note, in the table, concentration is relate to activity by a constant called activity coefficient which gaps the difference between real solution and ideal solution.

$$a_i = \gamma_i C_i \qquad \text{Eq 1.25}$$

Where C_i is concentration of the reactant of interest, γ_i is its corresponding activity coefficient.

1.5.3. Differentiation from Equivalent Potential

The difference between the electrode potential given certain current and its equilibrium potential of the electrochemical cell reaction is referred to as overvoltage[16].

The difference between the electrode potential given certain current and its zero current potential of electrodes is called polarization.

So the difference between overvoltage and polarization in the same pair of electrodes lies in the deviation from equilibrium potential of the principle reaction to the potential measured at zero current. This deviation is the summation of multiple different factors which are addressed here.

The list of different overvoltages and polarizations includes: charge transfer overvoltage for charge transfer reaction, diffusion overvoltage for ion transportation in electrolyte and interfaces, crystallization overvoltage for crystal forming reaction, reaction overvoltage for chemical reaction and resistance overvoltage caused by ohmic drop.

Charge transfer overvoltage is caused by the electrical double layer formed on the interface between electrode and electrolyte.

Table 1.5 Activity of Water and Sulfuric Acid and Equilibrium of Lead Acid Cell[17][18]

Concentration					
mol kg^{-1}	mol L^{-1}	γ	a_{H_2O}	$a_{H_2SO_4}$	E,V
0.5	0.49	0.144	0.9819	0.00148	1.881
0.7	0.68	0.131	0.9743	0.00307	1.900
1	0.96	0.121	0.9618	0.00716	1.922
1.5	1.42	0.117	0.9387	0.0214	1.951
2	1.86	0.118	0.9126	0.0522	1.975
2.5	2.28	0.123	0.8836	0.1158	1.996
3	2.69	0.131	0.8516	0.2440	2.016
3.5	3.08	0.143	0.8166	0.4989	2.035
4	3.46	0.157	0.7799	0.9883	2.054
4.5	3.82	0.173	0.7422	1.888	2.072
5	4.17	0.192	0.7032	3.541	2.090
5.5	4.50	0.213	0.6643	6.463	2.106
6	4.83	0.237	0.6259	11.48	2.123
6.5	5.14	0.263	0.5879	20.02	2.139
7	5.44	0.292	0.5509	34.21	2.154

Diffusion overvoltage is caused by the difference in concentration of reactants in electrolyte and reaction surface. This is overvoltage is relate to the rate of reaction or the current going through the battery. At reaction site, the interface of electrode and electrolyte and the pores in the active material, the lack of reactants to participate discharge and charge reaction limits the current delivering or receiving capability of the

cell. Higher current will lead to higher diffusion overvoltage, in extreme cases this overvoltage will cause the potential over battery terminals to collapse.

Reaction overvoltage is a phenomenon due to the presence of a rate-limiting chemical process in electrode reactions. The slow step is a rate-limiting factor for the cell and usually it is reaction rate is not affected by battery potential.

Crystallization overvoltage is caused by crystal growth. Metal ions in the solution need to find sites on the surface of lattice plane where it can be incorporated in the lattice. This insertion process is energy consuming which hinders the process causing a potential different between the area near the surface of the electrode and electrode. This overvoltage is affected by the concentration of the ion of interest. It can be calculated using Nernst equation under equilibrium state.

Resistance overvoltage can also be called resistance polarization, both names are extensively used in literature. When current runs through a conductor, the resistance or impedance of the conductor will cause a voltage difference on the terminals of the conductor. In an electrochemical cell, the path of electrical current includes electrolyte, active material or mass, electrode grid and terminal connectors. Each part of this path will introduce extra resistance in the cell. In literature, this polarization has also been related to the diffusion layer at the surface of electrode thus lead to overlapping of concept with diffusion overvoltage.

The overall equation for the voltage at the terminals of the cell can be express using the equation:

$$V_{cell} = E_{PbO_2/PbSO_4} - E_{Pb/PbSO_4} + (\eta_+ - \eta_-) - R * i \qquad \text{Eq 1.26}$$

Where η_+and η_- account for the overvoltages at positive and negative electrodes. The last term accounts for the resistance polarization.

2. LEAD ACID BATTERY FAILURE MECHANISMS AND FAILURE MODES

To study the failures of lead acid battery banks, the first step is a thorough study of failures in individual lead acid battery.

Batteries of all chemistry are doomed to fail after certain number of cycles. The causes of their failures can be vastly different due to the variety of reactions involved in the process.

Research into battery failures has always been a hot topic. Multiple approaches have been attempted in battery of every chemistry. Making accurate measurement and observation has been a tough task as site of the specific reaction can be hard to reach and measurement can be noisy and unobtainable. Experiments specifically designed for testing hypothesis about battery failures have been carried out. To this day, even though explanation of every battery failure known has been proposed, some of them are still not verified. One good example is on the reason for thermal runaway in valve regulated lead acid battery, even though the failure has been well known, there are still two contradictory explanation for its causes. In the later sections of this chapter, the two contradictory explanations are thoroughly investigated and a method to mitigate the two different explanations is proposed.

The sections of this chapter are arranged as follows. In section one, two basic and confusing concepts of failure mode and failure mechanism are differentiated, the failure modes for single battery and banks are defined. In section two, failure mechanisms of lead acid battery are introduced, choice on the failure mechanisms that needs to be included in battery model is discussed. In sections three, failure mechanisms of interest:

mechanical stress, thermal runaway and positive grid corrosion are discussed in detail, and modeling approach for each is introduced.

2.1. Failure Modes and Failure Mechanisms

Two important different concepts, failure mode and failure mechanism, need to be clearly differentiated before going into any detailed discussion. These two concepts are sometimes used in literature in an interchangeable manner which can cause great confusion when interpreting the material.

There are various definitions of both concepts, but generally speaking:

Failure mechanisms are associated with deviant physical condition or physical state, and can be identified as the cause of failure modes given enough information. ISO14224 and IEC 60050 define failure mechanism as "a process that leads to failure. The process can be physical, mechanical chemical, or a combination thereof."

Failure modes are associated with deviant function or behavior and the direct effect of one or certain combination of failure mechanisms[19].

One of the well accepted definitions is from Effective FMEAS by Carl Carlson:

A “Failure Mode” is the manner in which the item or assembly could fail to meet the intended function and its requirements[20].

For a battery, failure modes are user defined cases when it fails to meet the performance requirements: providing enough stored energy (capacity), providing enough power to support load, maintaining charge for an amount of time (low self-discharge), replenish within reasonable time and operating safely.

For a battery bank, the performance requirements are most likely just scaled to the size of the battery bank as a group of individual batteries acting essentially as one larger battery.

So failure modes of single battery and battery bank can be identified as follows[21]:

Capacity failure

Power failure

Charge failure

Thermal failure

Definition of failure modes are related to battery or battery bank operations. A few concepts concerning operation of battery or battery bank need to be addressed.

A cycle of operation needs to be defined. The definition of a cycle consists of how battery is discharged, load condition, how battery is charged, charge condition, when to stop battery from discharging, end of discharge condition, when to stop battery from charging, end of charge condition, how charge in the battery is maintained when not in service, float charge condition.

Even though the failure modes of single battery and battery bank share identical definitions, the failure mechanisms behind these failure modes might be vastly different. A simple example would be comparing capacity failure in a single battery and a pair of parallel connected batteries in a simple battery bank setup. Full capacity is delivered when end of discharge condition is reached. So the theoretical case would be twice amount of charge is delivered by the battery bank compared to the single battery; when in reality, this ratio can be smaller due to two imbalanced charge batteries used in the

battery bank, as one battery need to charge the other to compensated the other. Detailed examples concerning differences in failure mechanisms of battery and battery bank will be discuss in later chapters.

The performance requirements can be translated to battery specifications and measurable parameters, i.e. capacity, internal impedance, self-discharge rate, charge acceptance rate and thermal dissipating capability, etc.

These measurable parameters are used as indicators of different failure modes.

Battery temperature can be measured using sensors either mounted on the case or even directly inside battery case. The main limitation of battery temperature measurement is the time delay between the event causing battery to overheat and heat flow conducted to sensor location. Mount multiple sensors on a single battery will cause unnecessary increase of complexity of the system. Thermal event is best monitored using more information coming from different sources.

Battery capacity can be tested using a variety of method. A full charge and discharge cycle usually yield the most accurate result. Note for lead acid battery, usable battery capacity is related to multiple factors, including discharge current rate, battery temperature and battery internal impedance. The relationship between discharge current rate and usable capacity in battery can be expressed with Peukert's law[22]:

$$C_p = I^k t \qquad \text{Eq 2.1}$$

C_p is the capacity at one-ampere fixed current discharge rate in Ah (ampere hours), I is the actual discharge current in amperes, t is the time used to discharge the battery in hours, k is the Peukert constant (dimensionless).

As C_p is a given constant for the specific battery, the amount of time to completely discharged state is different for different discharge current, thus yield different usable capacity. This law was first proposed on lead acid battery and has been shown not applicable to battery of other chemistries. K is specific to lead acid battery of each technology and is also affected by age of the battery.

However, as a full charge and discharge cycle test can be time-consuming and expensive, different research has been conducted to investigate the correlation between battery capacity and other easily accessible parameters. The concept of battery state of health (SOH) is purposed, it is essential the ratio between the remaining usable battery capacity and nominal battery capacity. SOH has been related to battery impedance which is usually evaluated by sending current pulses into battery while monitoring its voltage response. As battery ages, its impedance increases over time. Even with other means of estimating battery capacity, a scheduled full charge and discharge test is still recommended for battery in float service[23].

Battery impedance can be tested using the same method mentioned in the paragraph above. For lead acid battery, crank capability is expected which requires battery to deliver large current for a short duration. This capability is greatly affected by battery impedance, a short circuit test is usually conducted to guarantee lower internal impedance of battery.

Battery internal discharge rate is usually calculated using the amount of charge loss over the time period of the loss. This is usually given in the datasheet offered by battery manufacturer. Battery self-discharge rate is tested extensively under different conditions.

The theoretical rate of self-discharge can be calculated using data in literature [24]. For lead acid battery used for float service, self-discharge rate is also related to thermal runaway thus needs to be carefully considered.

Everything is designed to have a life span, nothing will last forever. In case of battery capacity failure, what we care about the most is premature capacity failure which means battery remaining capacity drops below threshold before it reaches its designated life span.

There are a variety of causes for premature capacity failure in lead acid battery. High discharge rate and high internal impedance can lead to premature capacity failure. Low operating temperature can also lead to premature capacity failure. The chemical and electrochemical reactions in the battery can also be traced as causes of failure. As been discussed earlier, these causes are referred to as failure mechanisms.

Failure mechanisms can be classified into two categories: operating condition based and physical-chemical based. Operating condition based failure mechanisms will be discussed in Chapter 4. In the next section, physical and chemical based failure mechanisms are introduced.

2.1.1. Failure Mechanisms of Lead Acid Battery

Below is a list of possible failure mechanisms in lead acid battery:

Loss of electrolyte, electrolyte stratification, hydration, positive grid corrosion, internal short, passivating lead oxide film formation at positive current collector(grid), electrolyte contamination, agglomeration of finely divided lead in the negative electrodes, sulfation, inter-cell connector failure, positive electrode active material

softening and shedding, hydrogen accumulation consequences, thermal runaway, lead sulfate accumulation on the negative plate.

Each of the failure mechanisms listed above are briefly introduced in this section.

2.1.1.1. Loss of Electrolyte[25]

The electrolyte in lead acid battery is aqueous sulfuric acid solution. As the equilibrium potential of lead acid cell is higher than the potential required for water electrolysis, loss of water through this mechanism is unavoidable. Different additives are add to active material of both electrodes to raise the potential required for hydrogen and oxygen evolution on electrode surface, these effort help to reduce the reaction rate of water electrolysis greatly. In flooded lead acid, water evaporation is also another factor that leads to loss of electrolyte. In sealed batteries, this failure mechanism is irreversible. The loss of electrolyte essentially causes the reduction of effective internal surface area for electrochemical reactions and the result induced is the rise of internal impedance. This loss is recoverable in flooded batteries by simply adding distilled water, but irreversible in VRLA batteries. The rate of loss is temperature dependent, as the rate of water electrolysis and evaporation are both affected by temperature.

Partial loss of electrolyte can cause uneven utilization of active material on both electrodes. This may cause other related issues, for example, unevenly distributed mechanical stress through cycling, as the difference in stress may cause the electrode to deform in unpredicted manner.

Lead acid battery with transparent casing are available commercially, in those battery, the level of electrolyte can be easily observed thus electrolyte can be timely replenished.

Figure 2.1 shows the electrolyte marker on a transparent battery case and the batteries in figure are in low electrolyte level state.

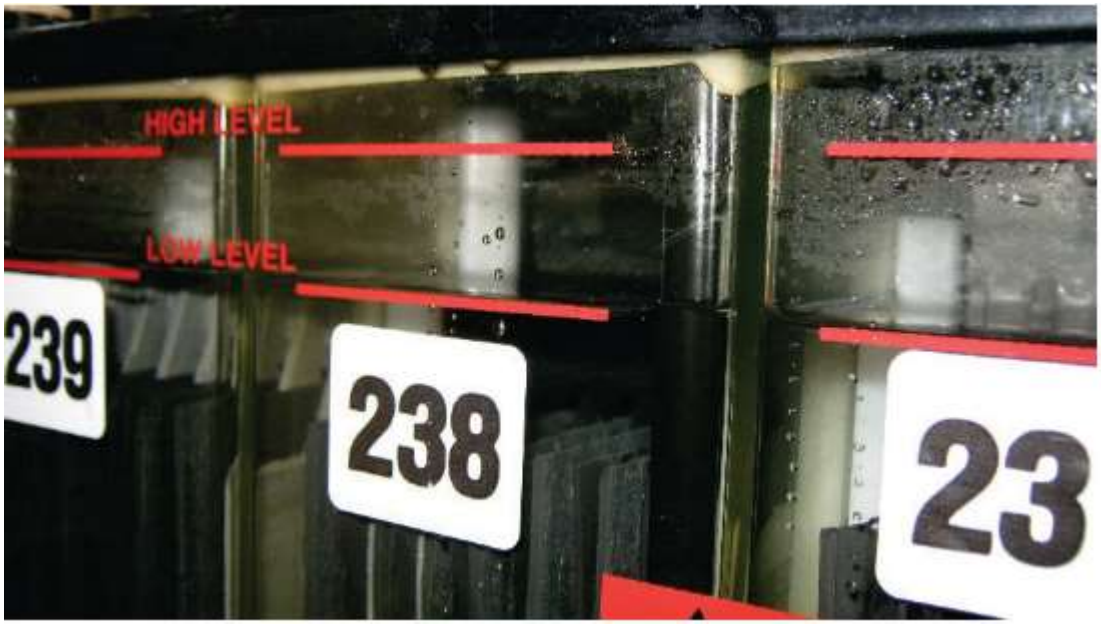

Figure 2.1 Battery with Transparent Case Showing Low Electrolyte Level. Reprinted from [26]**.**

2.1.1.2. Electrolyte stratification

Electrolyte stratification is best defined as the formation of a vertical concentration gradient of sulfuric acid within the cell container. Electrolyte stratification affects battery in different ways, first it induces a capacity loss which can be recovered by overcharging, and also encourages grid corrosion and hard stratification, and both are irreversible. This failure mechanism is almost unique in flood batteries. Electrolyte stratification can be mitigated by active electrolyte mixing. This is done through over charging battery causing gas evolution thus performs the duty as a mixer. In valve regulated lead acid battery, designs with horizontal plates are reported to be least affected by electrolyte stratification.

2.1.1.3. Hydration[27]

In batteries designed to have insufficient amount of sulfuric acid, as the capacity limiting reactant, electrolyte approaches the concentration of water when cell is completely discharged. Lead sulfate becomes soluble in the electrolyte and this is solubility is encourage by elevated temperature. If batteries exposed in this condition stay fully discharged for an extended period of time, lead sulfate in the electrolyte may cause mini-shorts between the plates. Although the mini-shorts have high resistance but they will greatly affect the batteries' capability of holding charge. Figure 2.2 below shows a hydrated battery, the white deposit on the battery case is lead hydrate formed in the process.

Figure 2.2 Hydrated Cell. Reprinted from [26]**.**

2.1.1.4. Positive Grid Corrosion[28]

The presence of contact between lead dioxide with metallic lead leads to a scenario that chemical reaction is thermodynamically and kinetically spontaneous. A mixture of different lead salts is formed as a result. Luckily, the rate of reaction is inherently very

slow. Lead acid battery has a finite life due to the positive lead metal alloy grids eventually dissolves through chemical corrosion. The rate of corrosion has been reported increases as the acidity of the electrolyte drops, this predicts that longer life expectancy of a charged battery compared to a battery that is often maintained in discharged state. Grid corrosion is one of the main life limiting factor in all lead acid battery.

2.1.1.5. Internal Shorting[29]

The inclusion of separators and pressure sealing of the electrodes largely eliminate the chance of existence of short circuits in a cell caused by active material shedding. Under normal cycling conditions, volume of the positive reactant changes by 30%. This volume change cycle put mechanical stresses on the packaging and separator material. As battery ages, these material ages and, occasionally, direct electrical contact is formed between two tightly packed electrodes in a cell, thus an irreversible short circuit is created.

2.1.1.6. Passivating Lead Oxide Film Formation[30]

A passive film forms on positive electrode current collector that serves to limit the corrosion rate by separating the two reactants. As this film grows thicker, an increase in internal impedance is observed in lead acid battery. Passivating layer grows quicker when battery is maintained in long periods at low state of charge. This film can be destroyed by charging battery at higher constant voltage over an extended period of time when battery is essential overcharge to penetrate the active material to reach active material and grid interface. The recoverability is limited by thickness of the passive film and the grade of grid corrosion. This film also limits the charge acceptability of positive electrode. However, due to protective function of this film performs, its growth in very early stage of battery service life is encouraged.

2.1.1.7. Agglomeration of Finely Divided Lead at Negative Electrodes

Direct fusion is often observed in pure metal at temperature way below its melting point. Such effect is most noticeable when finely grains of metallic powders are used. To neutralize this effect, certain different material is added to deliberately contaminate the surface of electrode and reduce contact fusion. In electrochemical batteries, these contaminants are called expanders. When the amount of expander is insufficient or expander particles are consumed during normal cycling, rapid capacity fading is observed. The consequence of this effect can be easily observed by polishing the plate in post mortem battery disassembly[30]. Chucks of lead can be directly observed in negative electrode. This effect will lead unrecoverable failure.

2.1.1.8. Electrolyte Contamination

Manufacturer instruction for battery maintenance usually states that distilled water should be added to fill water lost during operation of lead acid batteries. Daily practice has proven that water at hand is the most commonly used source of added water. Available water usually contains unknown mineral contents and leads to higher rate of self-discharge in battery. Self-discharge rate can reach to a point that the battery can no longer accept charge from observer point of view. In some situations, this effect can be reversible. Some even go no to suggest that accepting battery failure from water loss by not adding water at all is often a better choice. Such reasonable argument is deemed reasonable due to the fact that this happens at such a low rate that the chance of water loss related failure and failure caused other sources can be almost equal. These arguments lead to the introduction sealed type batteries, among them VRLA is the most common. It should be mentioned that certain performance limitation needs be tolerated

for achieving a fully sealed enclosure, for example, lower current limit and charge speed limit. Figure 2.3 below shows a battery with its electrolyte contaminated by dissolved copper. Copper is thus being electroplated onto the negative strap and plates.

Figure 2.3 Electrolyte Contamination. Reprinted from [26]**.**

2.1.1.9. Sulfation

Sulfation refers to the sedimentation of a thin film of irreversible lead sulfate crystal that forms on both battery electrodes under extended period of low state of charge state. As been reported in literature, that after a certain extended period of time under low state of

charge conditions, the recrystallization of lead sulfate could lead to scenarios that result in difficulty in recharge the battery, if not entirely impossible, by employing conventional charging method. Sulfation has led to the development of pulse based charging methods. This problem becomes more prominent as passenger vehicles are increasingly equipped with electric drives as well as other auxiliary loads that demands additional power. With the prevailing battery usage for grid energy storage, the number of batteries suffering from sulfation might greatly increase due to the float the float conditions batteries have to be put in for energy acceptance.

2.1.1.10. Intern-cell Connector Failures

Recent batteries often use so called “through the wall” welding to connect multiple electrode pairs in mono-block battery cases. Such welds are usually thoroughly tested before final battery assembly and shipment to costumer. Bad welds do happen in a relatively rare number of scenarios. Failures of such nature are relevant and may affect performance late in battery service life. This failure mechanism is irreversible.

2.1.1.11. Positive Electrode Active Material Softening and Shedding[31]

This phenomena is also known as positive active material softening and degradation. The positive electrode is formed with lead oxide of two different morphology, α-PbO2 and β-PbO2, where one serves as skeleton of the active material offering mechanical support and the other gets involved in charge/discharge reaction.

The shift of active material crystal structure or morphology, usually a result of overcharging and discharging, results in the softening and shedding of the active material from the positive electrode and grid assembly. The positive electrode assembly is usually encapsulated in a porous envelope, called gauntlet, that serves both as

separator between electrodes and barrier limiting the resulting products shed from the positive electrode. Even with gauntlets restraining active material, the contact between active material and grid is still loosened after excessive cycling. This failure mechanism is irreversible. An example is shown in Figure 2.4.

2.1.1.12. Thermal Runaway[32]

Thermal runaway is a prevalent failure mode in sealed lead acid batteries or valve regulated batteries. When a battery is decommissioned due to high temperature reported during constant voltage charging, thermal runaway is reported. This rapid heating is the combined consequence of exothermic recombination of oxygen at the negative electrodes through inner gas cycle and Joules heating from resistive components.

Figure 2.4 Shed Active Material at Bottom of Lead Acid Battery. Reprinted from [26]**.**

Under normal operating conditions, charging of lead acid batteries using constant voltage results in a decay in current approaching a limit to a trickle charge current. This current can reach above power supply current delivering capability in case of the thermal runaway. As higher temperature increases the reaction rate of oxygen evolution on positive electrode and oxygen recombination on negative electrode, battery will be driven into a spiral positive feedback loop. The Joule heating can heat electrolyte to boiling temperature leading to intense venting of steam. If not stopped timely, cell dry out can be observed.[33]

A different explanation of the same phenomena has also been proposed which contradicts the commonly accepted oxygen cycle explanation. Detailed discussion on this topic will be covered in later section.

2.1.1.13. Hydrogen Accumulation Effects[34]

Valve regulated batteries are designed to evolve oxygen in overcharged state. The built-in recombinant mechanism then collects oxygen from available gas space, i.e. micro-pores in separator and electrolyte, in the battery. Meanwhile, hydrogen is also produced during the self-discharge process in lead acid battery. Hydrogen is not efficiently consumed in the battery and is trapped in the battery forming a higher pressure. The pressure caused by this accumulated hydrogen occasionally leads to the venting out pf gas in the battery through a single direction valve that prevents back propagation of possible ignition. When the condition is met, for example the presence of high temperature in thermal runaway, where strongly exothermic chemical reactions present inside the battery. This pressure cycle leads to deform and swelling of battery case. The

resulting effect is usually very apparent and can usually be directly observed. Note that this failure mechanism has a low chance of occurrence.

2.1.1.14. Mechanical Stress

The volume of active materials, metallic lead and lead dioxide, and the product of electrochemical reaction, lead sulfate, differs by 30% percent. As shown in Figure 2.5 below, the volume difference is clear with the same number of lead atoms. After the charging process, on the positive electrode, lead sulfate is converted back to lead dioxide, but it will not restore its original volume. This constant change or pulsating of volume of the positive electrode will cause mechanical stress to accumulate, as well as cause more active material to disconnect electrically[35]. The same phenomenon is also observed on the negative electrode. This phenomena differs from the aforementioned positive electrode active material softening and shedding as the cause being pure mechanical.

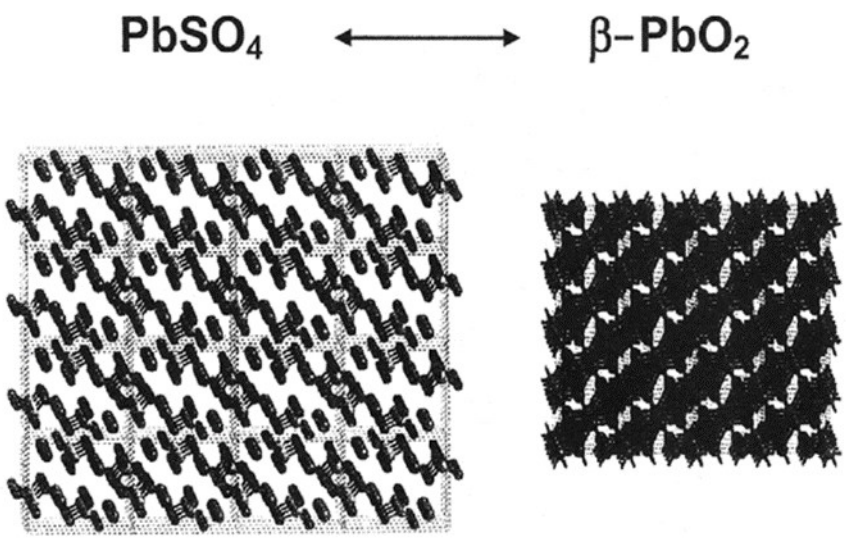

Figure 2.5 Volume Difference of Lead Dioxide and Lead Sulfate. Reprinted from [14]**.**

2.1.1.15. Polarity Reversal[16]

Polarity reversal is a frequent observed failure mechanisms during deep discharge of lead acid batteries. As in most lead acid battery, the two electrodes are rarely designed to have the same capacity, under a deep discharge, the electrode with less capacity will first suffer for polarity reversal. Since in the manufacturing process same materials are used for positive and negative plates, for lead acid battery with one single pair of plates, theoretical, it is still usable after polarity reversal, but due to the difference in electrodes, its performance will be heavily affected. For lead acid battery with multiple pair of plates, polarity reversal of one of the electrode will cause complete failure of the battery.

2.2. Detailed Discussion on Failure Mechanisms

With all the failure mechanisms briefly introduced, the next step is to classify these failure mechanisms. Here, they are classified in a different manner as opposed to most other classifications.

Certain failure mechanisms are caused by manufacturing defects when should be screened out by quality inspection of the manufacturer in the first place. In this work, these failure mechanisms are not considered.

Certain failure mechanisms are specific to very old battery, battery designed for a sole purpose. As the battery of interest is here is deep cycle battery and battery for standalone applications, these failure mechanisms are also not considered.

Certain failure mechanisms are completely random based, thus cannot be included in a deterministic model. As this is a model based study, these failure mechanisms are not incorporated in this study. However, these failure mechanisms can be added if needed using evolving failure rate that usually follows Weibull distribution.

There are also failure mechanisms that has such a low possibility of occurring that very few literature can be found about it, for example: hydrogen accumulating effect. There is just not enough information for it to be clearly studied, let alone included in the battery model.

The case for electrolyte stratification is a bit special. In flooded lead acid battery, electrolyte stratification can be mitigated by planned over charge procedure. Evolved hydrogen and oxygen help mix electrolyte in the bubbling process. Electrolyte stratification still exists in valve regulated lead acid battery, but has been shown can be easily mitigated by employing batteries with horizontal plate design.[4] As it is well counter, it will thus not be included in this study.

The left of the failure mechanisms are the ones that are incorporated in our study. The later part of this section is dedicated to the detailed discussion on these failure mechanisms.

2.2.1. Thermal Runaway

Thermal runaway describes the condition when rate of heat generation within the battery exceeds its heat dissipation capability.

Lead acid battery, or battery in general tend to go into thermal runaway when experiencing overcharge. In lead acid battery, the cases are different for batteries of flooded and valve regulated type.

In flooded battery, when overcharging, oxygen and hydrogen is released. Water electrolysis is an endothermal reaction, the amount of energy supplied by the charger is partially absorbed for this reaction to proceed, only a fraction of the energy is thus left to

heat up the battery. This is exactly what has been observed on overcharging flooded lead acid battery, battery becomes just sensibly warm to the touch. This is essentially built-in mechanism for overcharging energy dissipation.

In valve regulated battery, when overcharging, a different set of reactions fall under the name of oxygen cycle are involved. Valve regulated battery are designed to recombine as much gas evolved on positive electrode as possible. Valve regulated battery is observed to rise in temperature quickly, heat related battery case distortion can often be observed. The figure below shows a valve regulated battery after thermal runaway. Elevated temperature helps to increase the rate of this reaction cycle, thus makes battery going into a positive feedback loop.

Since valve regulated battery is the battery of focus of this research, and thermal runaway being one of the most prominent failure mechanisms, a detailed discussion on its causes and the dilemma mentioned above are presented here.

The mechanism of oxygen evolution on the lead dioxide electrode in lead acid battery is very complicated and there is no general agreed upon explanation of the corresponding mechanism. Still, for the purpose of thermodynamic deriviation, it is sufficient to give the overall reaction with its initial and end products disregarding its kinetics [5].

Oxygen evolved on the lead dioxide electrode reaches the lead electrode through the pores in the separator partially filled with immobilized electrolyte.

Evolution of oxygen at lead dioxide electrode:

$$2H_2O \rightleftharpoons O_2 + 4H^+ + 4e^- \qquad \text{Eq 2.2}$$

Heat of reaction is:

Reduction of oxygen at lead electrode:

$$\Delta H_{f,H_2O} = -285.8\,kJ/mol \quad liquid \qquad \text{Eq 2.3}$$

$$\Delta H_{f,O_2} = 0\,kJ/mol \quad gas \qquad \text{Eq 2.4}$$

$$\Delta H_{f,H^+} = 0\,kJ/mol \quad ion \qquad \text{Eq 2.5}$$

$$\Delta H_f = 285.8\,kJ/mol \qquad \text{Eq 2.6}$$

Water electrolysis is endothermic, absorbing 571.6 kJ of energy per mole of oxygen involved.

Two known mechanisms proceed at lead electrode, oxygen is either reduced chemically or electrochemically:

Chemical reduction of oxygen:

$$2Pb + O_2 \rightleftharpoons 2PbO \qquad \text{Eq 2.7}$$

$$PbO + H_2SO_4 \rightleftharpoons PbSO_4 + H_2O \qquad \text{Eq 2.8}$$

$$PbSO_4 + 2e^- + 2H^+ \rightleftharpoons Pb + H_2SO_4 \qquad \text{Eq 2.9}$$

Heat of reaction of each reaction is:

Lead oxidizes to lead oxide:

$$\Delta H_{f,O_2} = 0\,kJ/mol \quad gas \qquad \text{Eq 2.10}$$

$$\Delta H_{f,Pb} = 0\,kJ/mol \quad solid \qquad \text{Eq 2.11}$$

$$\Delta H_{f,PbO} = -271.9kJ/mol \qquad \text{Eq 2.12}$$

$$\Delta H_f = -543.8\,kJ/mol \qquad \text{Eq 2.13}$$

543kJ of heat is released through this process when a mole of oxygen is involved.

Lead oxide to lead sulfate:

$$\Delta H_{f,PbO} = -271.9 kJ/mol \quad \text{Eq 2.14}$$

$$\Delta H_{f,H_2SO_4} = -811.3 kJ/mol \quad \text{Eq 2.15}$$

$$\Delta H_{f,PbSO_4} = -920 kJ/mol \quad \text{Eq 2.16}$$

$$\Delta H_{f,H_2O} = -285.8 kJ/mol \quad \text{Eq 2.17}$$

$$\Delta H_f = -122.6 kJ/mol \quad \text{Eq 2.18}$$

The reaction is exothermic, 245.2 kJ of heat is released in this process.

Lead sulfate reduction to lead:

$$\Delta H_{f,PbSO_4} = -920 kJ/mol \quad \text{Eq 2.19}$$

$$\Delta H_{f,H_2SO_4} = -811.3 kJ/mol \quad \text{Eq 2.20}$$

$$\Delta H_{f,Pb} = 0\, kJ/mol \quad solid \quad \text{Eq 2.21}$$

$$\Delta H_{f,H^+} = 0\, kJ/mol \quad \text{Eq 2.22}$$

$$\Delta H_f = 108.7 kJ/mol \quad \text{Eq 2.23}$$

217.4 kJ of heat is absorbed in this process.

The total amount of heat released in this cycle:

$$\Delta H_f = 571.6kJ - 543.8kJ - 245.2kJ + 217.4kJ = 0kJ \quad \text{Eq 2.24}$$

So this cycle where oxygen is chemically reduced, no heat is released or absorbed.

The other mechanism is electrochemical reduction of oxygen, the corresponding reaction is:

$$O_2 + 4H^+ + 4e^- \rightleftharpoons 2H_2O \quad \text{Eq 2.25}$$

Heat of reaction is:

$$\Delta H_{f,H^+} = 0\, kJ/mol \quad ion \quad \text{Eq 2.26}$$

$$\Delta H_{f,O_2} = 0\,kJ/mol \qquad gas \qquad \text{Eq 2.27}$$

$$\Delta H_{f,H_2O} = -285.8\,kJ/mol \qquad liquid \qquad \text{Eq 2.28}$$

The reaction is exothermic, 571.6 kJ of heat is release. The amount of heat released at negative/lead electrode is the same as the amount of heat absorbed at positive/lead dioxide electrode.

The total amount of heat released in this cycle:

$$\Delta H_f = 571.6kJ - 571.6kJ = 0kJ \qquad \text{Eq 2.29}$$

The correlation between heat of reaction, Gibbs free energy change and entropy of reaction:

$$\Delta H = \Delta G + T\Delta S \qquad \text{Eq 2.30}$$

By Hess's law or first law of thermodynamics, the sum of enthalpies is zero for all closed chemical cycles. If the system ends in the same state that it started in, the enthalpy of the system will not change.

As can be show through the calculation above, no matter which mechanism oxygen evolved at positive electrode goes through to be reduced at the negative electrode, no net change of heat is present. One argument may be that since the locations of the endothermal and exothermal reactions are not the same, the exothermal reactions will cause battery to heat up locally thus increase the rate of reaction. The reality is in lead acid battery, positive and negative electrodes are closely packed together, thus battery should not be heated up by the oxygen cycle. And since it is implausible to assume 100 percent recombination efficiency, the heat absorbed through endothermal water electrolysis should overpower the heat released through recombination.

The question is what is causing battery to rise in temperature?

The energy needed is fed to the battery from energy source used for charging the battery. The amount of electrons that need to be transferred for per mole of oxygen to be reduced through either path is 4 moles. The amount of energy needed for transferring the electrons is 4FV, where F is the faraday constant, V is the voltage used to charge the battery. When battery is fully charged, no energy is stored through electrochemical reactions, thus all energy is converted to heat.

Battery internal resistance also plays a minor role in Joule heating of the battery, the power of Joule heating is I2R. The problem being given how small the internal resistance of the battery is, Joule heating is almost negligible. Most amount of heat is generated through going over the voltage gradient present in the battery, as battery is fully charged, the gradient is the strongest at this point.

The explanation for thermal runaway is that the closed oxygen cycle requires electrons to be moved for oxygen recombination on the opposite electrode, thus requires current from the source used for charging. The rate of reactions involved in this cycle will increase with the increase of battery temperature, thus more current is required from the charging source and this will heat up the battery even more. If the current supplying capability of the charging source is not limited, this positive feedback loop demanding for higher current will go on forever, eventually the battery keeps heating up and will eventually completely melt down. This seems easily avoidable in single battery setting but is a lot harder for the case of battery bank.

Rise in internal resistance caused by electrolyte displacement is also been proposed[36]. The electrolyte displacement is caused by transportation of oxygen and hydrogen. It has been observed in battery with clear plastic case when overcharged electrolyte level is slightly elevated.

2.2.2. Positive Grid Corrosion

The grid in lead acid battery is casted using metallic lead alloy. As the active material on positive electrode is lead dioxide, reactions between the grid and active material is unavoidable. The corresponding reaction is shown below.

$$Pb + PbO_2 \rightarrow 2PbO \qquad \text{Eq 2.31}$$

This reaction can proceed even at solid state with no other agents present. Note, other reactions are listed in Figure 2.6.

A thin film of lead oxide is thus formed on the grid and active material interface.

Lead dioxide (PbO2) is highly conductive, whereas lead oxide (PbO) is more resistive. The formation of corrosion layer lead to the increase of internal resistance in lead acid battery.

As lead oxide can react with sulfuric acid to form lead sulfate, in the charging process the end product lead sulfate can be converted to lead dioxide. Thus a new interface between lead grid and lead dioxide is formed fueling the corrosion process.

Theoretically, this reaction path will go on forever until all the lead grid is consumed. In fact, even without other failure mechanisms of lead acid battery, positive grid corrosion will always to the life limiting mechanism in lead acid battery. It is quite sarcastic in most other applications, lead is chosen because of its corrosion resistant capability.

The only option is to seek different metal or alloy to substitute positive grid. Additives to negative electrode has always been an active area of research to improve its performance on high rate charge and discharge at partial state of charge, very little effort has been put into finding a new material for positive grid for lead acid battery, even though for standalone applications, long service life is always a preferred quality.

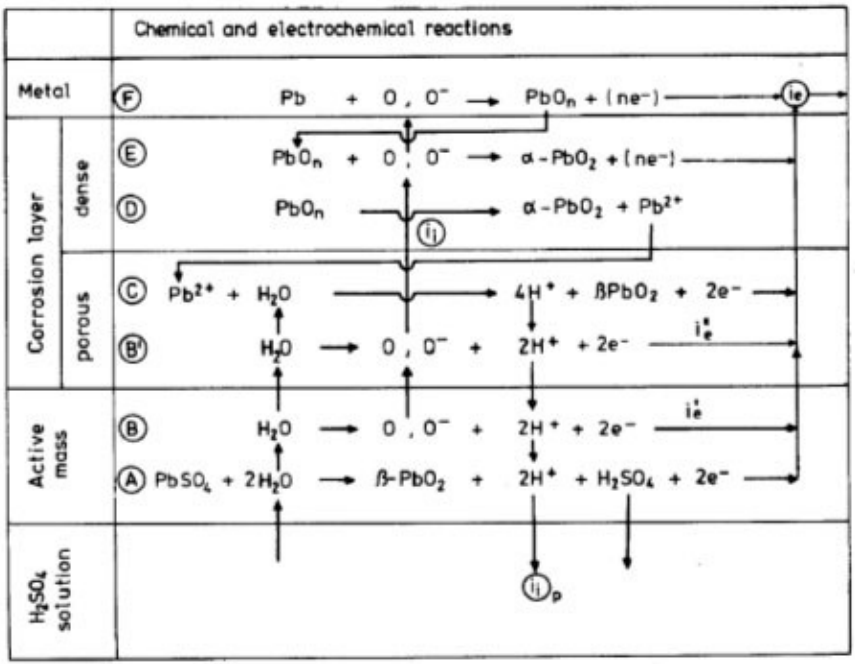

Figure 2.6 Reactions at Positive Electrode. Reprinted from [27] **.**

The rate of positive grid corrosion is limited by the formation of passivation layer on the grid. The exact composition of this passivating layer is discussed in [9]. It is usually considered to be formed by two different layer, a semi-permeable and resistive layer of lead sulfate and a semi-conducting layer of a mixture of lead oxide and lead dioxide. If the growth of the lead sulfate layer is not controlled, this will cause a different failure mechanism known as positive grid passivation.

2.2.3. Mechanical Stress in Lead Acid Battery

As in any battery, charge and discharge of battery cause its electrodes to change structure in cycle. In lead acid battery, this cycle of structure change is from metallic lead to lead sulfate and back to metallic lead on negative electrode and from lead dioxide to lead sulfate and back to lead sulfate on positive electrode, respectively. With the change in mechanical structure, the volume of the active materials in battery also pulsate in the due process. This has been shown in early section with the figure comparing the volume of lead dioxide and lead sulfate with same number of lead atoms.

The deeper the battery is discharged in the cycling process, the greater the change of volume is, thus the greater the mechanical stress is within the battery. This can be shown by Table 2.1 for lead acid battery lifespan versus of depth of discharge, the specific data for each battery can usually be found from battery manufacturers.

DOD%	**20**	**30**	**40**	**50**	**60**	**80**	**90**	**100**
Number of cycles								
VRLAB1	4250	2750	2125	–	1375	1000	–	800
VRLAB2	6250	4200	3200	–	2080	1500	–	1250
VRLAB3	–	5800	4300	3500	2800	–	1800	1650
VEB1	4500	3000	2250	–	1500	–	1000	900
VEB2	8400	5500	4250		2800	–	1800	1700
VEB3	6000	4000	3000	–	2000	1500	–	1200

Table 2.1 Number of Battery Cycles as a Function of Depth of Discharge (Manufacturer's Data)[38].

3. LEAD ACID BATTERY MODELING PORCESS

In this chapter, a model of lead acid battery with failure mechanisms built-in is presented.

3.1. Review of Different Modeling Methods

Model of a specific subject has to serve its purpose. To fulfil its purpose well, a balance between different aspects of the modeling choices has to be carefully considered. Accuracy, complexity and the ability for interpretation are among the most important aspects of these considerations.

Accuracy addresses the problem of output of the model tracking output of the subject when subjected to the same set of input. The problem of complexity is usually twofold: configuration complexity and computation complexity. Configuration complexity addresses the number of configurable parameters that are included in the model; computation complexity addresses the amount of resources, time and memory, needed for simulating the model. Ability for interpretation addresses the possibility for a qualitative and intuitive understanding of the behaviors of the model thus behaviors of the subject. This is especially important when design choices need to be made for a certain purpose for the subject.

An ideal model of the subject would be highly accurate, require very little resource to implement and self-explanatory. This is rarely the case in almost all studies. Compromises of different types are unavoidable. In many cases, details of the subject of interest are so scarce that educated guesses, hypotheses, have to be made and waiting to be verified either through observations or experiments. A quick survey of literature can easily reveal that many models are indeed built on these hypotheses.

Plethora of models of rechargeable batteries can be easily found in literature. Mathematical descriptions of the battery of interest are either based on detailed processes inside the battery, empirical observations of the battery or a mix of the two. These different approaches has been summarized as white box model, grey box model and black box model, respectively[39].

Generally, a white box model, also known as electrochemical model, includes most of the nitty-gritty details inside the battery. A good example of white box battery model can be found in [40]. In models of this type, a cell is usually is presented in great detail where electrolyte is discretized to model the process of ion transportation, electrodes are divided into layers or fragments so the effect of difference in active material concentration can be addressed 'properly'. Model of this type is usually designated for battery design purposes so tweaks on battery dimensions and other design parameters can be made to optimize for the specific application. This is clearly not the type of battery model needed for this research. The finite element analysis approach used can greatly increase computation and configuration complexity. The model is also too rich to be well interpreted as decoupling the large number of configurable parameters requires serious effort.

A black box model looks at battery as nothing more than a system with inputs and outputs. Effort is put into mapping the outputs to its corresponding inputs. The intermediate part, the battery itself, can be completely ignored in the process. It is clearly developing a black box model can demand a large collection of data. If the data collected can cover the input-output space entirely and evenly, very accurate model can be

developed based on the black box model approach. Machine learning algorithms and artificial neural networks are often employed for black box modeling process. Computation complexity is usually low, configuration complex varies per the algorithm used. Very little useful information can be directly interpreted.

Grey box model sits somewhere between the two aforementioned modeling approaches. A grey box model includes enough details of the processes on the battery and often addresses these processes using lumped parameter components. Certain part of the model can be built based on simple input-output mapping as per the black box approach. Complexity, either computational or configurational, depends on the amount of details required for the application. The ability to interpret is usually very high as lumped parameter components offer intuitive paths for parameter dependence. The one area grey box model lacking in is accuracy. To increase accuracy of the model, usually more components need to be included and thus increasing its complexity. In some extreme case, the addition of components can increase the order of the model thus greatly increase its computational complexity. The decision on adding components to the model needs to be considered carefully; and there is also a limitation on how much extra accuracy can be gained through this approach. Trying to match the accuracy of white box model with grey box model is unrealistic.

The topic of this research is failure of lead acid battery bank. The conventional choice of model for failure studies is usually either of white box model type where all the details is included, or a black box model where large amount data is available for an accurate model. For failure of lead acid battery bank, a detailed white box model brings great

computational complexity as a battery bank is consisted of multiple batteries, a black box model offers nothing on the interaction between batteries and very little information on what is going on in each individual battery, the great amount of data needed is also not available. The modeling approach used in this study is of grey box type.

A brief review of grey box type model is presented here.

There are two general sub-genres of grey box type: empirical model and equivalent electrical component model.

By lumping battery distributed dynamics, equivalent electrical component models use a selection of electric elements, such as voltage source, resistors, current source, capacitors, and often non-linear elements, such as Warburg impedance, to model the terminal behavior of battery. A large portion of these models can be referred to Randle models ,shown in Figure 3.1, which consist of different combinations of resistor and capacitors in the form of RC ladders. Adding more shunts to RC ladder increases the order of the model and helps to track the dynamic performance of battery more accurately. The figure below shows a typical Randle model. These models are used for studying the dynamic performance of batteries, as impedances of batteries at different frequencies and different magnitude of currents are measured and the results from these measurements are related to other battery parameters such as state of charge and usable capacity. These models albeit helpful in correlating measurable parameters of the battery to inaccessible parameters are not very practical, as measurements has to be taken on the battery when it is completely disconnected and requires highly specialized instruments.

In a battery bank setup, where multiple batteries even hundreds of batteries are involved, doing these tedious measurements is utterly impossible.

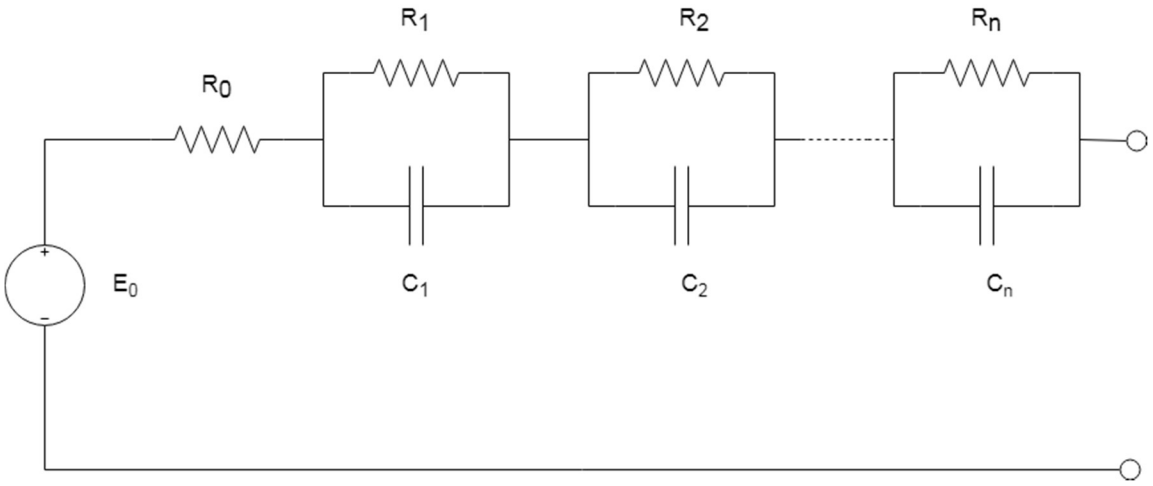

Figure 3.1 Randle Model[41]

Empirical models employs simple equations to describe characteristics of interest in battery behavior. The well-known Shepherd equation is a perfect example of empirical model where battery terminal voltage is expressed with its dependence on internal resistance and current drawn. The corresponding equations are[42]:

$$U_{Cell} = U_{oc} - g_c H + \rho_c \frac{I}{C_N} + \rho_c M_c \frac{I}{C_N} \frac{F}{C_c - F}, \qquad charge \qquad \text{Eq 3.1}$$

$$U_{Cell} = U_{od} - g_d H + \rho_d \frac{I}{C_N} + \rho_d M_d \frac{I}{C_N} \frac{H}{C_d - H}, \quad discharge \qquad \text{Eq 3.2}$$

A comparison of different modeling approach is summarized in Table 3.1.

3.2. Lead Acid Battery Model with Ageing and Failure Mechanisms

Further decisions need to be made on what should be included in the model used for this study. As from terminal user point of view, a battery offers voltage support while

suppling current the load; the load is cut off when the battery can offer enough voltage support.

Table 3.1 Comparison of Different Types of Models[43]

Model Type	Accuracy	Complexity, Computational	Complexity, Configuration	Interpret-ability	Application
Electrochemical	Very high	Very high	High	Low	Battery Design
Reduced-order	High	High	Medium	Medium	Control, SOC estimation
EECMs	Medium	Low	Medium	High	Real-time Control, SOC estimation
Empirical	Low	Very Low	Low	Medium	Only for constant operation conditions
Black-box	Medium	Medium	Medium to High	Low	Off-line analysis

In a battery bank, the interaction between batteries is purely electrical, current is distributed through difference in voltages and impedances. Temperature affects both voltage and impedance of the battery. This gives a rough figure on elements that needs to be included in the battery model: battery open circuit voltage, rate depend capacity, thermal effect, aging mechanisms and parasitic effects.

For a general battery model, its terminal voltage is always of interest. However, terminal voltage can be only be measured since it depends on multiple other variables including but not limited to open circuit voltage, internal resistance and current drawn. Open circuit voltage and internal resistance will be modeled separately.

The time frame used for study is based on battery or battery bank failure rate, which are in terms of hundreds of cycles. Factor that in the average number of cycles a deep cycle battery experiences in real life scenario, the time frame is in years. At this time frame, the dynamic of battery which are modeled using RC ladders are completely drown in the back ground. A thorough survey of literature reveals that even with multiple RC ladders used in lumped parameter model, the fast transient dynamic of battery is still cannot be properly present. A good example of this would be high rate discharge at partial state of charge for lead acid battery used in hybrid vehicles. This transient is widely known to harm battery greatly, it is still not well explained with models. Luckily, this is not included in the scope of this study.

But purposefully ignoring battery dynamic, the model that is of interest in this research is of semi-steady state type.

The model consists the following parts: electrical model, thermal model and aging model. Parasitic reactions and other failure mechanisms are addressed as separate modules of the model. Model composition is shown in Figure 3.2.

The electrical model is shown in Figure 3.3 below. This structure has been used extensively in literature for modeling lead acid battery.

Here, I_p is a voltage controlled current source that handles self-discharge. The magnitude of its current is also affected by battery temperature, battery open circuit voltage and age of the battery.

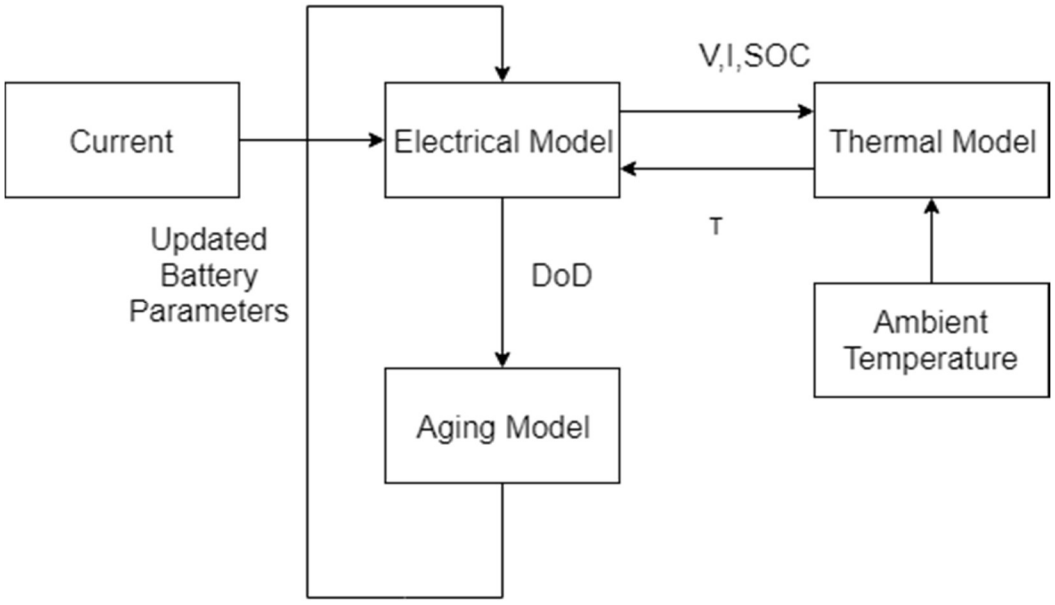

Figure 3.2 Model Composition

Ideally, all the parameters in the model should be able to be directly related to state of charge as SOC is the status most useful for the end user. So the relationship of battery parameters to SOC will be discussed in detail. As a reminder, the definition of state of charge is show here.

SOC is defined as:

$$SOC = SOC_0 + \frac{\int Idt}{Capacity} \qquad \text{Eq 3.3}$$

Where, SOC_0 is the initial SOC. SOC is usually calculated using columbic counting, even though widely adopted, this method can be very inaccurate due to omission of charge acceptance rate in the equation.

3.2.1. Modeling Battery Open Circuit Voltage

From last chapter on the principle of lead acid battery, the following equation has been explained in detail:

$$E_{cell} = E_{PbO_2/PbSO_4} - E_{Pb/PbSO_4} \quad \text{Eq 3.4}$$

$$E_{cell} = 2.041 + (1.98 * 10^{-4}) * T * \lg(a_{H_2SO_4}/a_{H_2O}) \quad \text{Eq 3.5}$$

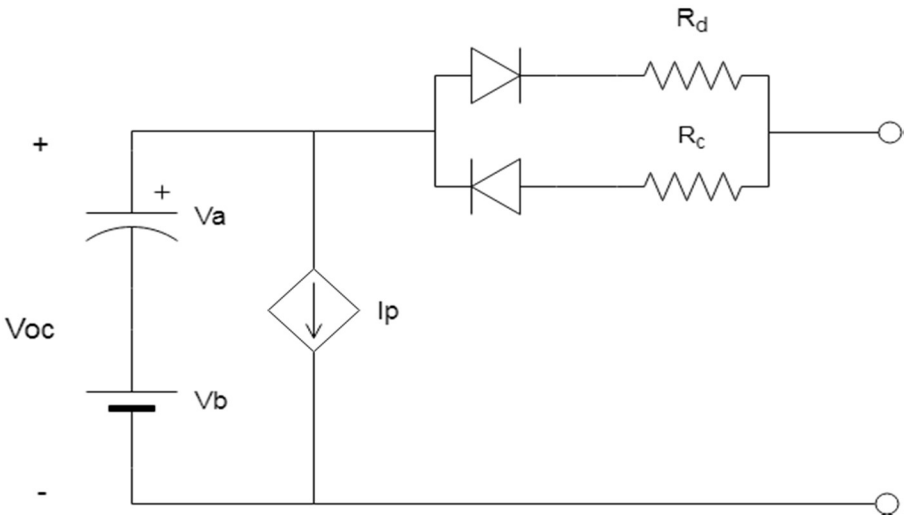

Figure 3.3 Electrical Model

This equation relates lead acid cell equivalent potential to temperature inside the cell and activity of sulfuric acid and water which are related to their individual concentration respectively. This relationship has been widely adopted in lead acid battery models to estimate battery state of charge. Conventionally, in flooded lead acid battery, electrolyte density can be directly measured and thus related to battery state of charge through sulfuric acid concentration, the same measurement is also used as status indicator for regular replenish of distilled water. In valve regulated batteries, electrolyte density

measurement is impossible, but the same relationship still stands. This is true because in most lead acid batteries, the amount of sulfuric acid, or more accurately its concentration, is the usable capacity limiting factor.

Figure 3.4 below shows the linear relationship between battery open circuit voltage and its internal state of charge in four different VLRA batteries. Note the batteries shown in the figures are constructed with 6 cells connected in series.

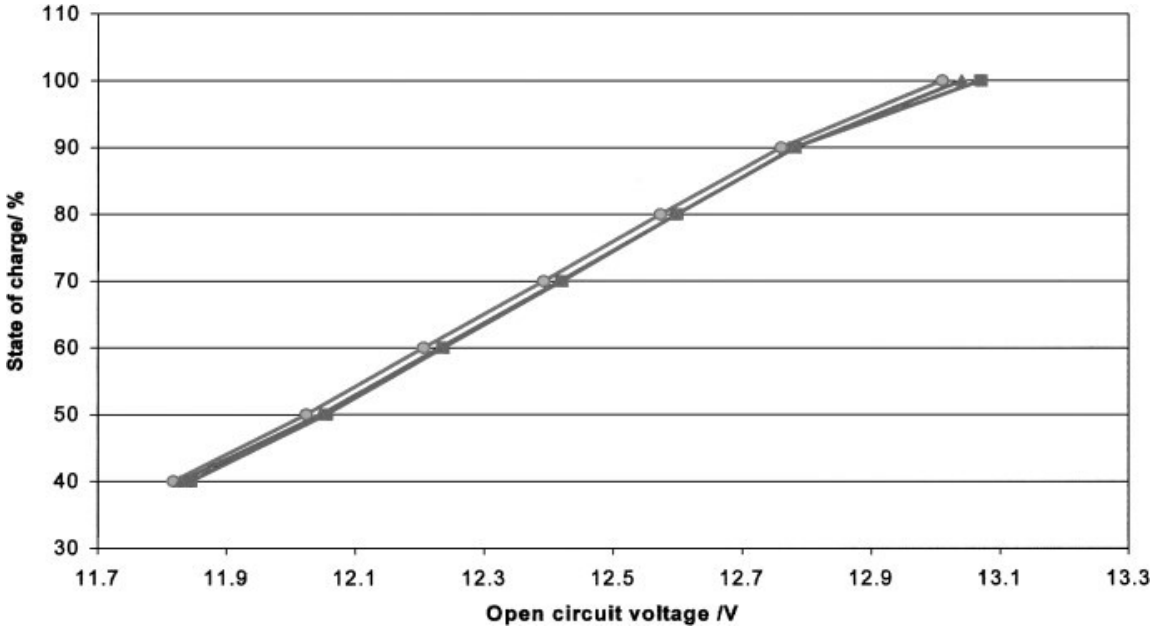

Figure 3.4 Dependence of the State of Charge on Open Circuit Voltage from Four VRLA Batteries of the Same Type. Reprinted from [44].

The equation used to model this relationship is:

$$V_{OC} = V_a * SOC * \left(1 + \alpha\left(T_{batt} - T_{ref}\right)\right) + V_b \qquad \text{Eq 3.6}$$

Rearrange the electrochemical relation, replacing cell temperature with a reference temperature and deviation from it, reference temperature is chosen to be 300K:

$$E_{cell} = 2.041 + (1.98 * 10^{-4}) * (T_{ref} + \Delta T) * \lg(a_{H_2SO_4}/a_{H_2O}) \qquad \text{Eq 3.7}$$

Again rearrange the equation to factoring out activity of water:

$$E_{cell} = 2.041 + (1.98 * 10^{-4}) * (T_{ref} + \Delta T) * \lg(a_{H_2SO_4}) \quad \text{Eq 3.8}$$

$$-(1.98 * 10^{-4}) * (T_{ref} + \Delta T) * \lg(a_{H_2O})$$

As the molar concentration, molarity, of water in the electrolyte remains relatively unchanged, the third term that includes water activity can be seen as a constant. A table showing the activity of water against its molar concentration can be found in chapter one. So compare this equation with the above, it can be seen:

$$V_b = 2.041 - -(1.98 * 10^{-4}) * (T_{ref} + \Delta T) * \lg(a_{H_2O}) \quad \text{Eq 3.9}$$

By substituting the corresponding values:

$$V_b = 1.75 \quad \text{Eq 3.10}$$

Table 3.2 is used to reference activity of sulfuric acid at different concentration.

The range of electrolyte relative density during a flooded lead acid battery operation can be found in literature, an empirical equation has also been established between the relation of specific weight of electrolyte and cell open circuit voltage:

$$E = specific\ weight + 0.845 \quad \text{Eq 3.11}$$

So, the molarity of sulfuric acid is directly related to cell open circuit voltage.

Another approach can be used to calculate the temperature coefficient through change of enthalpy. The detailed procedure are presented here.

Consider the reaction below:

$$Pb + PbO_2 + 2H_2SO_4 \rightleftharpoons 2PbSO_4 + 2H_2O \quad \text{Eq 3.12}$$

Enthalpy of Reaction:

$$\Delta H = -360kJ \quad \text{Eq 3.13}$$

Change of free Gibbs energy:

$$\Delta G = -372kJ \quad \text{Eq 3.14}$$

Heat of reaction:

$$T\Delta S = \Delta H - \Delta G = 11.6kJ \quad \text{Eq 3.15}$$

As:

$$nFE = \Delta G \quad \text{Eq 3.16}$$

Table 3.2 Electrolyte Parameters for Dilute Sulfuric Acid (Room Temperature)[46]

Wt.%	Relative Density	Concentration (g/L)	Concentration (mol/L)
8.0	1.0541	84.2	0.858
10.0	1.0068	106.6	1.087
12.0	1.0821	129.6	1.322
14.0	1.0966	153.3	1.563
16.0	1.1114	177.5	1.810
18.0	1.1265	202.4	2.064
20.0	1.1418	228.0	2.324
22.0	1.1575	254.2	2.592
24.0	1.1735	281.1	2.866
26.0	1.1893	308.7	3.147
28.0	1.2052	336.9	3.435
30.0	1.2213	365.7	3.729
32.0	1.2353	395.3	4.030
34.0	1.2518	425.6	4.339
36.0	1.2685	456.7	4.656
38.0	1.2855	488.5	4.981
40.0	1.3028	521.1	5.313

It can be easily sorted out that:

$$\frac{\partial E}{\partial T} = \frac{\Delta S}{nF} = 0.20mV/K \quad \text{Eq 3.17}$$

Note, the above calculation is done at temperature of 295K. This temperature coefficient is small and is sometimes neglected in practice, but for the purpose of this research, as interaction between batteries can be solely driven by temperature difference, thus this cannot be neglect.

$$\alpha = \frac{\frac{\partial E}{\partial T}}{V_a} = 0.345 * 10^{-3}/K \quad \text{Eq 3.18}$$

3.2.2. Modeling Battery Internal Resistance

From the structure of electoral model, the charge and discharge resistances are modeled separately, this is a natural choice, as the reactions involved are inherently different.

A breakdown of the composition of battery internal resistance is shown in Figure 3.5 below.

Per the discussion above on the battery dynamics, the capacitor and inductor in the impedance composition is not considered.

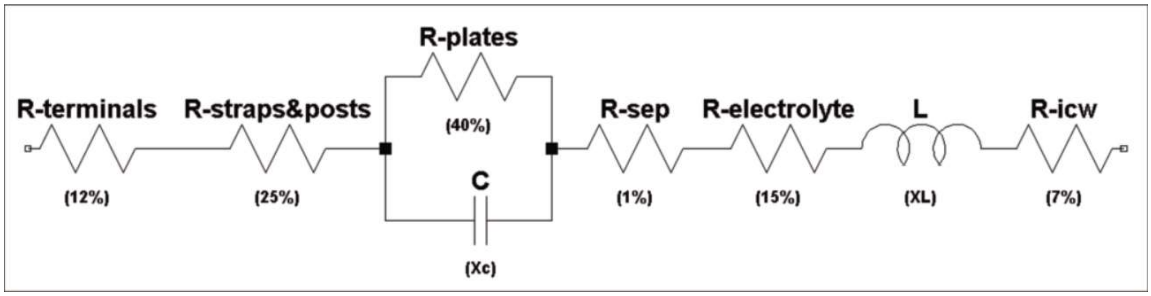

Figure 3.5 Battery Internal Impedance Composition. Reprinted from [47]**.**

Apparently, some components with the internal resistance of lead acid battery is not affected by battery state of charge. These components include: terminal resistance, strap

and post resistance, inter-cell connector resistance and separator resistance. These components account for about 45% percent of battery internal resistance. They are also not affected by the direction of reaction, thus will be considered as a separate component in the model and not discussed in here.

The components of interest are: plate resistance and electrolyte resistance. Both components have negative correlation with battery state of charge. As with the decrease of battery state of charge, the concentration of conducting ions also decrease, thus inducing the increase of electrolyte resistance; with the decrease of battery state of charge, lead sulfate is formed on both electrode, thus increase the resistances of both positive and negative electrodes.

The effect of temperature on the two components are different, plate resistance increase with higher temperature, electrolyte resistance decreases with higher temperature with increased ion mobility.

When battery is in discharging process, it is clearly its internal resistance increases with decreasing state of charge. When battery is in charging process, this relationship is reversed, this phenomenon is sometimes referred to as varying charge acceptance rate. This reversal in relation can be easily verified with a thought experiment, assuming charge resistance decreases with increasing state of charge, a constant voltage charge scheme will requires a never ending increase in current. This is a clear contradiction to the real life scenario.

Even these fairly natural deduction on the relationship between battery internal resistance and state of charge, very little literature can be found covering these topics.

The equations below are used to model battery internal resistances:

$$R_c = R_{c,base} * \exp(c * SOC + d) * (1 + \beta(T_{batt} - T_{ref})) \quad \text{Eq 3.19}$$

$$R_d = R_{d,base} * exp(g * (1 - SOC) + f) * (1 + \beta(T_{batt} - T_{ref})) \quad \text{Eq 3.20}$$

Where, V_{oc} is the open circuit voltage of the battery, SOC is the state of charge, R_c and R_d are the charge and discharge resistances, T_{batt} is the battery internal temperature and C is the battery capacity in Ampere-hours. The other parameters are constants.

3.2.3 Modeling Parasitic Reactions in Electrical Model

There are multiple parasitic reactions co-exist within lead acid battery. The most prominent of them all is water electrolysis.

The rate of this reaction in lead acid battery has been carefully investigated. In battery at float state, the rate of this reaction can be directly related to float current within the battery. The figure below shows float current in the battery at different temperature and open circuit voltage.

The below equation of parasitic reaction current is obtained by curve fitting Figure 3.6 from literature[48][49].

$$I_p = {}^{C}/_{100Ah} * I_{p,base} * \exp(r_1 * V_{oc} + r_2 * T_{batt} + r_3) \quad \text{Eq 3.21}$$

The values of the constants are:

$$r_1 = 16.17 \quad \text{Eq 3.22}$$

$$r_2 = 0.11 \quad \text{Eq 3.23}$$

$$r_3 = -30.3 \quad \text{Eq 3.24}$$

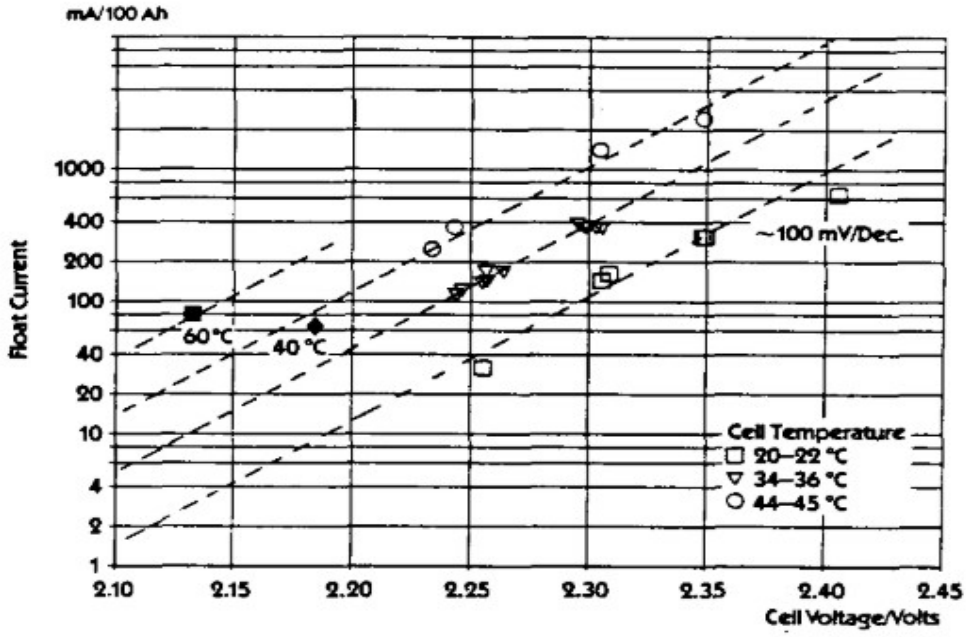

Figure 3.6 Float Current at Different Temperatures in a VRLA battery. Reprinted from [50]**.**

3.3. Battery Thermal Model

The composition of the thermal model is shown in Figure 3.7 below. The major sources of heat in a battery are the reaction heat and the ohmic heat. Heat generated are then dissipated through the casing of the battery. A temperature gradient exists between the all sides of battery case.

In Figure 3.7, C_T is the thermal capacity of the battery, T_{batt} is the temperature inside the battery case, $T_{outside}$ is the temperature outside the battery case, R_{tcd} , R_{tcv} and R_{tr} are the equivalent thermal conduction, thermal convection and thermal radiation resistances, respectively, and dQ/dt is the rate thermal energy is generated in the battery.

The amount of reaction heat generated in discharging process can be calculated, as charging process is just the reverse of discharging process, per Hess' law the amount of

heat either generated or absorbed in the due process is just the reverse of its reverse process.

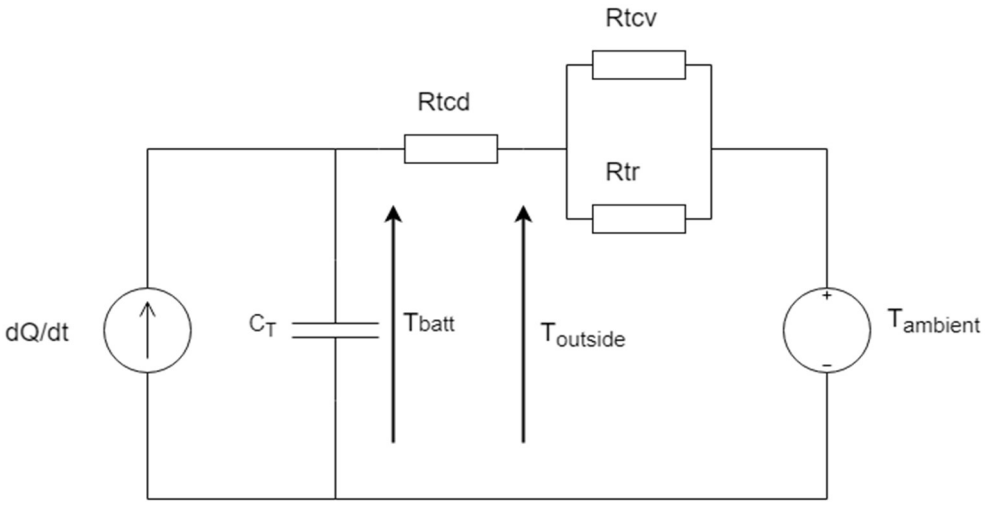

Figure 3.7 Thermal Model[51]

Revisit the equation:

$$Pb + PbO_2 + 2H_2SO_4 \rightleftharpoons 2PbSO_4 + 2H_2O \quad \text{Eq 3.25}$$

$$T\Delta S = \Delta H - \Delta G = -315.6kJ \quad \text{Eq 3.26}$$

In the discharging process, 11.6kJ of heat is absorbed when 2 moles of electrons are transferred through the load.

For charging process:

$$2PbSO_4 + 2H_2O \rightleftharpoons Pb + PbO_2 + 2H_2SO_4 \quad \text{Eq 3.27}$$

$$T\Delta S = \Delta H - \Delta G = 315.6kJ \quad \text{Eq 3.28}$$

In the charging process, 11.6kJ of heat is absorbed when 2 moles of electrons are transferred through the charger. As Faraday constant gives the amount of charge carried by a mole of electrons, the amount of heat generated or absorbed per coulumb of charge is:

$$\Delta Q = \pm 1.635 J/C \quad \text{Eq 3.29}$$

This value is used in the model to calculate reaction heat.

Heat dissipation of battery has to go through battery case and then to the atmosphere. The process of transferring heat from inside the battery to its case is usually the bottle neck. The amount of heat can be transferred from battery case to its surrounding through heat radiation can be evaluated using its emissivity.[52] For most commonly used battery case material, polypropylene, is 0.97.

The amount of heat that can be transferred through convection of cooling air outside battery case can be found at [53], value of 100W/m^2 *K is chosen. Battery dimensions are chosen per manufacture's product manual.

Calculation is carried out for a set of combinations of battery internal temperatures and ambient temperatures. The results from these calculations show that the amount of heat dissipated through radiation can be neglected and heat conduction through the battery casing is the major limiting factor for dissipation.

3.4. Battery Aging Model

The aging model addresses how battery capacity(C), $R_{c,base}$, $R_{d,base}$ and $I_{p,base}$ evolve. It is effectively addressing the problem of accumulated mechanical stress. The aging model is based on the Ampere hours, Ah, through put method with penalty for deeper depths of discharge.

A weighted discharge is calculated. Weighted Discharge is defined as:

$$Weighted\ Discharge = Capacity * (DoD + 0.05 * DoD^2) \quad \text{Eq 3.30}$$

Thus, the deeper depth of discharge is, the larger the weighted discharge will be.

Then, the weighted discharge is accumulated through cycles. The accumulated weighted Discharge is defined as:

$$AWD = \sum_i Weight\ Discharge_i \quad \text{Eq 3.31}$$

Batteries are assigned an expected lifespan. The aging factor is defined based on this expected lifespan and the AWD. Aging factor is defined as:

$$Aging\ Factor = \frac{Capacity_o * Expcycle - AWD}{Capacity_o * Expcycle} \quad \text{Eq 3.32}$$

Where, the $Capacity_o$ is the nominal capacity of the battery.

The battery capacity and the aging factor are related as:

$$Capacity = Capacity_o \cdot Aging\ Factor \quad \text{Eq 3.33}$$

The internal resistances are related in a similar manner, with the only difference being that the internal resistances grow with the aging of the battery:

$$R_{d,base} = R_{d,base,o} \cdot 1/Aging\ Factor \quad \text{Eq 3.34}$$

$$R_{c,base} = R_{c,base,o} \cdot 1/Aging\ Factor \quad \text{Eq 3.35}$$

Where, $R_{d,base,o}$ and $R_{c,base,o}$ are the resistances when the battery is new.

Self-discharge rate grows with battery aging. It is related to the aging factor as:

$$I_{p,base} = I_{p,base,o} \cdot 1/Aging\ Factor \quad \text{Eq 3.36}$$

3.5. Modeling Prominent Failure Mechanisms

Thermal runaway as the most prominent failure mechanism is reflected in battery temperature rise, capacity and resistance change.

Per the discussion in last chapter, thermal runaway is handled in two different cases.

The rate of water electrolysis thus the amount of current need for recombination can be calculated using the same equation for modeling parasitic reaction current:

$$I_p = {}^{C}/_{100Ah} * I_{p,base} * \exp(r_1 * V_{oc} + r_2 * T_{batt} + r_3) \quad \text{Eq 3.37}$$

When current supplied from the charger can sufficiently fuel the oxygen cycle, all excess energy is just used to heat the battery. No water loss is accounted for, thus only battery temperature change is calculated. The amount of heat inject into the battery per unit time through charger is simply:

$$\Delta Q = VI \quad \text{Eq 3.38}$$

Where, V is battery voltage, I is the charger current. Battery state of charge remains unchanged.

When current supplied from the charger is insufficient to fuel the oxygen cycle, rate of water electrolysis is calculated at the positive electrode potential, all the current supplied is considered to be used in oxygen recombination, the excessive oxygen and hydrogen generated is considered as loss of water. This is the reason why loss of electrolyte should not be neglected as a failure mechanism even for valve regulated lead acid batteries. The amount of water loss per unit time is calculated using the equation below:

$$\Delta m = 18 * \Delta I / 2F \quad \text{Eq 3.39}$$

Where ΔI is the deficient of current, F is faraday constant, 18 is the atomic weight of water.

This is shown as a capacity loss as resistance increase, which are calculate as:

$$C = C_0 \frac{m - \Delta m}{m} \quad \text{Eq 3.40}$$

$$r = r_0 \frac{m}{m - \Delta m} \quad \text{Eq 3.41}$$

Where the amount of water in electrolyte. Note the increase in resistance applies to both charge and discharge resistance.

The amount of heat generated in this process is:

$$\Delta Q = V(I - \Delta I) \quad \text{Eq 3.42}$$

Reaction heat is neglected, as calculation at different conditions has shown its two orders of magnitude smaller than the heat accounted for using the above equation. Battery is also discharge be the deficient of current.

Positive grid corrosion is also modeled as a capacity decrease and resistance increase. Rate of positive grid corrosion has been studied extensively.[54][55][56][57][58] Corrosion rate is impeded by the formation of a passive layer on positive grid.

This tendency needs to be reflected in the model. The basic assumption is that the life of lead acid battery is limited by positive grid corrosion[59][60]. The capacity loss at the end of battery life cycle is set to be 20%, resistance is set to increase by 25%. The following equations are used to model positive grid corrosion:

$$C = C_0 * e^{-u_c t} \quad \text{Eq 3.43}$$

$$r = r_0 * e^{u_r t} \quad \text{Eq 3.44}$$

4. MODEL BASED FAILURE STUDY

Application scenario of single battery is very limited, mostly in consumer electronics only. A single battery, while offering a media for energy storage and power delivery, is greatly limited by its sheer size and capability. To fulfill the voltage and current requirement, batteries are usually connected either passively or actively to form battery banks of different topologies. This is quite significant in grid energy storage applications where hundreds even thousands of batteries are used. Choice of battery bank topology depends greatly on the application. Finding optimal topology of battery bank for each specific application is challenging even when certain requirements are already given. Many questions concerning battery bank go unaddressed. The general idea of having a large of number of batteries connected in series might be suboptimal is widely accepted but never thoroughly investigated. The general idea of having a large battery bank consist of many individual batteries might raise reliability and safety issues has also been mentioned in multiple sources, but the claims have also never been carefully verified. Carrying out real life experiment on single battery failure is usually costly and time consuming, doing the same for battery banks of different scales and topologies is utterly impossible. Certain failure modes have very low chance of occurrence that may cause catastrophic damage. These failure modes can easily be neglected even in single battery case. Battery models is a powerful tool that can help to mitigate the problem, as simulation of batteries and battery banks can be easily staged, repeated and perturbed for sensitivity analysis.

A whole branch of engineering is dedicated to the study of failures of complicated systems, reliability and system safety engineering; different methods have been developed for failure analysis, either top-down or bottom-up. However, these methods can hardly be used for our study, for a battery bank with hundreds of batteries pin point the reason of a single failure is almost next to impossible.

Failure of battery bank is studied statistically in this chapter. First a test cycle is defined. Then, single battery case is tested as a baseline. Effect of different choices operating condition is verified with specific interest in the effect of float charge. Effect of topology and bank size is then tested. A simple improved topology is introduced and tested. Step failure is introduced to different battery banks as test of their reliability and robustness.

4.1. Defining A Test Cycle

Testing battery model requires a specific test cycle. Ideally, collect a number of cycles taken from real world scenarios and form a sequence of cycles from the collection will serve as the best test cycle for batteries or battery banks. This ideal case, however, requires a specific mix for every different application. Testing for failure requires a mix of normal use and extreme cases so all the possibility of failure can be identified and examined.

In this study, a simple test cycle is proposed. This test cycle consists of full charge and discharge of battery bank which put maximum stress on the test subject and is thus chosen for failure study purpose. This is not representative of real-world scenario, as battery banks are seldom exposed to cycles like this, shallower depth of discharge and long hours of float operation is typical of energy storage devices used in grid

applications. Since failure is the focus of this research, the choice of maximum stress test is adequate.

The test cycle is shown in Figure 4.1 below. Each part of the test cycle is discussed in the following section.

4.1.1. End of Discharge Condition

End of discharge condition is defined as voltage threshold which is temperature and current compensated. The higher the current drawn from the battery, the lower the voltage threshold, the higher the battery temperature, the higher the voltage threshold. Define a proper end of discharge threshold is closely related to defining the usable capacity of the battery. From the discussion in last chapter, the shallower the cycles the battery goes through in a discharge-charge cycle, the longer the battery's life span; the shallow the cycle, the lower the usable capacity. Improperly defined end of discharge voltage threshold can lead to false positive report on capacity failure.

4.1.2. End of Charge Condition

The definition of end of charge condition needs to be considered with the charging method used. The charge method used in this research is current limited constant voltage charging. Using this method, in later stage of charging, charging current will be reduced greatly, and essentially goes into the range of trickle charge.

Thus, end of charge condition is defined as combination of voltage and current threshold. As the voltage of battery is inaccessible in the charging process. Using the combination of measured battery voltage and current will ensure the battery get fully charged.

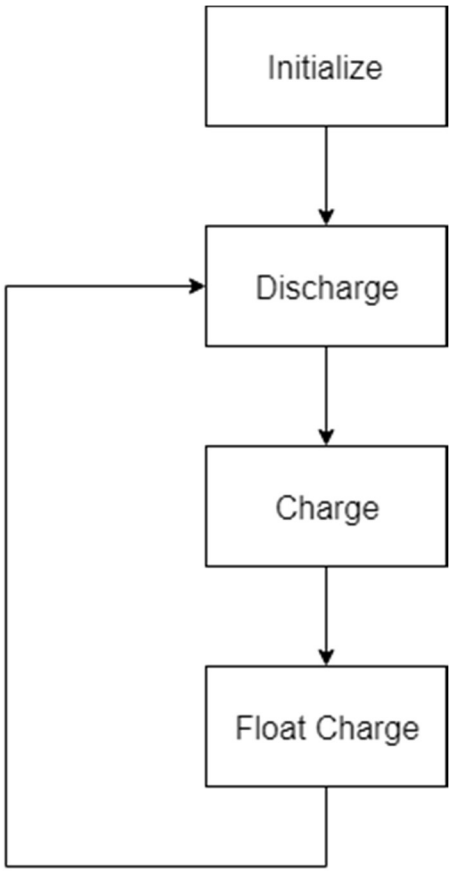

Figure 4.1 Defined Test Cycle

4.1.3. Float Charge

For lead acid battery or battery of any chemistry, self-discharge is unavoidable. The rate of self-discharge depends on many different factors. Modeling self-discharge current has been discussed in detailed in last chapter. In single battery or battery bank used for stationary applications, float charging method is used for compensating self-discharge. A voltage slightly higher than the battery fully charged voltage is applied to the battery, then the current supplied to the battery is closely monitored to prevent excessive over-charge that may lead to thermal runaway. Improved methods for self-discharge

compensation has been proposed [1], but the method mentioned above is still the most wide used.

The method of float charge is applied to battery or battery bank simulated in this study, float current is controlled within upper and lower thresholds to guarantee safe operation.

4.1.4. Choice of Battery Parameters

Parameter of 12v 300ah battery :		
Nominal Voltage		12V
Rated Capacity (10 hour rate)		300AH
Size (Length*Width*Height*Total Height)		520*270*228mm
Weight Approx		73KG
Capacity 25°C (77°F)	10 Hour Rate(9.0A)	300AH
	5 Hour Rate(14.4A)	240AH
	1 Hour Rate(54.0A)	120AH
	1.5 Hour Discharge To 10.5V	120A
Internal Resistance	Full Charged Battery at 25°C(77°F)	3.2mΩ
Capacity Affected By Temperature (10 Hour Rate)	40°C(104°F)	102%
	25°C(77°F)	100%
	0°C(32°F)	85%
	-15°C(5°F)	65%
Self-Discharge at 25°C (77°F)	Capacity after 3 Month Storage	91%
	Capacity after 6 Month Storage	82%
	Capacity after 12 Month Storage	64%
Terminal		COPPER /PB
	Voltage 14.40-14.80V Time 14~16h	
Float Charge (Constant Voltage)	Voltage 13.50-13.80V	
Warranty	3Years	
Color	Black, Grey	
Certificate	CE; ISO9001; MSDS	

Figure 4.2 Battery Parameters Used for Modeling

Figure 4.2 above is the base of parameter choice for this study, batteries of similar specifications are available from multiple suppliers.

Batteries of same specification will inevitably be different due to manufacturing tolerances. When used in single battery setup, these minor differences can usually be neglected as the parameters of all batteries fall within the acceptable margin. When used

in a battery bank setup, these differences will cause interactions between batteries that are usually neglected. To study these interactions and eventually battery bank failures, a proper range of these battery parameters needs to be given.

For the batteries used in this study, the parameters subjected to variation are battery initial capacity, charge and discharge resistances, base parasitic reaction current and its initial state of charge. All these parameters are assumed to follow normal distribution, their ranges are list below. These ranges can be varied in simulation to study the impact of variation in each parameter or conduct sensitivity study on these parameters.

$$Capacity_o \sim N(300,10)\ \ Ah \quad \text{Eq 4.1}$$

$$R_{c,base,o} \sim N(20,2)\ \ mOhm \quad \text{Eq 4.2}$$

$$R_{d,base,o} \sim N(5,0.25)\ \ mOhm \quad \text{Eq 4.3}$$

$$SOC \sim N(1,0.05) \quad \text{Eq 4.4}$$

4.1.5. Test Sequence and Logic

As in the model procedure, different resistances are attributed to charge and discharge path, one of the major issue in the algorithm is choosing which resistance to use for each specific battery in the battery bank.

A check sum is given to the bank and refreshed to equal the number of batteries in the bank at every time interval. Each battery in the bank is given a status flag. Battery in charging stage is given status -1, battery in discharging stage is given status 1. Initially, the status flag of each battery in the bank is given according to the operating stage of the bank, i.e. if the battery bank is in discharging stage, all batteries within the bank are assumed in discharge stage thus given status flag of 1. Current distribution is then

calculated based on these initial status flags, discharge and charge resistance are chosen accordingly for this purpose. Calculating current distribution is relatively simple by solving linear equations. After initial current distribution is calculated, current attributed to each current is multiplied with the battery's status flag. Since current coming out the battery is considered positive, if direction of current in the battery calculated is the same as indicated by its status flag, the result of the aforementioned multiplication will come out as positive, otherwise the result will come out as negative. If the result come out as positive, the check sum will be deducted by one, if the result come out as negative, the check sum remains the same. This process will be done iteratively for each battery in the bank, if the result of one battery come out as negative is status flag will be flipped. After this whole process, if the check sum is zero, then simulation can go to the next time step, otherwise check sum will be reinitiated to equal the number of batteries in the bank, current distribution will be recalculated based on the altered status flags of the batteries in the bank. This will be done repetitively, until the check sum is zero. In the next time step in simulation, status flag of each battery will be reassigned based on the operating status of the bank.

After current distribution is calculated, each battery is related to its corresponding current. The following procedure will be carried out in the same time step in simulation. State of charge of each battery is updated based on the current and its current capacity.

$$SOC(t) = SOC(t-1) - I(t) * dt/C(t) \qquad \text{Eq 4.5}$$

The amount of heat generated in this time step is also calculated using current and its resistance, resistance is chosen based on its status flag used in current distribution calculation.

$$Q(t) = I^2(t) * R(t) * dt + I(t) * dt * q \qquad \text{Eq 4.6}$$

q is the amount heat generated or absorbed by the electrochemical reactions involved per amount of charge transferred, q is calculated using thermodynamics data of the reactants separately for charge and discharge. The amount of heat dissipated is also calculated based on the battery temperature from last time step. Batteries with the bank are assumed thermally isolated, so heat dissipation only happens between the batteries through surface of battery case with atmosphere.

$$Q_{diss}(t) = c_1 * (T(t-1) - T_{am}) + c_2 * (T^4(t-1) - T_{am}^4) \qquad \text{Eq 4.7}$$

The first term in the above equation accounts for heat dissipation through convection, the second term accounts for heat dissipation through radiation. c_1 and c_2 are two constants related to the surface area of battery case and battery case material.

Change in battery temperature can thus be calculated.

$$T(t) = T(t-1) + (Q(t) - Q_{diss}(t))/C_T \qquad \text{Eq 4.8}$$

The current introduced by parasitic reactions is also calculated within this time step. Details concerning the above equations can be found in last chapter.

$$I_p = {}^{C}/_{100Ah} * I_{p,base} * \exp(r_1 * V_{oc} + r_2 * T_{batt} + r_3) \qquad \text{Eq 4.9}$$

Battery resistances, both charge and discharge, is updated accordingly with battery state of charge and battery temperature. The corresponding equations can be found in last chapter. The reason for updating both resistances is because battery status flag in the

next time step needs to be determined in the next round of current distribution calculated.

After the status of each battery is updated, the measured voltage of the battery bank is calculated with the voltage drop in each battery's resistance included. This voltage is then compared to two different thresholds. If the battery bank is in discharge stage and voltage of the battery bank is lower or equals to end of discharge voltage threshold, discharge is stopped. If battery voltage is higher or equals to end of charge voltage threshold, the battery bank remains in charging stage until the end of charge current threshold is met, then charge is stopped. Battery bank can either go through charge, discharge cycles directly or go through float charge stage in between. In this study, the length of float charge stage is predefined, battery bank goes to discharge stage after timer for float charge stage runs out. Float charge is not implemented at end of discharge, as it has been shown in multiple studies that keeping battery in discharge status in extended period of time has detrimental effects on it. Note current distribution in three stage is done in the same manner, but in discharge stage the total amount of current coming the battery bank is controlled, in charge stage, the charge voltage applied to the bank is controlled, in float charge stage, the voltage applied to the bank is controlled to limit the current going into the bank lies with the upper and lower threshold.

Battery parameter update is done at the end of each discharge stage. The amount of charge taken from each battery is summed up to calculate the depth of discharge of the

corresponding cycle, then battery capacity, charge and discharge resistance and base parasitic current are updated accordingly per the detailed equations in last chapter. Failure modes of the battery bank is evaluated different. Thermal failure is the most prominent failure mode that need the most attention, in simulation temperature of each battery is constantly updated and compared to a temperature threshold. If the temperature of any battery goes above the preset temperature threshold, thermal failure is reported and simulation is stopped.

Capacity failure is evaluated at the end of each discharge stage, the total amount of charge deliver by the bank can be calculated and compared to a capacity threshold. This is threshold is set to be 70% of the nominal capacity. Note, connecting batteries in series will not increase their combined charge capacity even through more energy can be delivered with the same amount of charge transferred, connecting batteries in series will increase their combined charge capacity as well as deliver more energy when compared to a single battery. The nominal capacity is determined by the number of strings in parallel. The battery used in this simulation is rated at 300Ah, so the nominal capacity of the bank is 300Ah multiplies the number of strings in parallel.

Power failure is evaluated by comparing the amount of power delivered by each single battery to an upper power threshold. Power of each battery is calculated by multiplying its voltage with its corresponding current. Power failure is reported whenever a battery's power goes above its power threshold. Power failure is essentially set up a precaution measure, if power failure is detected that usually means there is fault with the circuit the battery bank connected to or fault with the inter battery connections in the battery bank.

As failure of inter battery connection and failure of load and charging circuit is not consider, it can be predicted that this failure mode is mostly unlikely to be observed in simulation.

Charge failure is detected by setting up a timer for charge stage, if battery bank fails to reach end of charge status before the time preset for charging runs out, charge failure is reported.

These details are included in the flow charts in Figure 4.3 to Figure 4.6.

4.1.6. Choice of Cycle Parameters

End of discharge voltage is set to be 10 V multiplies the number of batteries in series. Note, this is lower than the zero state of charge voltage, 10.5V. This choice is made based on the overvoltage caused by discharge resistance.

End of charge voltage is set to be 15 V multiplies the number of batteries in series, end of charge current is set to 0.5 A multiplies the number of battery strings in parallel.

Temperature threshold for thermal failure is set to be 400K for each battery.

Power threshold for power failure is set to be 1000W for each battery.

Discharge current is set to be 15A multiplies the number of battery strings in series.

Charge voltage is set to be 15V multiplies the number of batteries in series, a current limit of 45A per string is also set.

Float charge current is limited to between 0.2 A and 0.01 A per string to compensate self-discharge.

Ambient temperature is set be 300K.

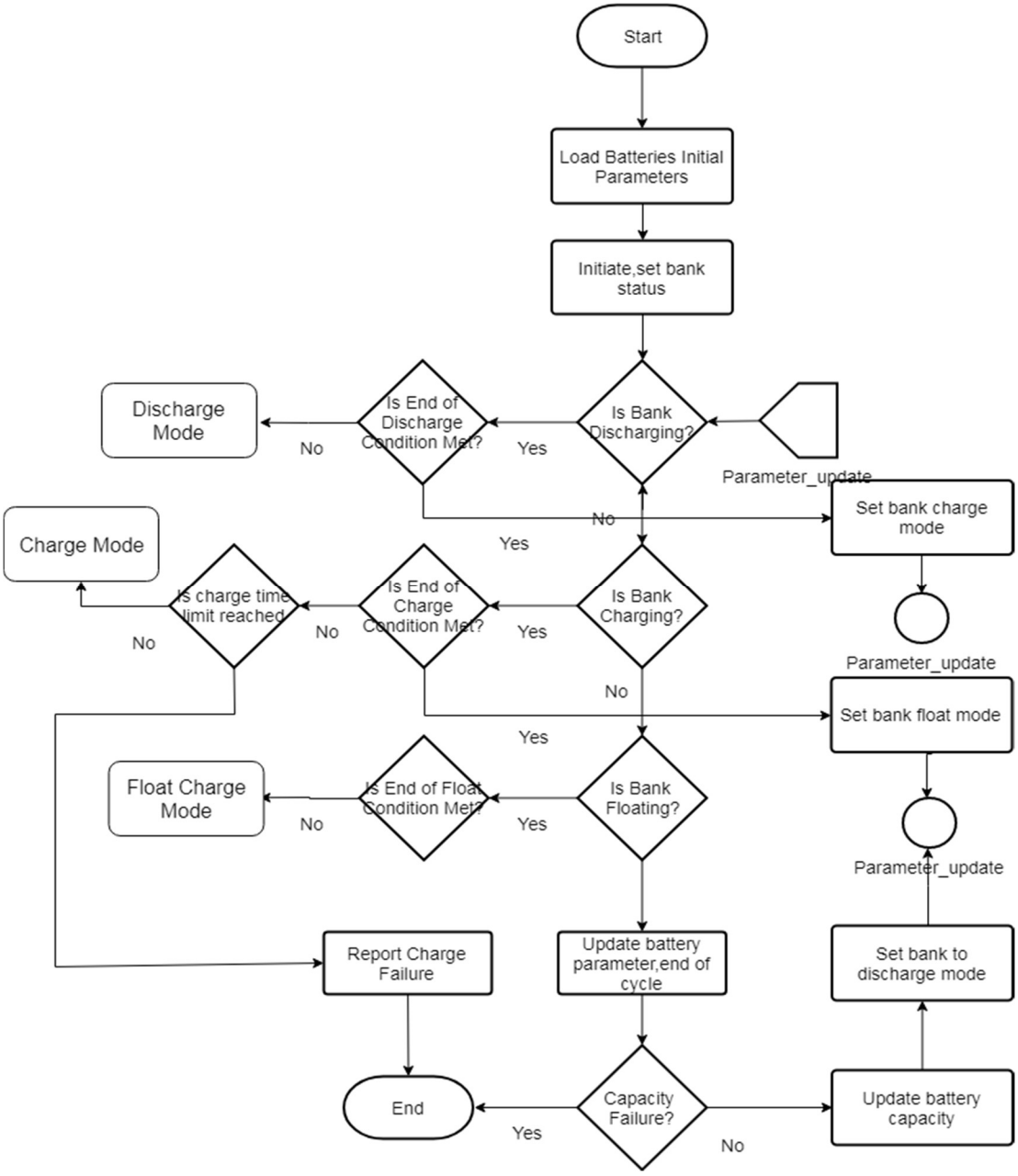

Figure 4.3 Flow Chart Part 1

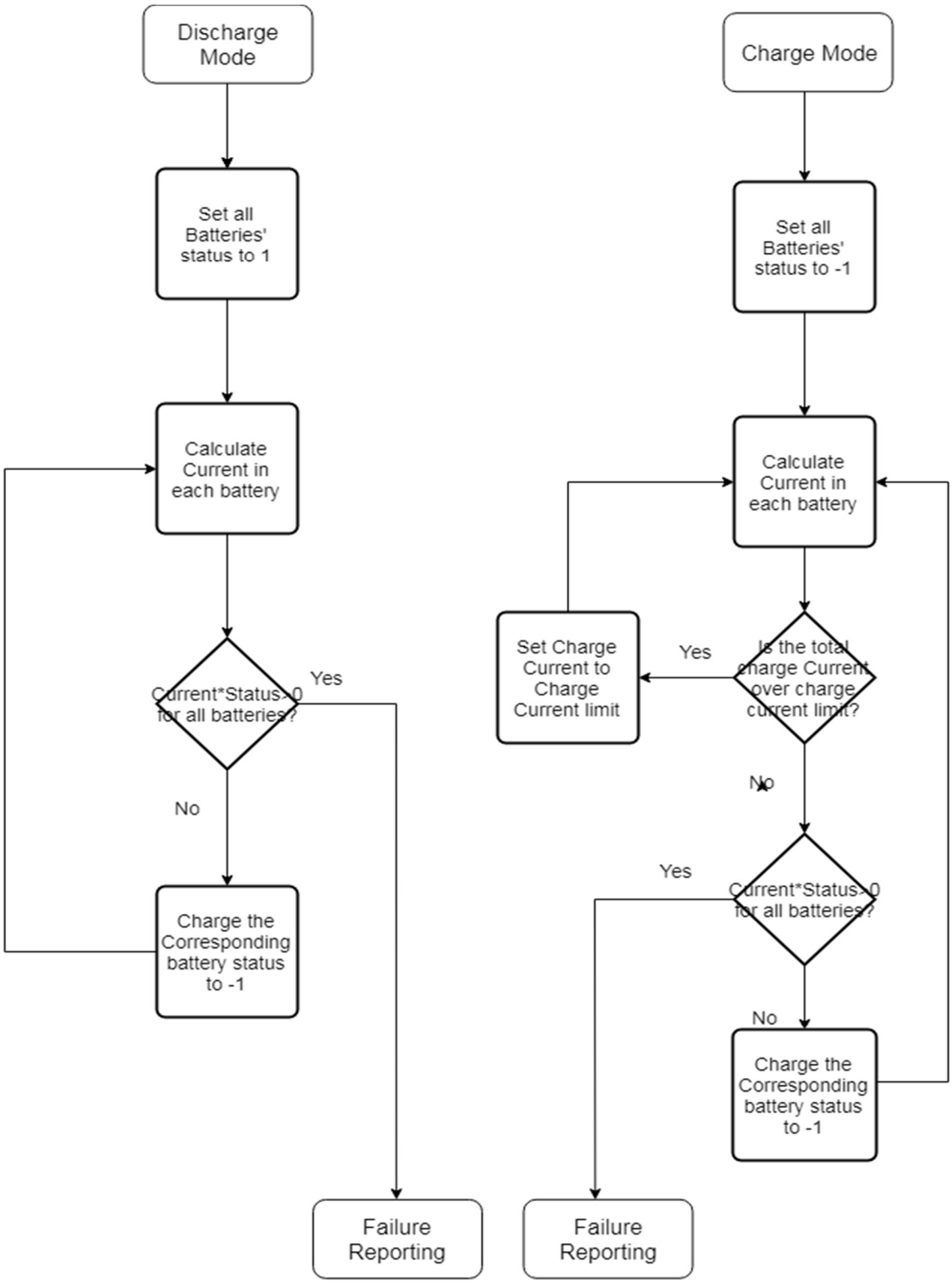

Figure 4.4 Flow Chart Part 2

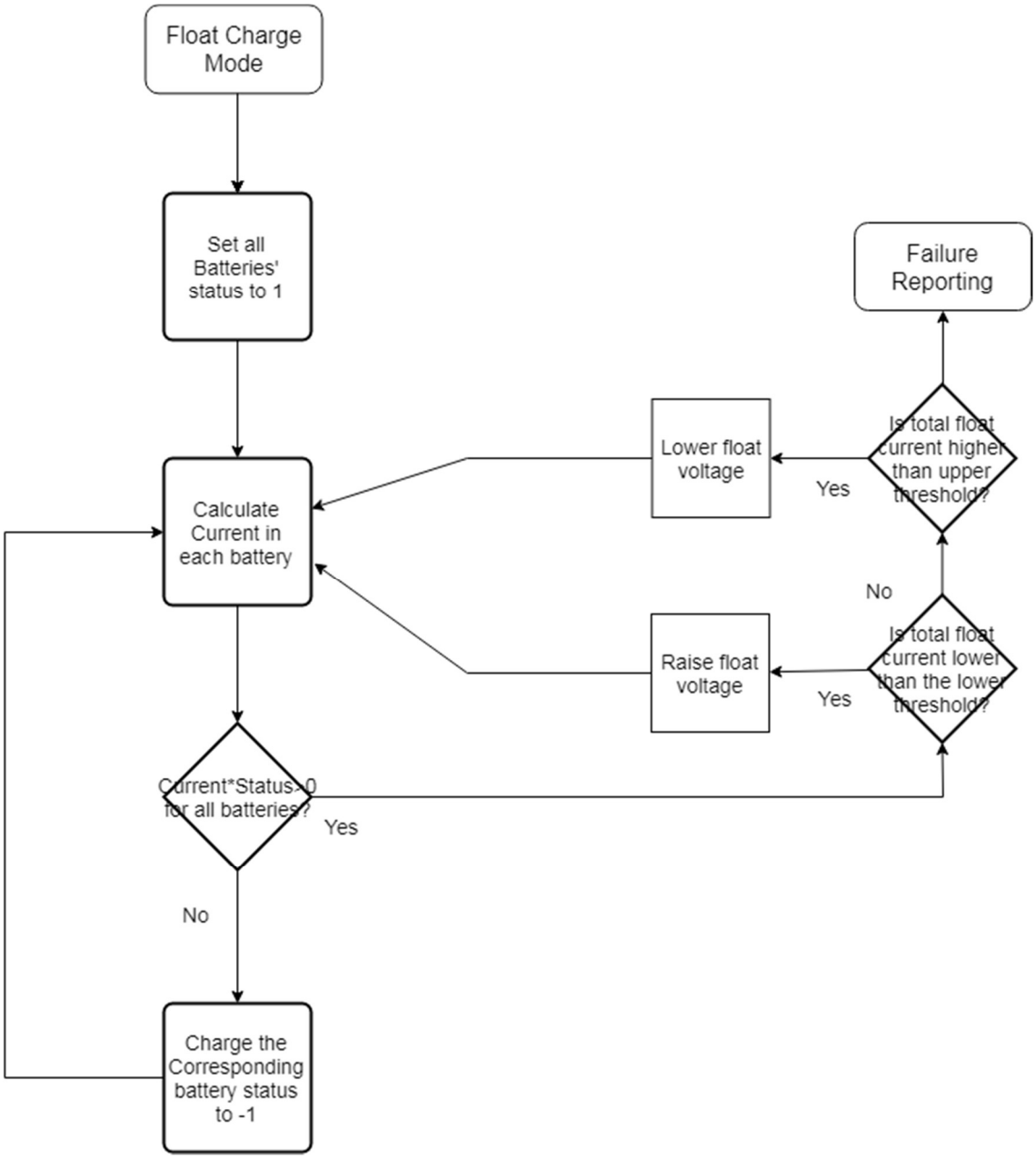

Figure 4.5 Flow Chart Part 3

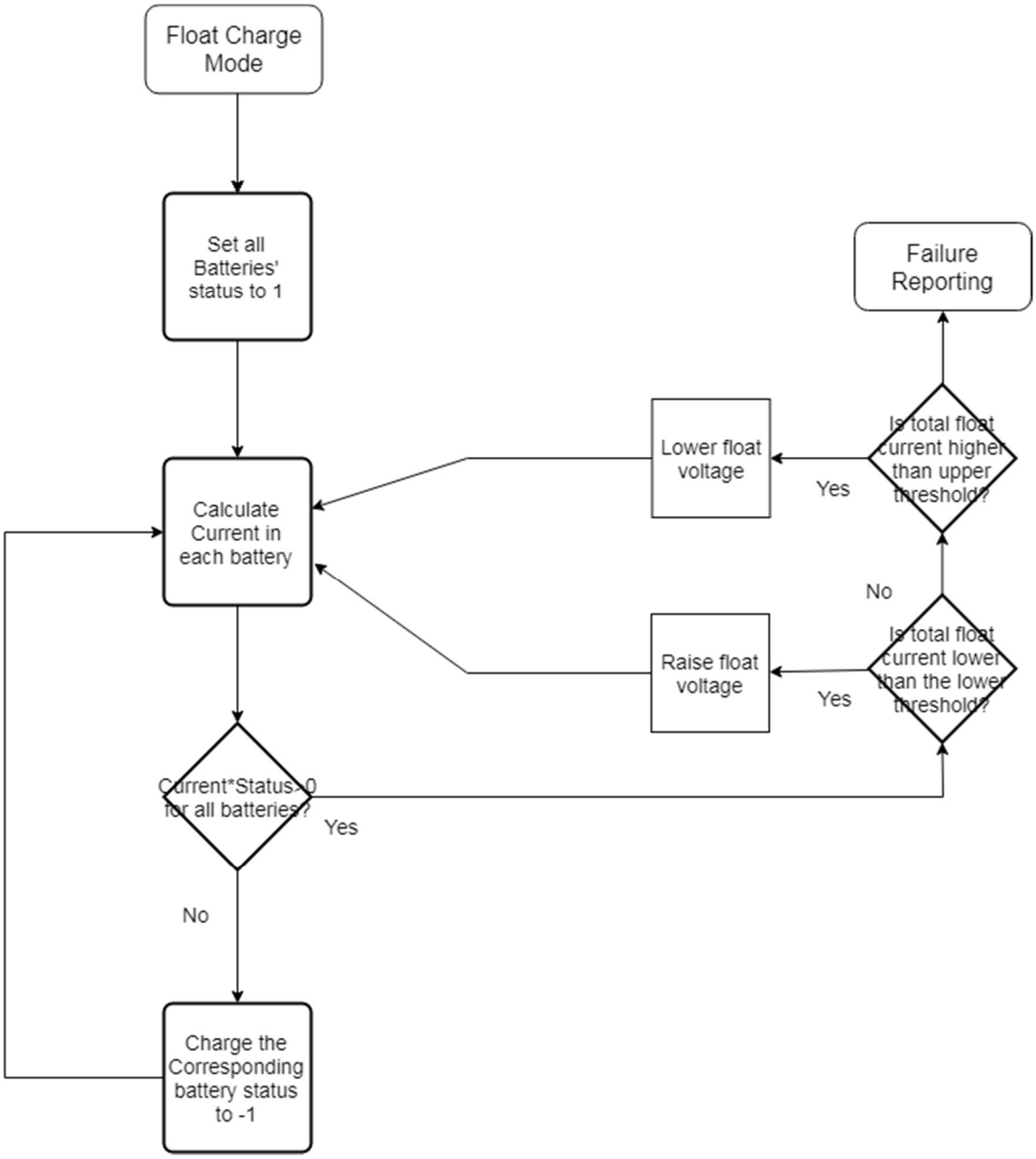

Figure 4.6 Flow Chart Part 3

4.2. Single Battery Testing

With the aforementioned algorithm, the first step is to test single battery as a baseline. Testing is done to a large number of batteries with randomly generated parameters with the distributions given above. Testing procedure is shown Figure 4.7 below. Testing is done to randomly generated single batteries in batches of 100, at the end of each batch average number of cycles to failure as well as its standard deviation to failure is calculated based all the accumulated test results. Test will be terminated either the max batch number is reached, or the difference between 5 consecutive average number of cycles to failure and its standard deviation is less than 0.5% of the observed values. This is done to ensure the statistic characteristics of the subject is observed following loose law of large numbers.

A single battery with all parameters at reference values are tested as a benchmark. Under normal operating condition specified above single battery fails at 720 cycles under capacity failure.

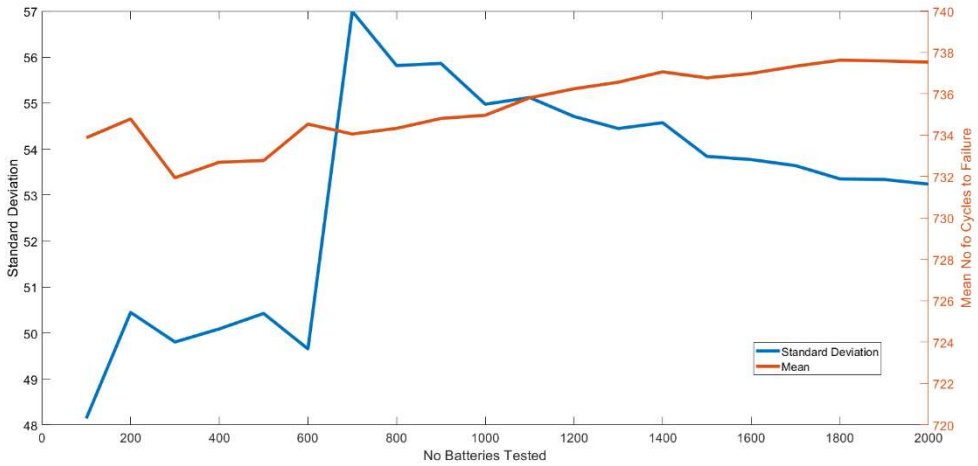

Figure 4.7 Test Procedure for Statistical Characteristics

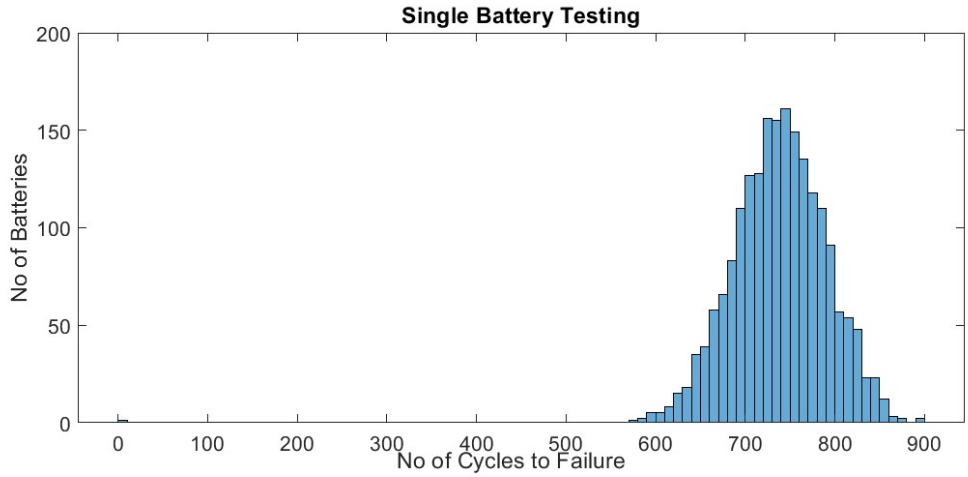

Figure 4.8 Histogram of Number of Cycles to Failure for Single Battery, Float Charge Disabled

As can been from Figure 4.8, 20 batches, a total number of 2000 batteries, were tested when the condition for end of testing is met. Of the 2000 batteries tested, 1999 reported capacity failure. Only 1 battery reported charge failure at the end of first cycle. No thermal failure is reported.

This is supported by varies literature on single battery failure study. Only extreme operating conditions trigger thermal failure. Note, float charge is not implemented for single battery, as no balancing is needed for single battery setup.

Single battery model is then test with varying depth of discharge, this is achieved by adjusting end of discharge voltage. The threshold of capacity failure is also adjusted accordingly. Figure 4.9 summaries these tests, as can be seen from the data presented, the average number of cycles to failure is extended with lower depth of discharge, this conclusion agrees the data provided by multiple battery manufactures. Of all the batteries tested, no thermal failure is reported.

Single battery model is also tested with different load current profile, note low power threshold is disabled for this test. At higher load current, battery reports thermal failure. The result is shown in Figure 4.10.

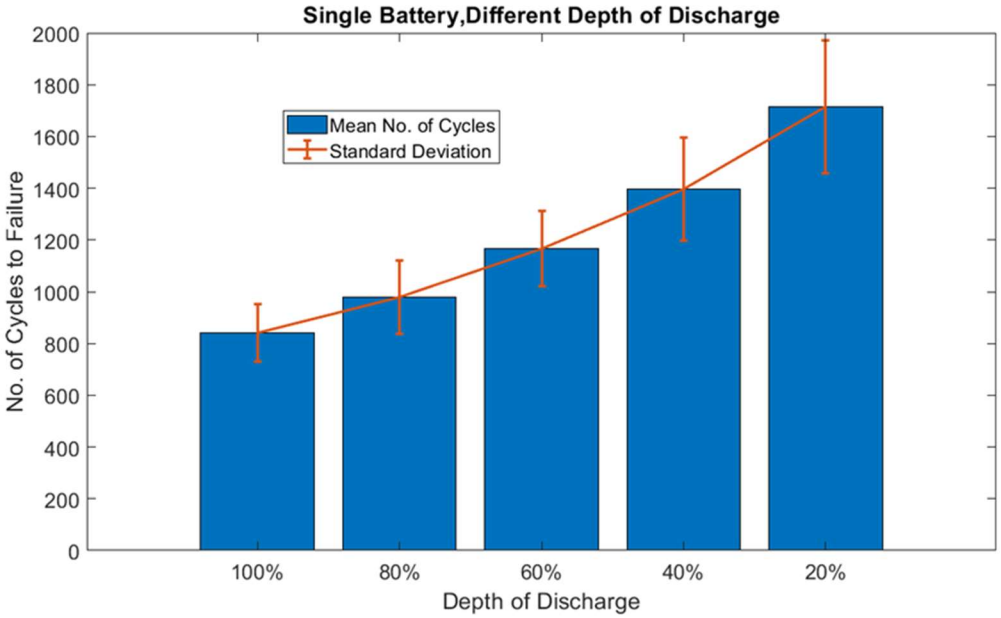

Figure 4.9 Single Battery Test with Varying Depth of Discharge

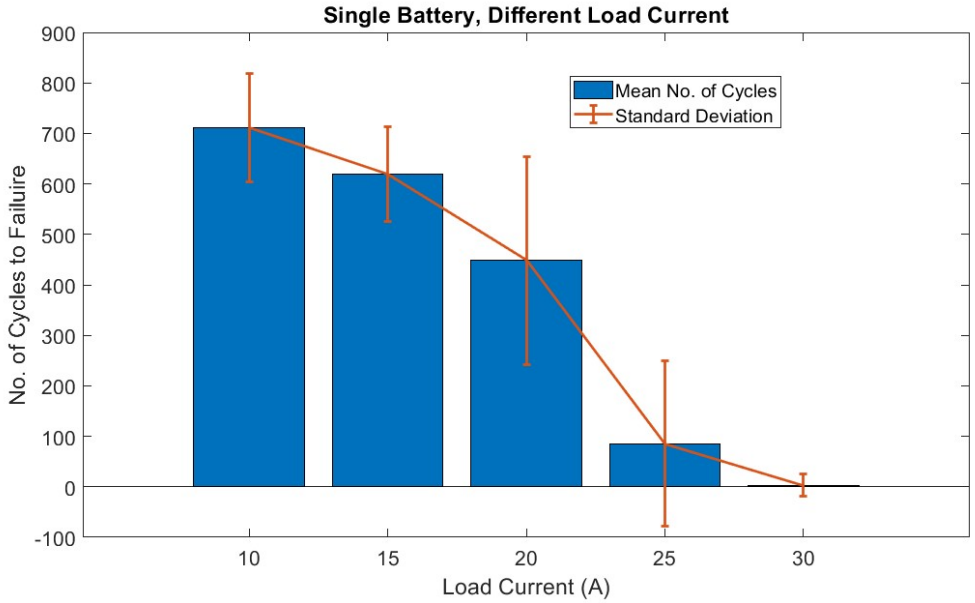

Figure 4.10 Single Battery Test with Varying Load Current

Single battery model is tested with different ambient temperature, thermal failures are starting to show at higher ambient temperature. The result is summaries in Figure 4.11.

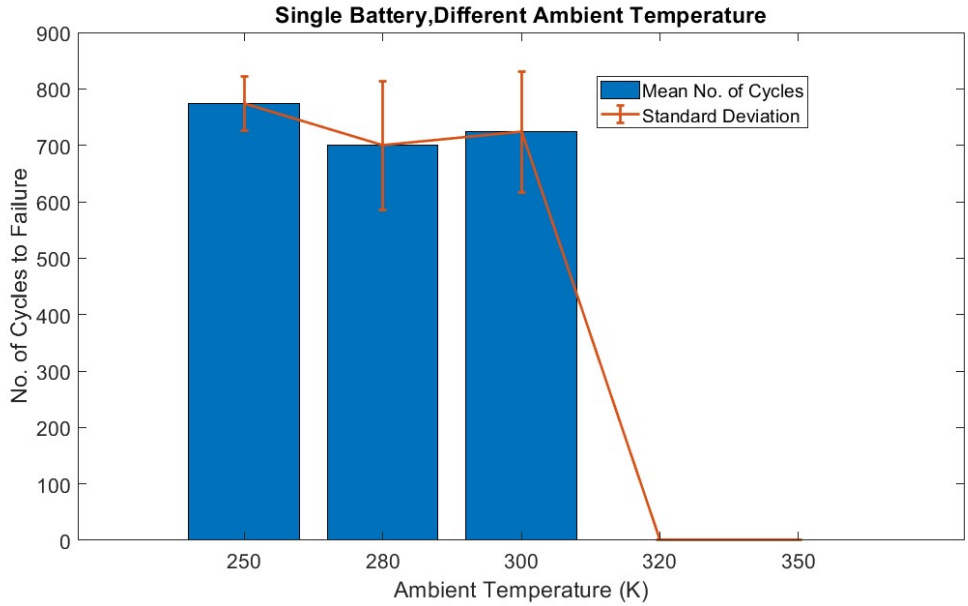

Figure 4.11 Single Battery Test with Varying Ambient Temperature

The effect of float charge on single battery is tested separately, all operating conditions are set to nominal.

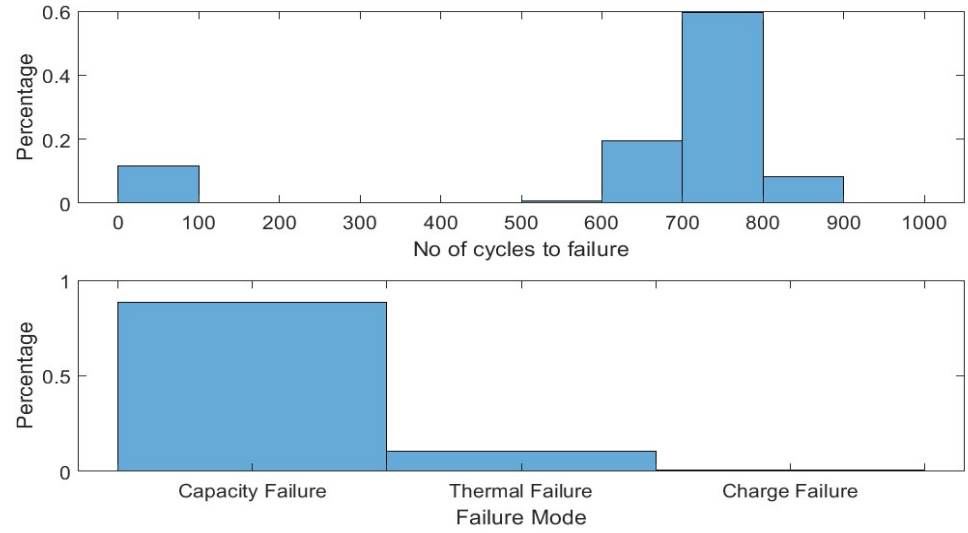

Figure 4.12 Single Battery Test with Float Charge Enabled

As can be seen from Figure 4.12, with float charge mode enabled, thermal failures account for 10 percent of the failures reported. This is a major shift in failure mode. Similar results have been reported in literature.

4.3. Battery Bank Testing

Battery banks are connected in a passive manner, meaning there is no active switch in any inter battery connections. There are studies on implementing active battery inter connection for battery active balance, but that introduces more sources of possible failure and is not wide adopted in the industry, so active connections are not consider in this study.

4.3.1. Effect of Series and Parallel Connection

The first question that needs to be addressed is the difference between choices of connecting batteries in series or in parallel if power rating of the battery bank is given. To show case the differences of series and parallel connections, the simplest scenarios are tested, batteries are connected in a single series string from one battery to a hundred batteries for the series case; batteries are connect in a single parallel column from one battery to a hundred batteries for the parallel case. Both are tested with float charge disabled and enabled. The result is shown in the Figure 4.13 to Figure 4.16. The bars in the figure are mean number of cycles to failure for each specific bank topology with its standard deviation overlaying on top in orange error bars.

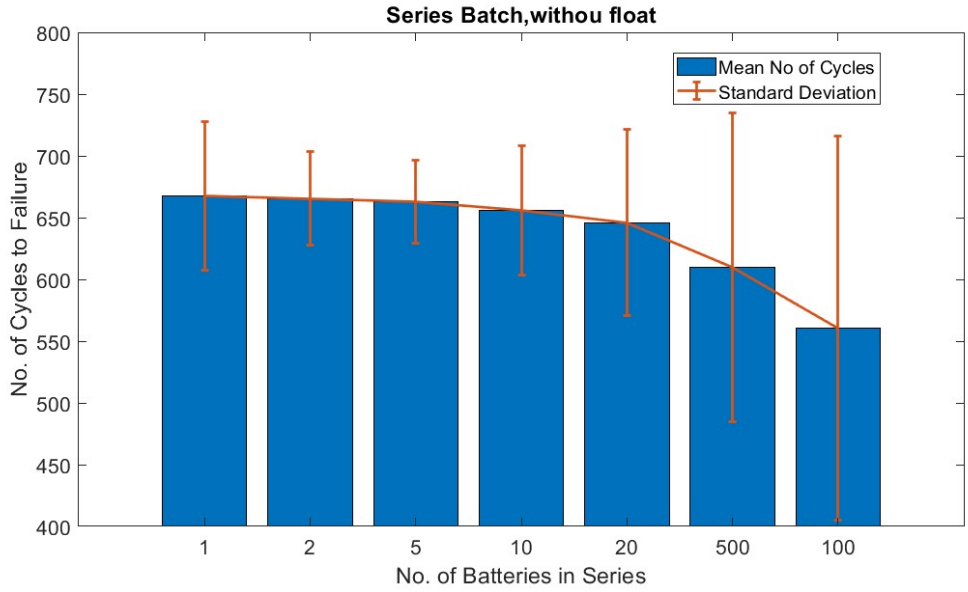

Figure 4.13 Series Battery Connections with Float Charge Disabled

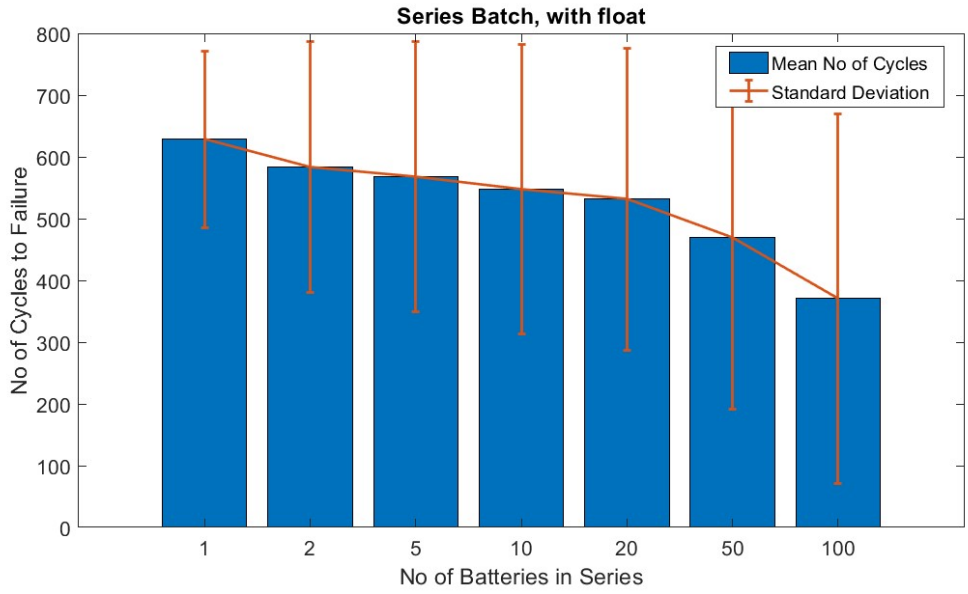

Figure 4.14 Series Battery Connections with Float Charge Enabled

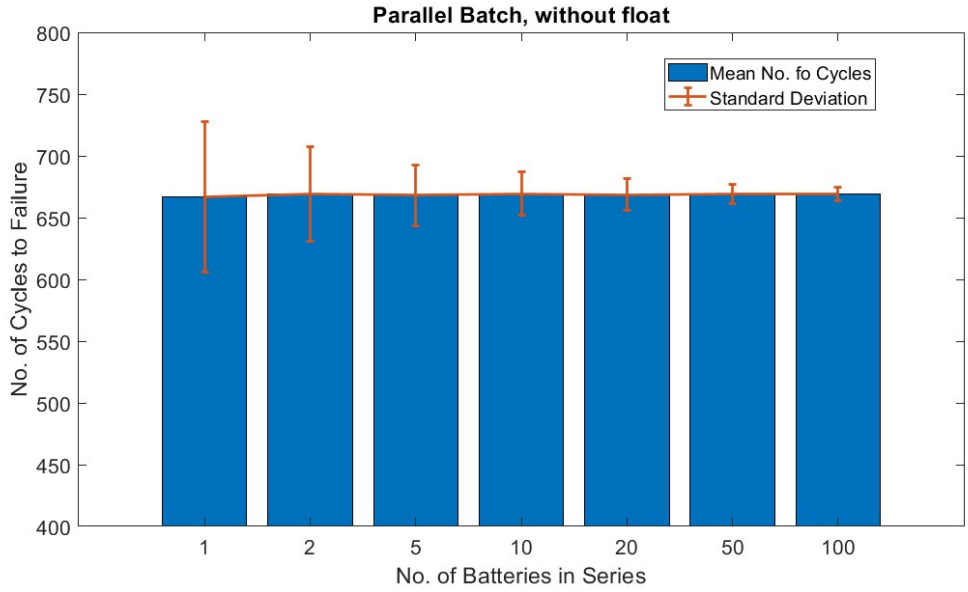

Figure 4.15 Parallel Battery Connections with Float Charge Disabled

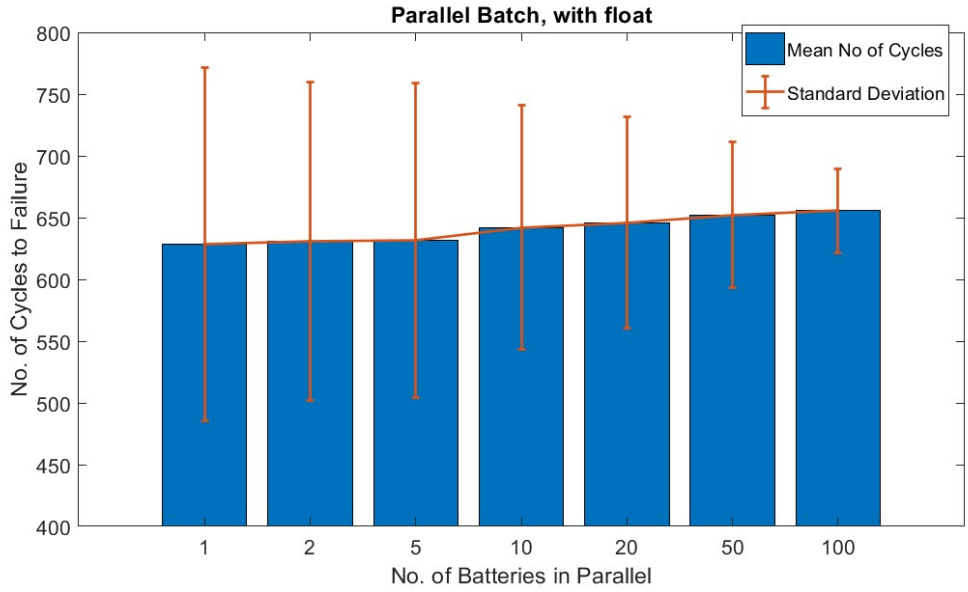

Figure 4.16 Parallel Battery Connections with Float Charge Enabled

It can be seen from above, that connecting batteries in series leads to shorter expected life span; connecting batteries in parallel has little effect on the mean number of cycles to failure. The inclusion of float charge has very little effect on series topologies; but

adding float charge to parallel topologies greatly increases the standard deviation on mean number of cycles to failure, i.e. increase uncertainty.

The desired purpose of float charge is twofold, maintain battery bank at full state of charge for an extended period of time by compensating self-discharge current, balance batteries in the bank to achieve even state of charge. In series case, battery balancing can only be done by overcharge every battery in the string thus causing other consequences, in batteries reach full state charge earlier when compared to others: water loss and temperature rise. If high temperature threshold is reached, then failures will be reported prematurely as can be seen from the decreased mean number of cycles to failure. The only solution to this problem is to introduce extra means of active battery balancing and is beyond the scope of this research. In parallel case, balancing of batteries can be achieved passively. In float charge, the distribution of float charge current cannot be controlled and may lead to other consequences as seen can be seen from the increased standard deviation in mean number of cycles to failure.

The result of the above test actually verifies the long existing ‘mythical’ belief of parallel connecting batteries is better than series connecting batteries.

4.3.2. Effect of Battery Bank Size

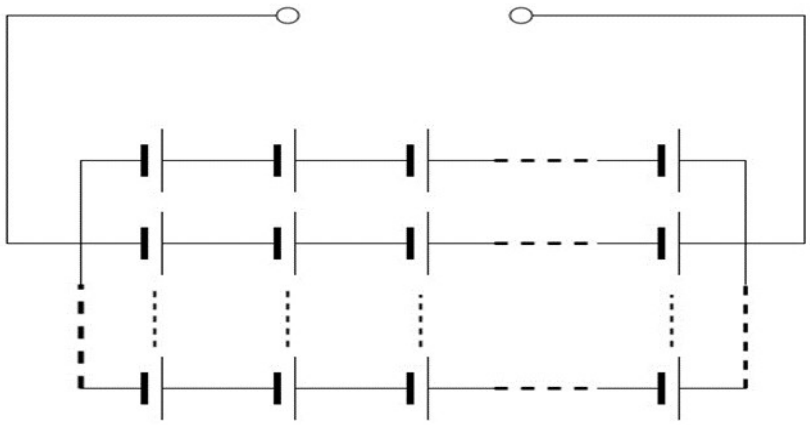

Figure 4.17 Typical Battery Bank with No Active Connections

Next question is the effect battery bank size on its average life span and failure mode. Tests are ran on battery banks with symmetrical topology, i.e. 2*2, 4*4 etc. Comparison is made on cases with float charge mode enabled and disabled. In cases where float charge is disabled, no interval between the end of charge and start of discharge is attributed. The corresponding results are shown in Figure 4.18 below.

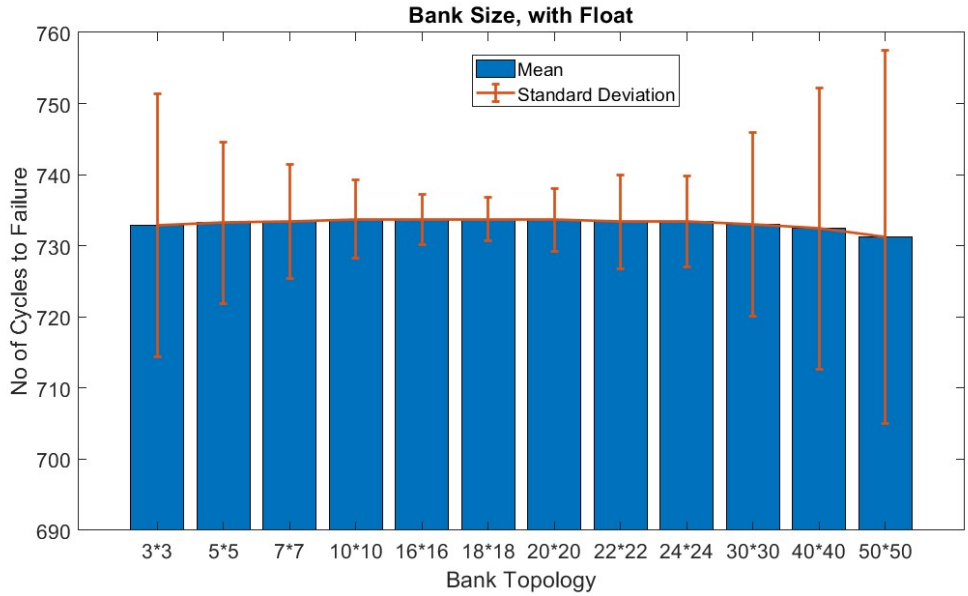

Figure 4.18 Effect of Battery Bank Size with Float Charge Disabled

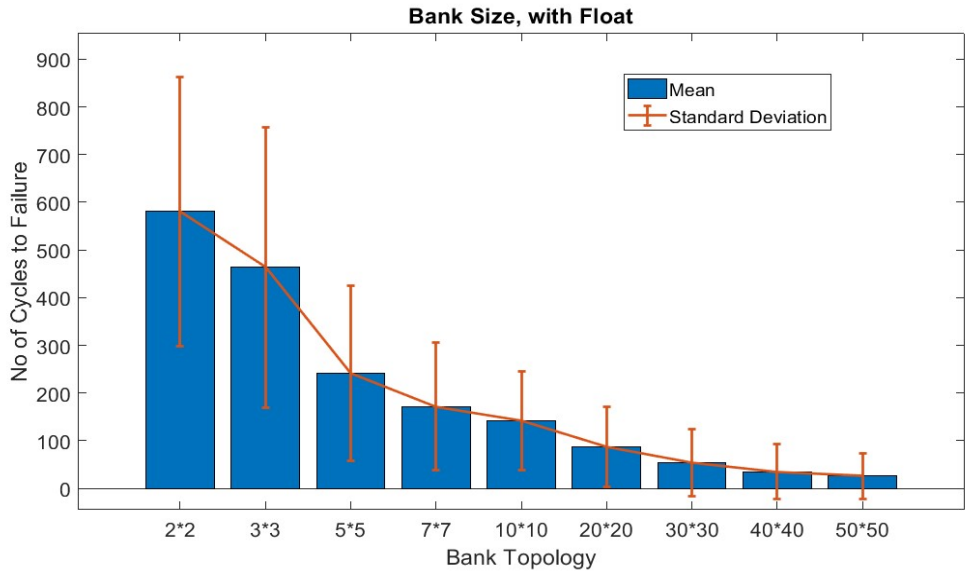

Figure 4.19 Effect of Battery Bank Size with Float Charge Enabled

In case where float charge is disabled, battery banks is insensitive to bank size, mean number of cycles of failure remain almost constant. The standard deviation takes an interesting path, it decreases first, reaches minimum at bank of 18*18 and then starts increasing again. The reasoning behind this phenomenon is the competing factors of

self-balancing of bank and randomness distribution of parameters of individual batteries. From reliability point of view, this offers the possibility of optimal sizing of battery bank. If the bank of such size and topology cannot meet the requirement, multiple banks can be used instead of a single bank.

In cases where float charge is enabled, shown in Figure 4.19,battery banks are more susceptible to thermal failures. The effect of such introduction is very prominent. Larger banks are affected immensely. This might raise the question of the adaptation of float charge, specific conventional float charge method used here. Similar concerns have been raised in literature and new methods for float charge have been proposed[61].

Simulation result agrees with the observations in real world scenarios where most thermal failures are reported when battery bank is in float charge mode. The conclusion from those reports, however, is ambiguous as battery banks are put on float charge mode for most of their life span. It is inconclusive whether failures are caused by float charge or failures are just more frequently reported due to the percentage of time on float charge.

In this research, it can be clearly identified that float charge is the cause of increase in chance of thermal failure.

4.3.3. Effect of Topology with Fixed Number of Batteries

With number of batteries used in the battery bank given, different available topologies are tested and compared in this section. The test is ran on a hundred batteries. All nine available topologies are tested, i.e. 1*100, 2*50, 4*25, 5*200, 10*10, 20*5, 25*4, 50*2

and 100*1. Note, float charge is disable for these tests. Result is shown Figure 4.20 below.

As can be seen above, mean number of cycles of failure and its standard deviation are insensitive to battery bank topology.

One notable shift in failure mode is observed in battery bank simulations. For single battery case, a very low percentage of the failure is charge failure and no thermal failure is reported under normal operating conditions. For battery bank case, no charge failure is reported in all the tests and thermal failure is the major failure mode besides capacity failure.

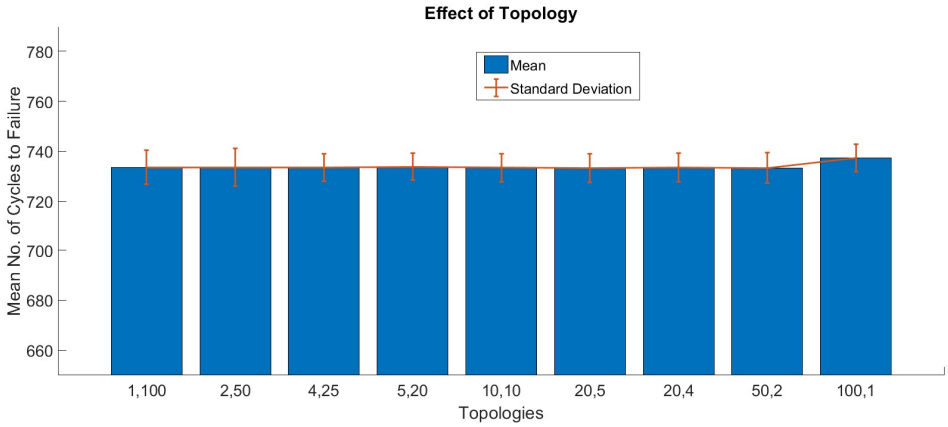

Figure 4.20 Effect of Battery Bank Topology on Fixed Number of Batteries with Float Charge Disabled

4.3.4. Discussion on Failure Mode

The absence of charge failure can be easily explained, the mismatch of battery parameters can lead to uneven charge of batteries, and end of charge condition can be reached for the bank without fully charge every battery in the bank. This problem can be

partially solved by float charge, but as can be seen from the above discussion, the introduction of float charge will cause more premature failures.

4.3.5. Introduction of Improved Battery Bank Topology

An improve battery bank topology is tested in this section, this topology is referred to as meshed topology for the inclusion of extra inter-string connections as can be seem in the figure below. Meshed topology helps balance between batteries better in all cases.

The same tests on the conventional battery banks are ran battery banks with mesh topologies, the corresponding result can be seen in Figure 4.21 below. Mesh topology solves the problem of increased chance of thermal failure with float charge. Note, for effect of battery bank size, meshed bank is limited to 20*20 as larger banks requires extra resource for simulation.

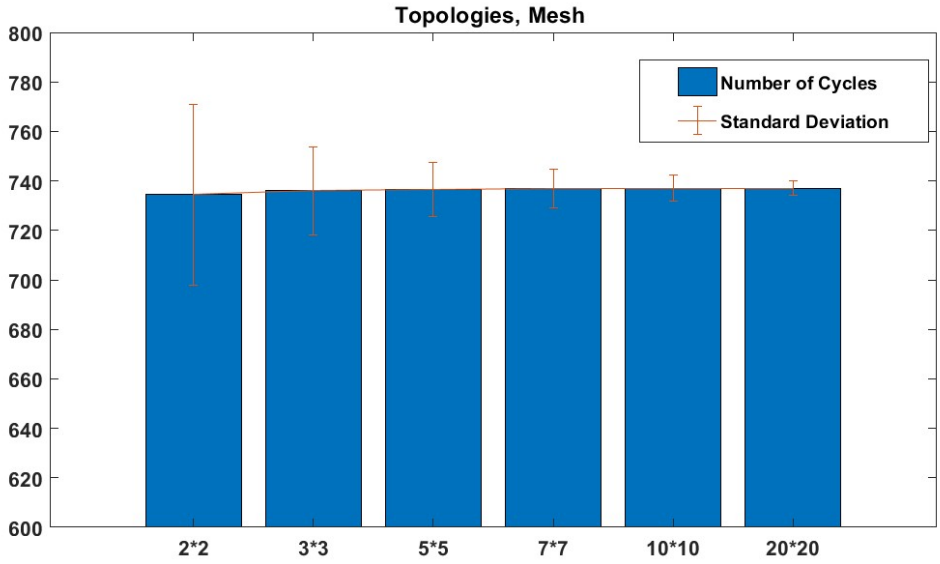

Figure 4.21 Effect of Battery Bank Size on Meshed Topology with Float Charge Disabled

The above result is achieved by introducing extra inter-string passive connections between every battery. Battery bank with more sparse inter-string connections is also tested. A battery bank of 10*10 is chosen with two different mesh intervals, 2 and 5, i.e. inter-string connection is put after 2 or 5 batteries. The result is shown in Figure 4.22 below. To test the effectiveness of sparse mesh connections, these test are done with float charge enabled.

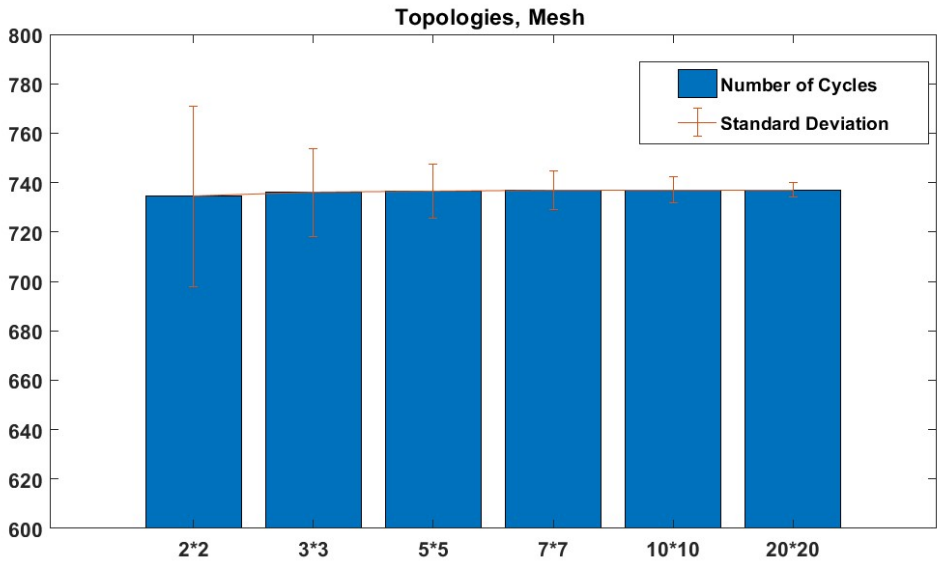

Figure 4.22 Effect of Battery Bank Size on Meshed Topology with Float Charge Disabled

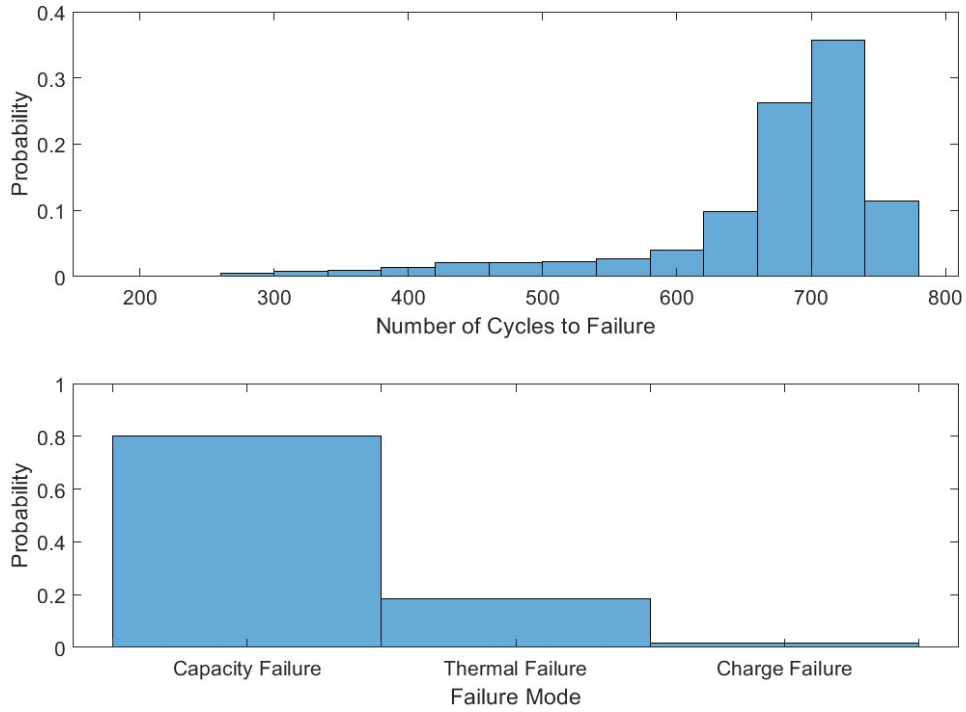

Figure 4.23 Meshed Topology with Sparse 2 Connections, Float Charge Enabled

As shown in Figure 4.23, sparse connection is not as effective as 'dense' meshed connections. In the case of sparse 2 connection, majority of battery banks still reports capacity failure, with a very low percentage of charge failure, about 20% thermal failure is unacceptable for bank operation. In the case of sparse 5 connection, shown in Figure 2.24, majority of battery bank reports thermal failure which deems this connection scheme completely ineffective even with great improvement when compared to conventional topology. The result of 10*10 battery bank with conventional topology is shown in Figure 4.26 as a reference for comparison. The result of 'dense' meshed bank is shown is shown in Figure 4.25.

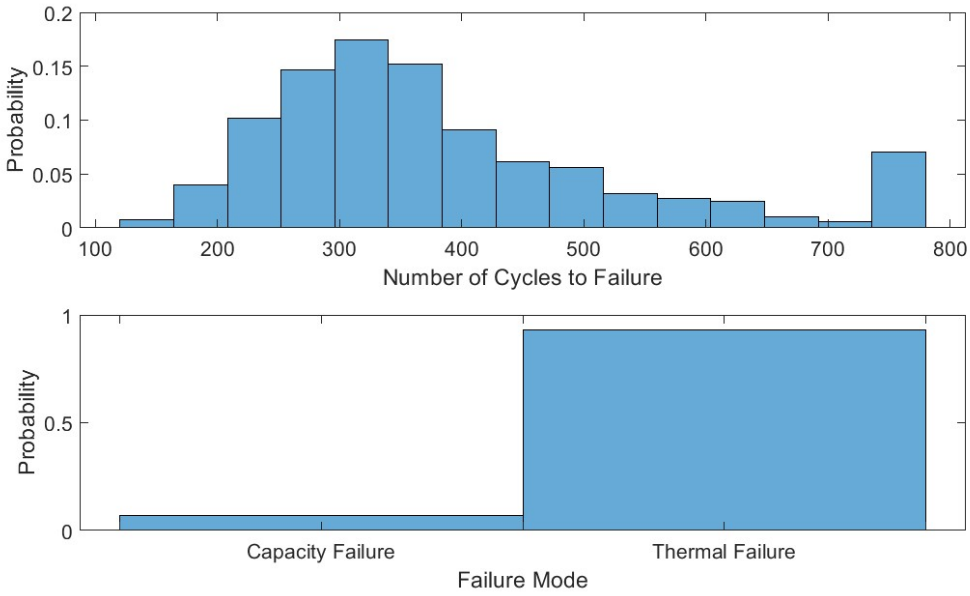

Figure 4.24 Meshed Topology with Sparse 5 Connections, Float Charge Enabled

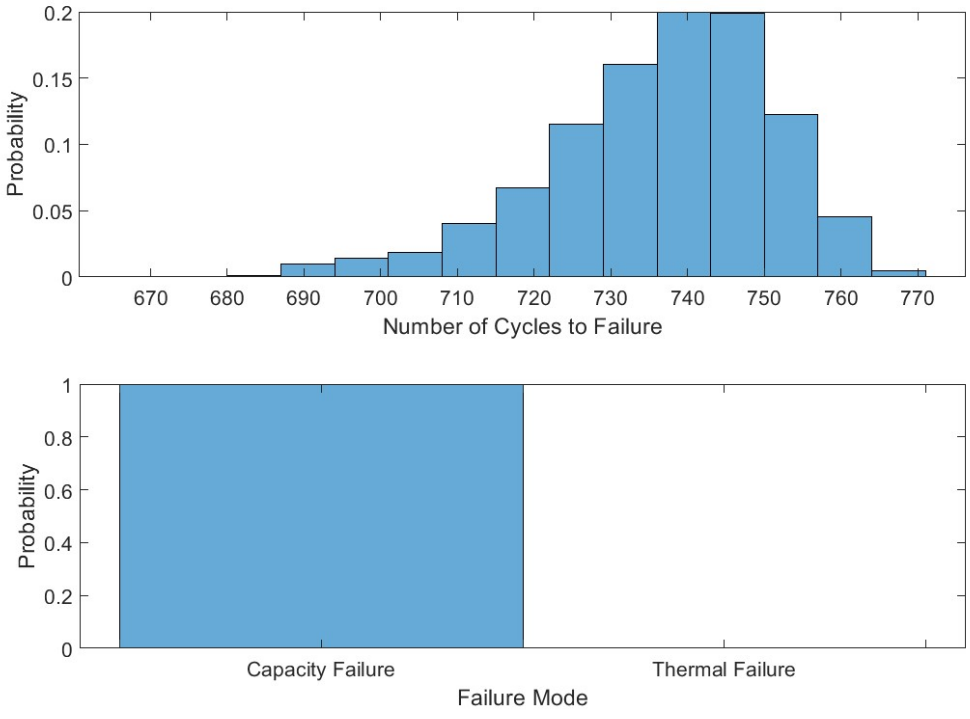

Figure 4.25 Meshed Topology, Float Charge Enabled

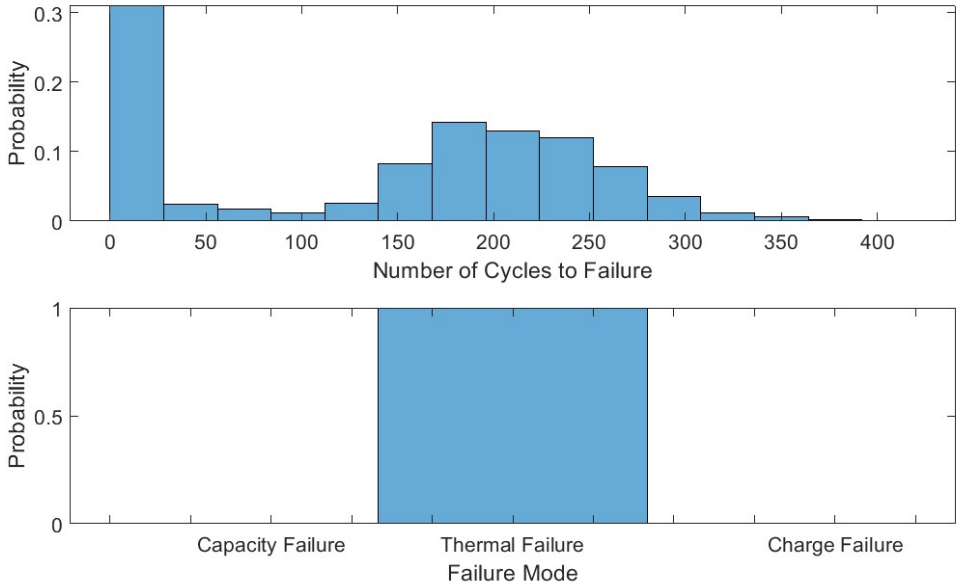

Figure 4.26 Conventional Topology, Float Charge Enabled

The current rating of the inter-string connection is also of great interest, since it is a matter of practical value, if the current rating of these connections is only fractional of the normal connections, the introduction of these extra wiring is more justifiable. To evaluate the current rating, the same batch based statistical testing is ran again with the maximum current going through meshed connections recorded for every test. Out of the 1,600 test of 'dense' mesh connections, the maximum current is recorded as 223.16A, with a 97 percentile of 145.82A; out of the 2,300 test of sparse 2 connections, the maximum current is recorded as 161.43A, with a 97 percentile of 113.96A; out of the 1,600 test of sparse 5 connections, the maximum current is recorded as 300.97A, with a 97 percentile of 93.48A. The maximum current rate of the inter string connection is thus 1C, i.e. 300A, depends on the rating on normal connection, this result does not show major saving in wiring.

Further advantage of the meshed topology is shown in the next section.

4.4. Step Failure Testing

The effect of single point failure in battery bank is studied in a comparative manner. Single step failures are introduced in both battery bank of conventional and meshed topologies. Two different categories of single point step failures are introduced, namely capacity and state of charge. The reason for such failures are not specified, and the same methodology can be extended to multi-point failure with single or mixed categories of failure.

Single point step failure is tested on battery bank of 10*10, a thousand set of parameters are randomly generated and used for base of comparison. For state of charge category, four different step sizes are chosen, 20%, 30%, 50% and 100%. For capacity category, three different step sizes are chosen, 50Ah, 100Ah and 150Ah. The locations of these step failures within the bank are randomly generated in simulation.

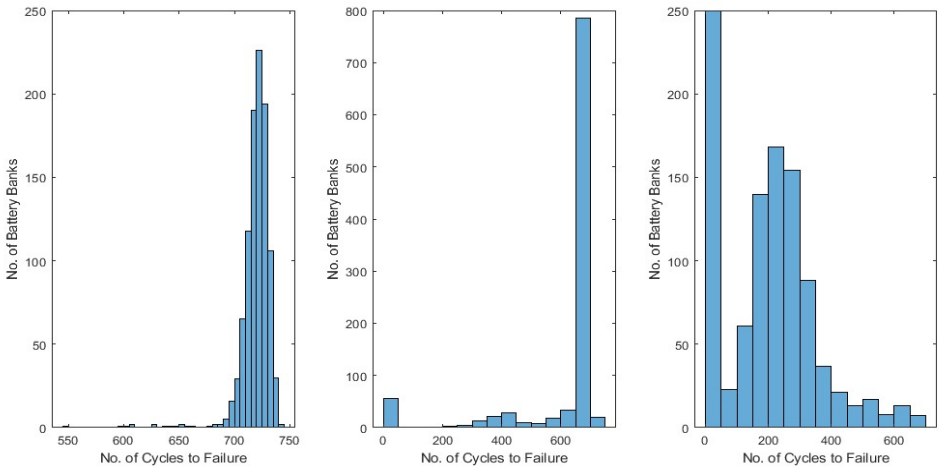

Figure 4.27 Capacity Step Failure, Number of Cycles to Failure, Conventional Topology

From Figure 4.27 to Figure 4.34, it is shown that both battery banks of conventional and meshed topologies are relative insensitive to smaller step failures, 50Ah step for capacity, 20% and 30% in SOC steps; as the step size increases, different topologies behaves very differently. Meshed topology is insensitive to all the step failures given, all banks are reported as capacity failure with very minor effect on the number of cycles to failure, conventional topology shows increase in percentage of thermal failure and eventually reports majority of the failure as thermal failures. No charge failure is reported in any of these test, float charge is disable in all these test.

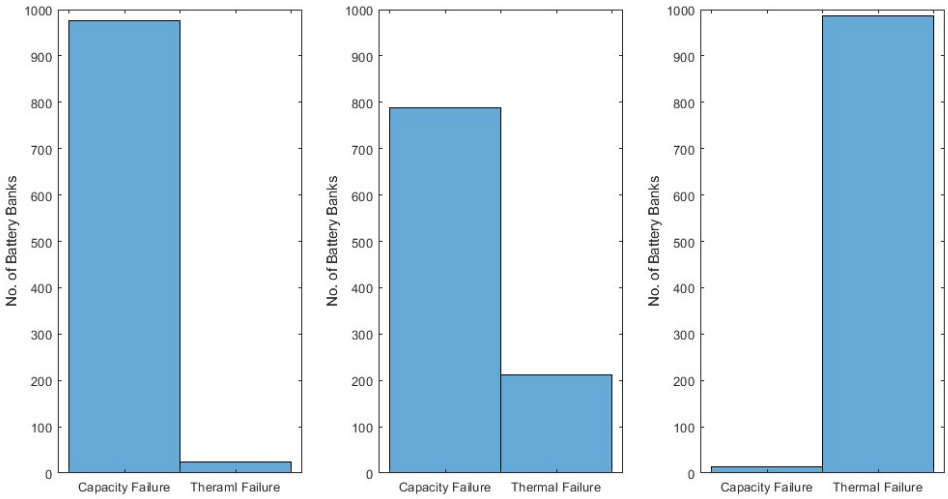

Figure 4.28 Capacity Step Failure, Failure Mode, Conventional Topology

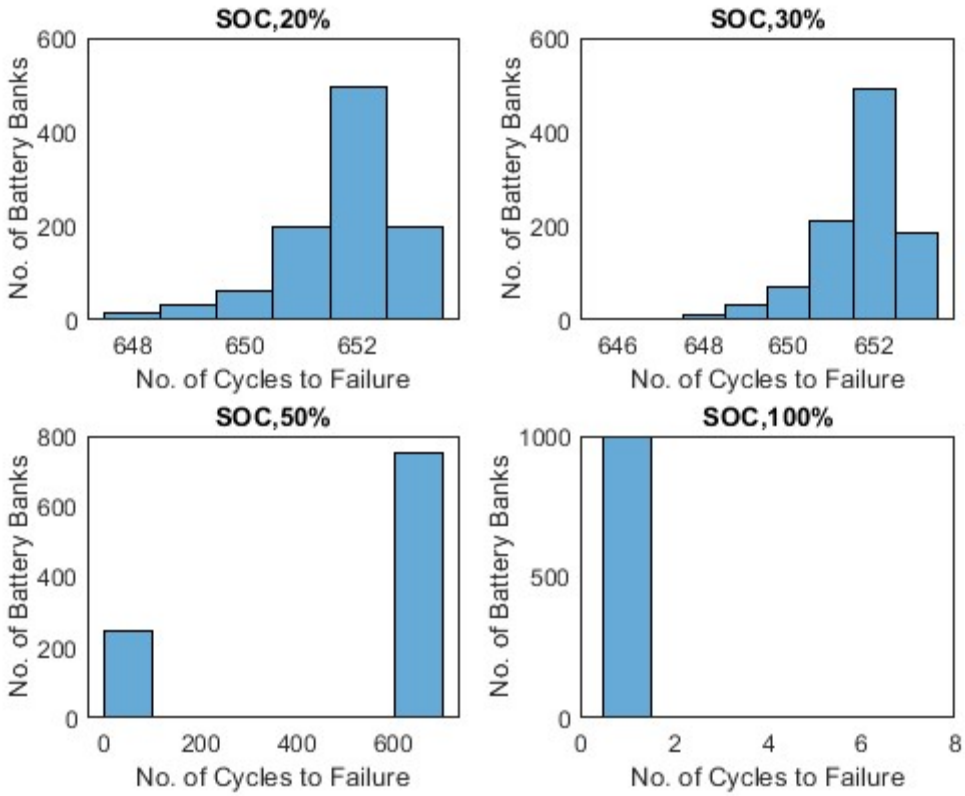

Figure 4.29 SOC Step Failure, Number of Cycles to Failure, Conventional Topology

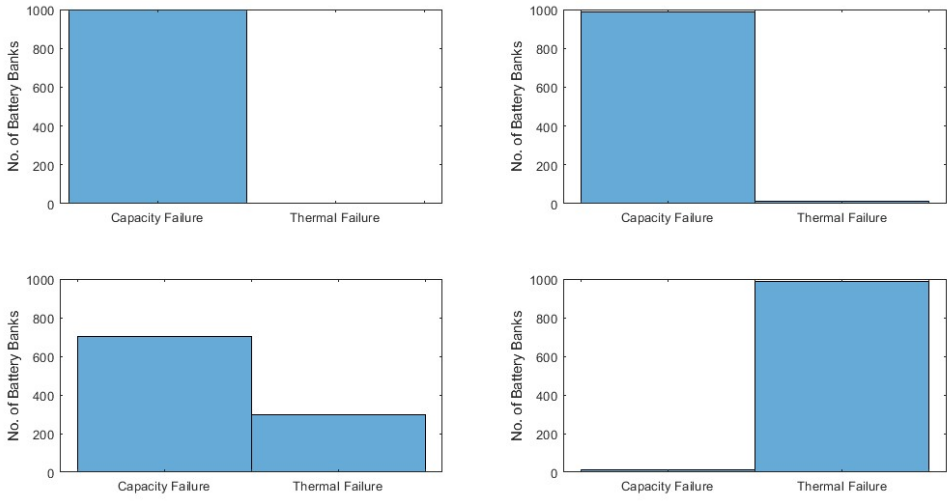

Figure 4.30 SOC Step Failure, Failure Mode, Conventional Topology

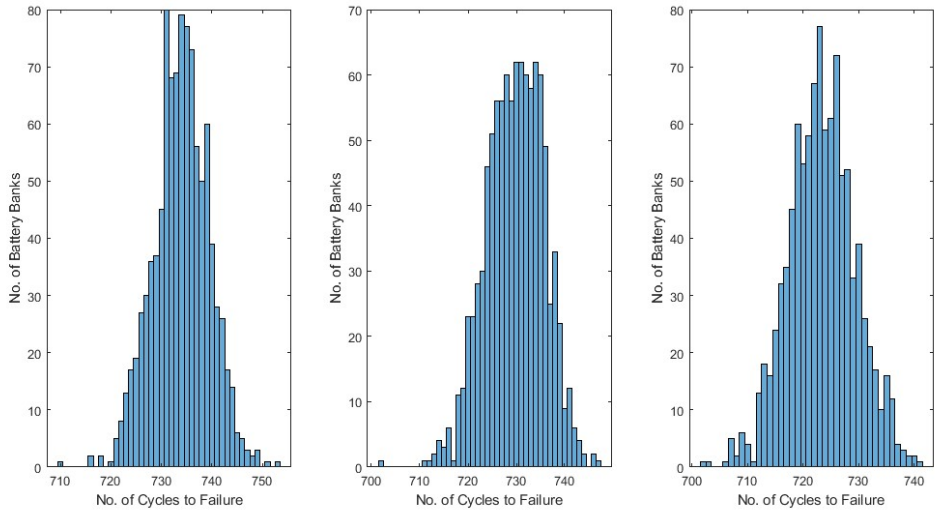

Figure 4.31 Capacity Step Failure, Number of Cycles to Failure, Meshed Topology

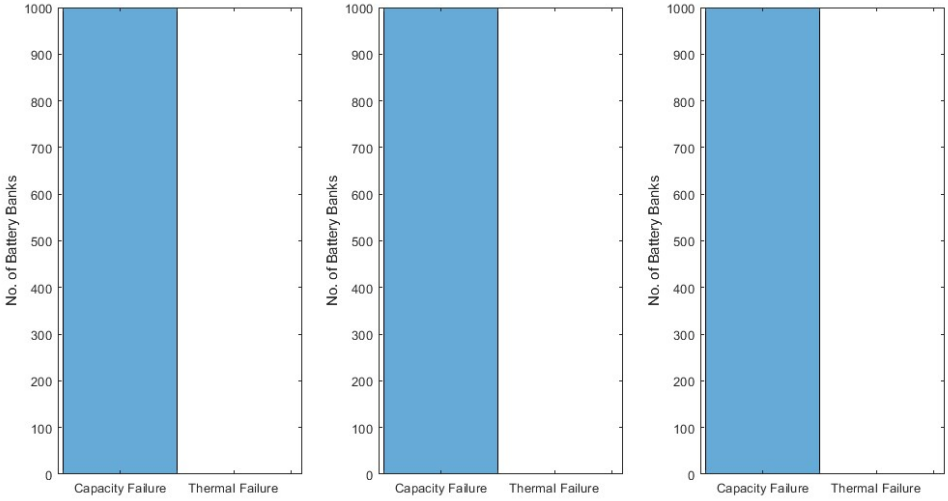

Figure 4.32 Capacity Step Failure, Failure Mode, Meshed Topology

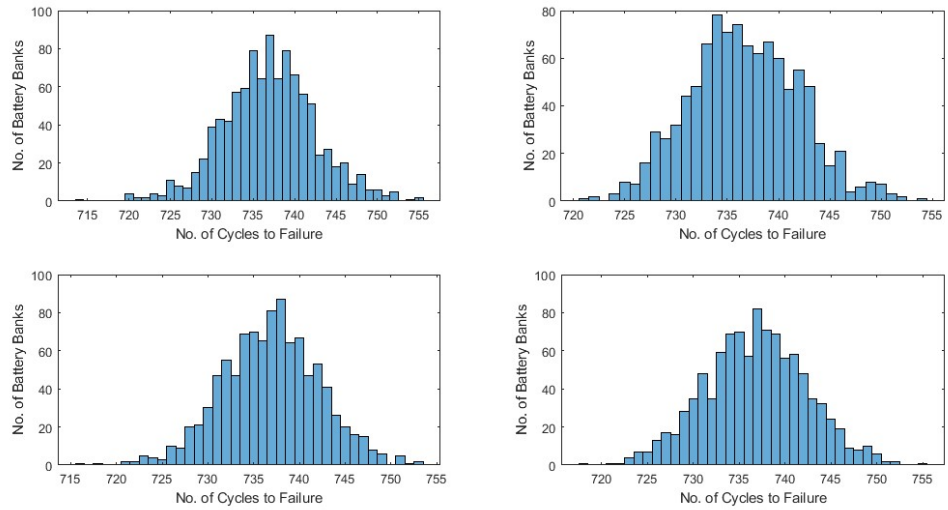

Figure 4.33 SOC Step Failure, Number of Cycles to Failure, Meshed Topology

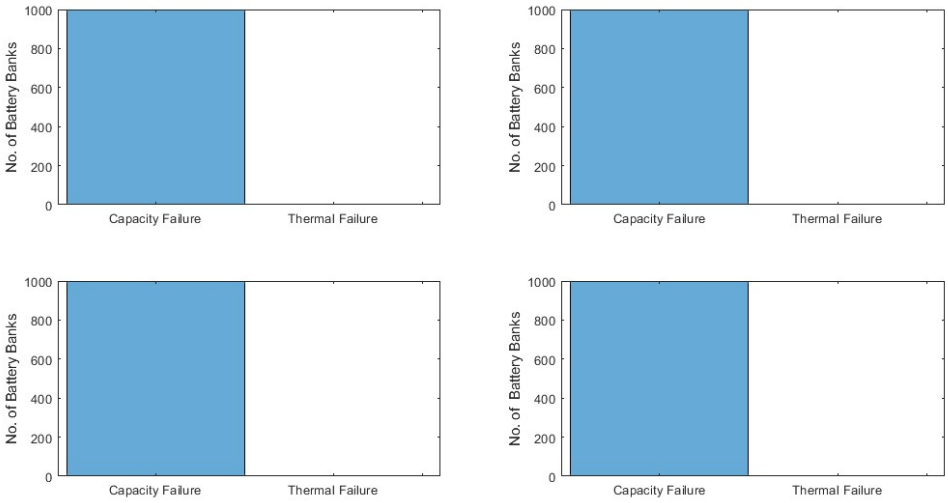

Figure 4.34 SOC Step Failure, Failure Mode, Meshed Topology

The result above clearly shows that meshed topology is more robust when exposed to single point step failures, even though the cost saving may not be as prominent per the

discussion on current rating in last section. This robustness is still a strong advantage over conventional topology.

5. MODLE BASED BATTERY BANK FAILURE PREDICTION

The ideal case for battery bank control is that end user has the capability to predict the failure of battery bank based on battery bank current state. This is however not an easy task.

First, state of battery bank is not easily accessible. Measurements can be made on the bank in real time which offer information on battery voltage, current and temperature, but the internal states of batteries are not available. Parameters of interest which include battery state of charge, battery internal resistance and battery capacity cannot be acquired directly. Thus, these parameters need to be estimated based empirical information and real time measurement[23].

Empirical information which is in form of battery model can have errors and bias, measurements can be noisy and fluctuation, how to combine the two to acquire high quality knowledge on the system is a well-studied problem.

Second, even when equipped with estimation of battery state with high fidelity, how can its failure be predicted? Failure is result of the systems initial state and its interaction with the outside world. In the case of a battery bank, this means both the bank's initial states and its full history of operations which includes its interaction with the environment around it are needed to how and when exactly it will fail. But when all this information is available, there is nothing that needs to be predicted. Conventionally, this is done by carrying a large amount of test on a fair number of identical or very similar systems with different initial conditions and different stress or load conditions until failure is observed. Thus, the average of life span of the system of interest can be

calculated based on even or weighted average, the probability of each type of failure can be calculated with respect of the amount of time in operation. If the states of these systems are recorded in these tests, preventative maintenance procedure and recommendations can also be proposed. This data collecting process is extremely expensive both in terms of monetary cost and the amount of time needed.

For a simple system with few components, this is still viable; for a battery bank with large number of batteries, this is next to impossible. This is the reason why very little study on battery bank failure is available, when the studies of individual battery failure are abundant.

Fortunately, this is grueling data collecting process can be greatly simplified using simulation. If a high-fidelity system model is known, simulation can be run on the model with different load and environmental conditions. Since varying system parameters and initial conditions is easy in a simulation environment, ample data can be collected in a fair amount of time. With this data, the procedure of life expectance calculation and failure probability calculation can be done in a straightforward fashion.

Once enough data is collected, battery failure prediction becomes a classification problem.

So, what it takes to make a high-fidelity model? What if there is no high-fidelity model available? If the model fits most available data collected on the subject, the model is considered of high fidelity. The lack of a high-fidelity data is usually caused by lack of available data on the subject itself. The true dependence of measurable quantities on the

subject and its real inaccessible state is sometimes unknown, this case is common in for battery models.

Failure of battery is just observed, sometimes postmortem analysis is available, but the procedure or the reason leading to the failure cannot be directly related to battery parameters. For a complicated setup such a battery bank, identify the specific reason for failure is an even hard task, the real origin of the failure can be easily masked by other less prominent effects.

The purpose of this chapter is to showcase a viable framework for battery bank failure prediction instead of universally predicting battery bank failure, given the latter is a task next to impossible.

This chapter is organized as follows. In section one, real time battery state and parameter estimation method is introduced. In section two, data collection process on a battery bank of specific topology is shown then battery bank failure is predicted using different classification methods.

5.1. Battery State and Parameter Estimation

Model used for state estimation is an incomplete model, it is acquired by simplify the model used for failure study. Measurement is generated using the model proposed in this thesis with inserted Gaussian white noise. This is arrangement made to showcase the capability of estimating the state of battery bank even with inaccurate model and noisy measurements.

The basis for the algorithm used in this study is particle filter. Three major concepts, Markov chain, Monte Carlo approximation and sequential Bayesian inference, are

indispensable in developing particle filter algorithm for battery state estimation, they are brief introduced in this section, clear similarity can also be observed when compared to evolutionary algorithms.

5.1.1. Markov Chain

As both measurement and state estimation is done in discrete time, the model used can be viewed of Hidden Markov Chain type. Since both the measurement and state at a particular time step is only related to the measurement and state as well as input of last time step, the model used is then of memoryless Hidden Markov Chain type. These assumptions serve to greatly simplify the estimation process.

A rough definition of the Hidden Markov Chain is a type Markov process that has a discrete state space, or a discrete index set that satisfies the Markov property which is often characterized as "memoryless". Markov Chain can be depicted in the following graphical model in Figure 5.1, where $(X_n)_{n\in N}$ denotes the dynamic process or the wanted quantity, $(Y_n)_{n\in N}$ denotes the measurement or observation made at each time step, both X_n and Y_n are available sequentially in time.[62]

$$\begin{array}{ccccc} \boldsymbol{X_1} & \rightarrow & \boldsymbol{X_2} & \rightarrow & \cdots \\ \downarrow & & \downarrow & & \\ \boldsymbol{Y_1} & & \boldsymbol{Y_2} & & \cdots \end{array}$$

Figure 5.1 Markov Chain Model

The mathematical model of the dynamic system of interest can be expressed in both state space form and probability distribution form. Both are shown in Figure 5.2 and 5.3.

$$\boldsymbol{X_1 \sim p(x_1)}$$
$$\boldsymbol{X_n | (X_{n-1} = x_{n-1}) \sim p(x_n | x_{n-1})}$$
$$\boldsymbol{Y_n (X_n = x_n) \sim p(y_n | x_n)}$$

Figure 5.2 Dynamic Model in Probability Distribution Form

$$\boldsymbol{x_n = f(x_{n-1}, u_{n-1})}$$
$$\boldsymbol{y_n = f(x_n, v_n)}$$

Figure 5.3 Dynamic Model in State Space Form

Where u_n is process noise sequence, v_n is measurement noise sequence, both u_n and v_n are white noise which satisfied the following fundamental property: any two instances of white noise are statistically independent no matter how close they are in time. The two equivalent models above cover the evolution of y_n and x_n, $f(x_{n-1}, u_{n-1})$ or $p(x_n|x_{n-1})$ is usually called the transition model, $f(x_n, v_n)$ or $p(y_n|x_n)$ is called observation model. Notice, there is no requirement on the linearity of the model, nor there is limitation on any of the distributions listed. If the dynamic model is linear and all distributions are Gaussian, there always exists a close form solution to the estimation problem. It is all easy to prove such a solution can be optimal. The method used for seeking such solution is called Kalman Filter. When the linearity of the model cannot be promised, linearization methods are used employing Taylor series, the most commonly used methods are extended Kalman filter and unscented Kalman filter. These approximation methods will inevitably introduce inaccuracy into the estimations. But the distributions are still required to be Gaussian. These requirements greatly limit the usage of Kalman filter type methods.[63]

In case of battery, it can easily show the state space model is nonlinear and no information on the distribution of parameters is available even though it is plausible to assume they follow Gaussian distribution. The method that will be employed in this study is particle filter, this greatly relaxes the requirements on the model and

distributions of interest which make it more flexible. The only problem with the method is that is computationally expensive. But thanks to the availability of ever-increasing computational power, it is already being widely employed in real- time estimation applications. The prerequisite of particle filtering method is Monte Carlo approximation, sequential Bayesian inference and sequential importance sampling and resampling. The detailed particle filter algorithm is presented after a brief introduction of aforementioned concepts. Then a modified particle filter method is introduce which handles modeling error when compared to conventional particle filter.[64]

5.1.2. Monte Carlo Approximation

Consider a random variable X having probability density function of $p_X(x)$ on a set of values χ, and g is a function of X. The expectation of $f(X)$ can be calculated as follows:

$$E\big(f(X)\big) = \int_{x\in\chi} f(x)p_X(x)dx \qquad \text{Eq 5.1}$$

If X is discrete, then the expectation can be rewritten as:

$$E\big(f(X)\big) = \sum_{x\in\chi} f(x)p_X(x) \qquad \text{Eq 5.2}$$

Where x_i denotes the *i*th sample from X. This is called a Monte Carlo approximation of $E\big(f(X)\big)$. It can be easily shown by the law of large number, if n is large enough $\hat{f}(x)$ can be arbitrarily close to $E\big(f(X)\big)$. A mathematical form of this is:

$$\lim_{n\to\infty} P(|\hat{f}(x) - E\big(f(X)\big)| > \epsilon) = 0 \qquad \text{Eq 5.3}$$

Where ϵ is arbitrarily small.

This method can also be used to approximate probabilities. If given a random variable X and its distribution $q(x)_{x\in\chi}$, the probability of X taking its value with $d\chi$

$$\hat{p}_{x\epsilon d\chi}(x) = \frac{1}{N}\sum_{i=1}^{N}\delta_{x_i}(d\chi) \quad \text{Eq 5.4}$$

Where $\delta_{x_i}(d\chi)$ is the Dirac delta mass located at x_i which equals 1 if $x_i \epsilon d\chi$ and equals zero otherwise. This approximation is often referred to as empirical measurement of a distribution in literature, which is a confusion caused by abuse of notation in the original reference.

5.1.3. Sequential Bayesian Inference

Bayes' theorem is well known way to describe the probability of an event based on prior knowledge and updated information. The simplest form of Bayes' theorem can be put as:

$$P(A|B) = \frac{P(B|A)P(A)}{P(B)} \quad \text{Eq 5.5}$$

One of its most popular application is Bayesian inference which closely related to our state estimation problem. Recall the goal is to acquire probability distribution $\{p(x_n|y_{1;n})\}_{n\geq 1}$ which can be rewritten as:

$$p(x_n|y_{1:n}) = \frac{p(x_n, y_{1:n})}{p(y_{1:n})} = \frac{p(x_{n-1}, y_{n-1})p(x_n|x_{n-1})p(y_n|x_n)}{p(y_{1:n})} \quad \text{Eq 5.6}$$

Divide the bottom and top of the above equation by $p(y_{1:n-1})$, reorganize:

$$p(x_n|y_{1:n}) = p(x_n|y_{1:n-1})\frac{p(y_n|x_n)}{p(y_n|y_{1:n-1})} \quad \text{Eq 5.7}$$

Where :

$$p(x_n|y_{1:n-1}) = \int p(x_t|x_{n-1})p(x_{n-1}|y_{1:n-1})dx_{n-1} \quad \text{Eq 5.8}$$

$$p(y_n|y_{1:n-1}) = \int p(x_{n-1}|y_{1:n-1})p(x_n|x_{n-1})p(y_n|x_n)dx_{n-1:n} \quad \text{Eq 5.9}$$

Substitute:

$$p(x_n|y_{1:n}) = p((x_n|y_n)|y_{1:n-1}) \quad \text{Eq 5.10}$$

And get:

$$p((x_n|y_n)|y_{1:n-1}) = p(x_n|y_{1:n-1})\frac{p(y_n|x_n)}{p(y_n|y_{1:n-1})} \quad \text{Eq 5.11}$$

This is indeed in the form of Bayes' theorem.

This offers a path for sequentially calculate $p(x_n|y_{1:n})$. $p(x_n|y_{1:n-1})$ is considered prior estimation as measurement at time step n is still not available. $p(x_n|y_{1:n})$ is considered posterior or update estimated estimation as measurement at time step is used to update $p(x_n|y_{1:n-1})$.

5.1.4. Importance Sampling and Resampling

Importance sampling is a very interesting mathematical manipulation that is proven to be very useful in different applications. Use the scenario setup for Monte Carlo approximation. Consider the following integral and identity.

$$\int f(x)dx = \int \frac{f(x)}{g(x)}g(x)dx \quad \text{Eq 5.12}$$

If $g(x)$ is a probability density function and $g(x) > 0$, the integral can be rewritten as:

$$\int f(x)dx = E(\frac{f(x)}{g(x)}) \quad \text{Eq 5.13}$$

This is the basic idea behind importance sampling, it does seem pretty useless at this point.

Now, consider a probability distribution $\pi(x)$ which can be formed into following form

$$\pi(x) = \frac{\gamma(x)}{Z} \quad \text{Eq 5.14}$$

$$Z = \int \gamma(x)dx \quad \text{Eq 5.15}$$

Where Z is nothing more than a normalization constant. $\pi(x)$ can also be written as:

$$\pi(x) = \frac{\omega(x)q(x)}{Z} \quad \text{Eq 5.16}$$

$$Z = \int \omega(x)q(x)dx \quad \text{Eq 5.17}$$

$q(x)$ is a probability density function defined on the same set of values. It is easy to find the Monte Carlo estimation of Z as:

$$\hat{Z} = \frac{1}{N}\sum_{i=1}^{N} \omega(x_i) \quad \text{Eq 5.18}$$

Where x_i are samples from the distribution $q(x)$. $q(x)$ can be manipulated in an interesting manner.

$$q(x) = \int q(y)\delta(x-y)dy \quad \text{Eq 5.19}$$

Since $q(x)$ is a probability density function, the Monte Carlo estimation of the right hand side can be write as

$$\hat{q}(x) = \frac{1}{N}\sum_{i=1}^{N} \delta(x-x_i) \quad \text{Eq 5.20}$$

Substitute the two estimations into $\pi(x)$:

$$\hat{\pi}(x) = \frac{\omega(x) * \frac{1}{N}\sum_{i=1}^{N}\delta(x - x_i)}{\frac{1}{N}\sum_{i=1}^{N}\omega(x_i)} = \sum_{i=1}^{N}\omega_n(x_i)\delta(x - x_i) \quad \text{Eq 5.21}$$

Where $\omega_n(x_i) = \frac{\omega(x)}{\sum_{i=1}^{N}\omega(x_i)}$, and is usually called normalized importance weight. This shows a very interesting way of estimating $\pi(x)$. Sampling can be done using an arbitrary distribution $q(x)$ as long as $q(x) > 0$ when $\pi(x)$>0, then $\pi(x)$ can estimated by evaluating those samples using $\omega(x)$. Since $q(x)$ can be as simple as possible, which can be show late the most commonly used particle filter is essentially sampling from uniform distribution, choosing a proper $q(x)$ can greatly simplify the problem.

But how can this importance sample method be carried out sequentially? Redefine probability density function $q(x)$ on a time sequence $x_{1:n}$ as $q_n(x_{1:n})$, the subscript n of q indicates that it is a distribution defined on a n-dimensional space. $q_n(x_{1:n})$ has the following property:

$$q_n(x_{1:n}) = q_{n-1}(x_{1:n-1})p(x_n|x_{n-1}) \quad \text{Eq 5.22}$$

$p(x_n|x_{n-1})$ is the transition probability density function.

$$\omega_n(x_{1:n}) = \frac{\gamma_n(x_{1:n})}{q_n(x_{1:n})} = \frac{1}{q_{n-1}(x_{1:n-1})}\frac{\gamma_{n-1}(x_{1:n-1})}{\gamma_{n-1}(x_{1:n-1})}\frac{\gamma_n(x_{1:n})}{p(x_n|x_{n-1})} \quad \text{Eq 5.23}$$

$$= \frac{\gamma_{n-1}(x_{1:n-1})}{q_{n-1}(x_{1:n-1})}\frac{\gamma_n(x_{1:n})}{\gamma_{n-1}(x_{1:n-1})p(x_n|x_{n-1})}$$

$$= \omega_{n-1}(x_{1:n-1})\frac{\gamma_n(x_{1:n})}{\gamma_{n-1}(x_{1:n-1})p(x_n|x_{n-1})}$$

This shows a clear path of calculating importance weight sequentially.

5.1.5. Particle Filter Algorithm

Set the following identities:

$$\pi_n(x_n) = p(x_n|y_{1:n}) \quad \text{Eq 5.24}$$

$$\pi_n(x_{1:n}) = p(x_{1:n}|y_{1:n}) \quad \text{Eq 5.25}$$

$$\gamma_n(x_n) = p(x_n, y_{1:n}) \quad \text{Eq 5.26}$$

$$\gamma_n(x_{1:n}) = p(x_{1:n}, y_{1:n}) \quad \text{Eq 5.27}$$

It can be easily shown:

$$\omega_n(x_{1:n}) = \omega_{n-1}(x_{1:n-1}) \frac{p(y_n|x_n)p(x_n|x_{n-1})}{p(x_n|x_{n-1})} \quad \text{Eq 5.28}$$

$$= \omega_{n-1}(x_{1:n-1})p(y_n|x_n)$$

Thus, given the choice above, the particle filter method base on sequential importance sampling is as follows.

If n=1:

sample $X_1^{(i)} \sim p(x_1)$

Calculate initial weight

$$\omega_1\left(X_1^{(i)}\right) = p(y_1|X_1^{(i)}) \quad \text{Eq 5.29}$$

If no measurement or observation is available at n=1,

$$\omega_1\left(X_1^{(i)}\right) = p(X_1^{(i)}) \quad \text{Eq 5.30}$$

Normalize $\omega_1\left(X_1^{(i)}\right)$.

For n>=2

Sample $X_n^{(i)} \sim p(x_n|\hat{x}_{n-1})$, where is $\hat{x}_{n-1}$the posterior of x from the last time step. This is the prediction part from a Bayesian point of view

Calculate weight

$$\omega_n\left(X_{1:n}^{(i)}\right) = \omega_{n-1}\left(X_{1:n-1}^{(i)}\right)p(y_n|X_n^{(i)}) \quad \text{Eq 5.31}$$

and normalize to get weight $\omega_n\left(X_{1:n}^{(i)}\right)$, this is the update part from a Bayesian point of view.

Approximate the distribution as

$$\hat{\pi}_n(x_{1:n}) = \sum_{i=1}^{N} \omega_n^{(i)} \delta_n(X_{1:n}^{(i)}) \quad \text{Eq 5.32}$$

$$\hat{\pi}_n(x_n) = \sum_{i=1}^{N} \omega_n^{(i)} \delta_n(X_n^{(i)}) \quad \text{Eq 5.33}$$

Calculate estimate of X_n

$$\hat{x}_n = \sum_{i=1}^{N} \omega_n^{(i)} X_n^{(i)} \quad \text{Eq 5.34}$$

In state estimation problems, the most wanted quantity is the expectation of X_n given $p(x_n|y_{1:n})$.

$$E_{p(x_n|y_{1:n})}[X_n] = \int x_n p(x_n|y_{1:n}) dx_n \quad \text{Eq 5.35}$$

Let $\pi_n(x_n) = p(x_n|y_{1:n})$, substituting its Monte Carlo estimation into the equation above:

$$\hat{E}_{p(x_n|y_{1:n})}[X_n] = \sum_{i=1}^{N} \omega_n^{(i)} X_n^{(i)} \quad \text{Eq 5.36}$$

This is the solution that we are looking for.

The major problem of this recursive method is weight degeneracy. If the initial sample starts with a low weight, after a few iterations, its corresponding weight will be so small that the sample contributes very little to the estimation itself while still taking up resources to update.

One way to solve this problem is to employ resampling methods. A commonly used method is sequential importance resampling. The basic idea of resampling is resample based on the calculated weight, and the new samples are given equal weight after this process.

$$\hat{E}_{p(x_n|y_{1:n})}[X_n] = \frac{1}{N}\sum_{i=1}^{N} X_n^{(i)} \quad \text{Eq 5.37}$$

5.1.6. Evolution based particle filter

The similarities between particle filter and evolutionary computation are easily recognizable. The possibility of merge the two different algorithms to improve computational performance has been presented in literature.

Evolutionary computation mimics the nature process of evolution by simulating the reproduction and selection of a population based on individual merits, such factors such as mutation are also considered in the process.

The basic steps of evolutionary computation are recombination, sometimes referred to as crossover, mutation and selection. Let $x^{(k)} = (x_1^{(k)}, \cdots x_n^{(k)})$ be the target population with $x_i^{(k)}$ denotes the ith component or characteristic of the population in kth member. Recombination, or crossover as in some literature, allows the mixing of information of two individuals in their descendants. A typical recombination rule is:

$$x_j' = x_{S,j} + \chi * (x_{T,j} - x_{S,j}) \quad \text{Eq 5.38}$$

Where T and S denote two parent of the descendant which selected randomly from the population. χ is random number, $\chi \in (0,1)$ following a uniform distribution.

Mutation introduces random changes to the population and is usually additive. It can be realized with the following equations.

$$\sigma_j' = \sigma_j * \exp\left(\tau' N(0,1) + \tau * N_j(0,1)\right) \quad \text{Eq 5.39}$$

$$x_j'' = x_j' + \sigma_j' N_j(0,1) \quad \text{Eq 5.40}$$

$N(0,1)$ denotes a normally distributed random variable with zero mean and unit variance. $N_j(0,1)$ is only employing the subscript to show that it is a different realization of the same distribution. σ_j indicates the step size chosen for mutation. τ' and τ are chosen according to population size. It can easily show the above process encourage small mutations or variations.

Selection process of evolutionary computation is based on fitness assessment of individuals and completely deterministic. Selection can be carried out either on the union of parent generation and its immediate descendant or on the immediate descendant only. Let μ denote the number of individuals in the parent generation and λ the number of

individuals in offspring generation. If selection is carried out on the union of parent and immediate descendant generations, μ members are selected out of the total of $\mu + \lambda$ members; if selection is carried out on the immediate descendants only, μ members are selected out of λ members. The underlying requirement here is $\lambda > \mu$.

When comparing the evolutionary computation with importance resampling particle filter method, the similarities are obvious. Recombination process can be viewed as state propagation through state space model. Mutation and selection process corresponds to importance sampling and resampling in sequential importance sampling particle filter, essentially using a different method to counter the problem of importance weight degeneration.

Combining particle filter and evolutionary computation to form a new algorithm has been proposed in [64] and been proven providing better estimation results when inaccurate state space model is used in [65]. A basic outline of the algorithm is shown below.

For $n = 1$

Sample $X_1^{(i)} \sim p(x_1)$

Calculate initial weight

$$\omega_1\left(X_1^{(i)}\right) = p(y_1|X_1^{(i)}) \qquad \text{Eq 5.41}$$

If no measurement or observation is available at n=1,

$$\omega_1\left(X_1^{(i)}\right) = p(X_1^{(i)}) \qquad \text{Eq 5.42}$$

Normalize $\omega_1\left(X_1^{(i)}\right)$.

For $n \geq 2$

Propagate $X_{n-1}^{(i)}$ to get $X_n^{(i,0)}$ and as parent generation

Sample for $X_n^{(i,j)} \sim q\left(x_n \middle| x_{n-1}^{(i)}, y_{1:n}\right)$ as immediate descendant, note $q\left(x_n \middle| x_{n-1}^{(i)}, y_{1:n}\right)$ is acquired by introducing extra randomness to the state space model.

And evaluate the weight of $X_n^{(i,0)}$ and $X_n^{(i,j)}$ by

$$\omega_n^{(i,j)} = \omega_{n-1}^{(i)} \frac{p(y_n|x_n^{(i,j)})p(x_n^{(i,j)}|x_{n-1}^{(i,j)})}{q\left(x_n \middle| x_{n-1}^{(i)}, y_{1:n}\right)} \quad \text{Eq 5.43}$$

And sort the combined samples by descending order of weight.

Take the first N members of sorted $X_n^{(i,j)}$, and normalize their weights as $\omega_n^{(i)}$.

Then:

$$p(x_n|y_{1:n}) \approx \sum_{i=1}^{N} \omega_n^{(i)} \delta(x - x_n^{(i)}) \quad \text{Eq 5.44}$$

5.1.7. State space model used for state estimation

When battery is the subject, the states that needs to be measured and estimated includes state of charge, internal resistance, terminal voltage, temperature and capacity. The measurements that can be applied to an individual battery or batteries in a bank in real-time are limited to terminal voltage, temperature and load current.

In models developed in numerous literatures, battery open circuit voltage and internal resistance are usually related to its state of charge, even though state of charge is not a measurable physical quantity. These models are built for the purpose of estimating internal state of charge from easy to access external measurements. However, for a

battery in operation, its open circuit voltage is not accessible. Bias caused by combination of current and internal resistance is impossible to avoid, over-voltages caused by factors introduced in early chapters just make the case worse. An equilibrium state or even a quasi-equilibrium state measurement of battery parameter is such deemed almost impossible. Luckily, these factors can be considered as noise and be filtered out by the weak law of large numbers.

The state space model used for particle filtering here is a purposefully simplified version of the model developed earlier. As particle filter algorithm use information acquired through measurements to calibrate the prior belief, an over simplified model is way to test its practicality when accurate model of the subject is not available. Since battery parameters are only known to follow certain distributions, it is also challenging to extract the exact value of the parameter for the state space model.

The state space model used is as follows, n is the index for states, dt denotes the time increment between two discrete time steps.

$$SOC_n = SOC_{n-1} - I_{n-1} * \frac{dt}{C} \quad \text{Eq 5.45}$$

$$R_n = R_{n-1} * \exp c(SOC_n - SOC_{n-1}) \quad \text{Eq 5.46}$$

$$V_n = a * SOC_n + b - I_n * R_n \quad \text{Eq 5.47}$$

$$T_n = T_{n-1} + I_n^2 * \frac{R_n}{C_T} \quad \text{Eq 5.48}$$

Where C is capacity of the battery and C_T is its thermal capacity.

The inaccessible states here are SOC_n and R_n, available measurements are V_n and T_n, I_n is a measurable input of the system. Note here, an accurate estimation of battery capacity C is also highly desirable.

When compared to the detail model, temperature dependency of open circuit voltage and internal resistance is neglected. The degrading of capacity and internal resistance over cycles are also not included as the evolving of these parameters are on a different time scale. But this model can still be used to estimate battery capacity and internal resistance in real time. It can be clearly seen from the model used above, the estimation of internal resistance is based on the estimation of state of charge, this cause the estimation result to be quite noisy. Another form of particle filter algorithm, smoothing, is used to partially alleviate this specific problem.

5.1.8. Generate Real-time Measurement

A battery bank of topology 10*10, ten batteries in series to form a string and then 10 strings connected in parallel, is used to generate real-time measurement data. Parameters of each battery in the bank is drawn from the same distributions used for failure simulation in last chapter.

To better test the practicality of particle filter, the time increment of data acquiring process has been set to 5 seconds. Later, the data collected will serve two purposes, current and voltage measurements with add on random noise are used as input to particle filter, other recorded parameters are used to test the accuracy of estimations.

5.1.9. Formatting Particle Filter for Battery Bank and Result Comparison

The evolution based particle filter is set up in the following way. 500 particles are used as parent generation for each parameter that needs to be estimated for each battery, 2

descendants are generated from each parent, refer to the algorithm discussed earlier for the details. So total number of 1500 equivalent particles used for each estimation, this greatly extend the coverage of Monte Carlo method thus providing better result.

Initial parameters of the batteries used in the bank are draw from the same distributions used for data collection. This set of newly drawn parameter is different from the set used above, as to simulate the lack of information on real state of batteries. Following the steps given in the above section it is not hard to complete the estimation of state of charge. The result can be shown in the figure below, the line in black line is state of charge acquired by running the complete detailed model, where the blue line is the estimated state of charge. Note, this is a random battery taken from the bank.

Develop the algorithm for state of charge estimation is straight-forward. This is not the same case with internal resistance estimation. There is no direct access to measurements on charge and discharge resistances, as update the resistance estimations from model propagation is the essence of particle filter algorithm, this presents itself as a major problem. Revisit the model on resistance propagation and terminal voltage.

$$R_n = R_{n-1} * \exp c(SOC_n - SOC_{n-1}) \quad \text{Eq 5.49}$$

$$V_n = a * SOC_n + b - I_n * R_n \quad \text{Eq 5.50}$$

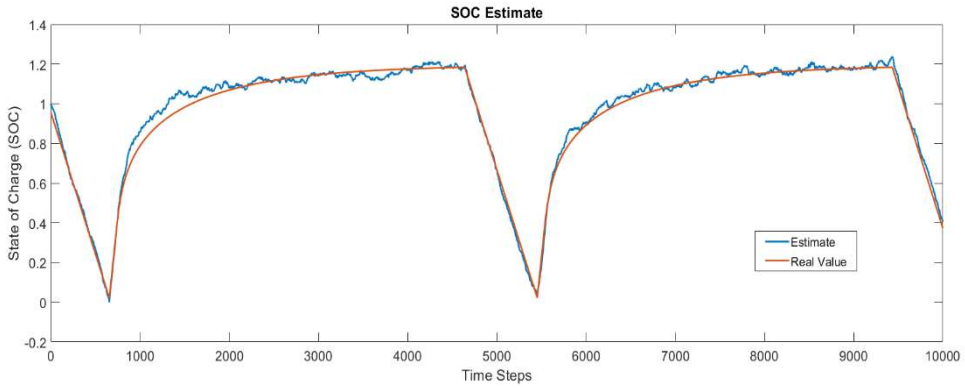

Figure 5.4 SOC Estimation Result

Using two consecutive voltage measurements:

$$V_n - V_{n-1} = a * (SOC_n - SOC_{n-1}) - (I_n * R_n - I_{n-1} * R_{n-1}) \qquad \text{Eq 5.51}$$

Reorganize, and substitute $SOC_n - SOC_{n-1} = I_{n-1} * dt$:

$$R_n = (V_{n-1} - V_n + a * I_{n-1} * dt/C + I_{n-1} * R_{n-1})/I_n \qquad \text{Eq 5.52}$$

From the equation above, R_{n-1} is the updated estimated estimate from last time step, a is a constant, all the other variables are directly available from measurement in the current and last time step. Thus this can be used as quasi-measured resistance.

When these quasi-measured resistances are used in the particle filter algorithm, the resultant estimation is compared to the resistance value acquired from detailed model. The figure below shows the charge and discharge resistance estimate of a random battery in the battery bank tested. As it can be seen the estimates are fairly accurate. Note, the choice of initial particles can affect the result greatly, such discussion however is beyond the scope of this research.

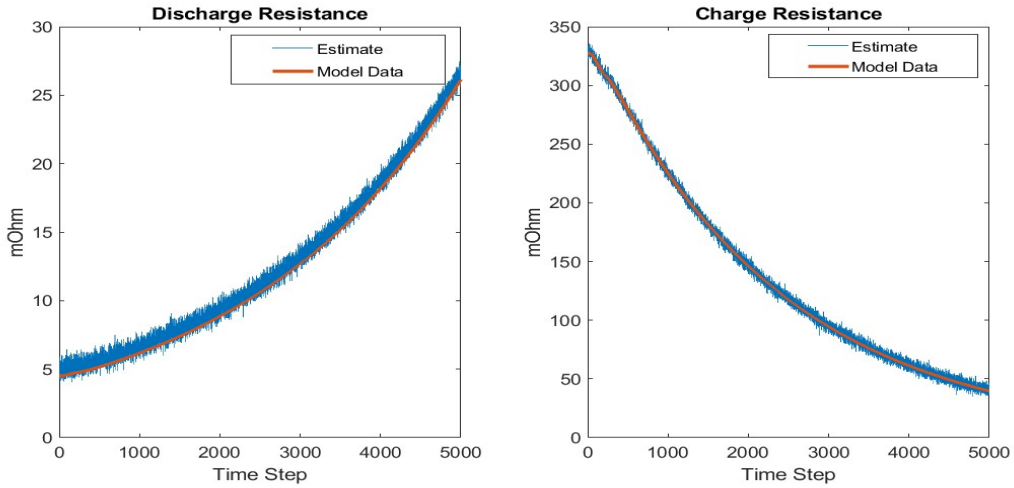

Figure 5.5 Battery Resistance Estimation Result

Capacity of the battery is another parameter that requires accurate estimation. In fact, capacity of battery is the hardest to measure of all the parameters of interest, and is often used as an indicator for battery state of health as end of life of battery is usually defined based on remaining capacity.

Since battery capacity is not fast varying parameter, it can be estimated based on differences in voltage measurements in adjacent time steps. The effect of temperature and internal resistance on battery terminal voltage can be largely neglected due to the adjacency of the measurements. This method is theoretically possible given noise free measurements. Given two consecutive voltage measurements denoted as V_n and V_{n-1}, the following equation can be used to estimate battery capacity:

$$C = a * \frac{I_{n-1} * dt}{V_{n-1} - V_n} \qquad \text{Eq 5.53}$$

Both voltage and current measurements are subject to noises, these noise can often be assumed of Gaussian White Noise type. These additive noise can make capacity estimate very inaccurate. The solution is to average the estimate over multiple time steps.

The result of SOC estimation is shown in Figure 5.4 and the result of resistance estimation is shown in Figure 5.5.

5.1.10. Section Conclusion

As it has been shown above by employing evolutionary particle filter algorithm, battery parameters can be estimated to various precision given the different amount resource used for computation. A major limitation of this type of algorithms is its time complexity. Given a large battery bank and precision requirement, the task of making real-time estimates can be challenging.

5.2. Battery Bank Failure Prediction

The interest of this research is on battery bank failure prediction which is inherent different from real-time battery control.

With the estimated parameters to a certain confidence, how the failure of battery bank can be predicted? As has been discussed at the beginning of this chapter, knowing the state of batteries in battery bank is only half of the picture. Battery bank failure depends on both its initial state and operational history.

Simulation can be ran on a large number of battery banks with different initial conditions, the number of cycles to failure and failure mode are recorded. The collected data is then used for classification.

To insure better classification results, better coverage of the parameter space is needed. Instead of select parameters within the Gaussian distribution used earlier, uniform

distribution with wider ranges are used for parameter generation. Parameter space used is shown below.

$$C \sim U(250,350) \quad Ah \qquad \text{Eq 5.54}$$

$$R_c \sim U(12,28) \quad mOhms \qquad \text{Eq 5.55}$$

$$R_d \sim U(1.5,5.5)\ mOhms \qquad \text{Eq 5.56}$$

$$SOC_0 \sim U(0.8,1.2) \qquad \text{Eq 5.57}$$

Again, the same battery bank topology is used, 10*10. The cycle chosen for this test is the same used in last chapter, full discharge, full charge and float charge for a predefined period of time. The distribution and failure modes and average number of cycles to failure is list in the table below.

Different number of banks are randomly generated and simulated for different classification method. Only two different failure modes are found in these simulated banks.

The first consideration is to combine the number of cycles to failure with failure modes to implement a multi-category classification. The mathematical difficulty encountered is beyond the scope of this research. The classification is then limited to classical two category classification. Different classification methods are used, including conventional deterministic methods and artificial neural network based method. Attempts have been made to use the convolution deep learning network based classification method. Structure of data greatly limited the success in this path, as the deep lying assumption for convolution network is not satisfied, i.e. data points spatially close to one another is

more connected logically. In the case of battery bank, switching the sequence of batteries in a string under a well-ventilated scenario will not yield a different result.

The parameters considered in classification are battery capacity, initial state of charge, charge and discharge resistance. Classification is first carried out on data in its original form, Z-score normalization is done on different parameters and the data as a whole, and this is how sensitivity of classification result is tested. The equation used for z-score normalization is[66]:

$$Z_i = \frac{X_i - \mu}{\sigma} \qquad \text{Eq 5.58}$$

Where μ is the mean of the data and σ is its standard deviation.

Deterministic classification is implemented using Matlab classification toolbox.

Artificial neural network classification is implemented using Matlab ANN toolbox.

A table is given below for a list of different conventional classification methods. The result is presented in term of confusion matrix. Visualization of confusion matrix is shown after the table. The classification listed in table is done without feature extraction where all data are used without sensitivity consideration.

Note due to the errors and inaccuracy in estimated battery parameters, the sensitivity of classification result versus battery parameters needs to be implemented. But due the high dimension of data used, this presents great difficulty and is left for future work.

Table 5.1 Original Classification Result

	Thermal Failure		Capacity Failure	
Classification Method	True Positive	False Negative	False Positive	True Negative
Tree, Fine	222	5019	301	74458
Tree, Median	43	5198	65	74694
Tree, Coarse	10	5231	25	74734
Linear Discriminant	0	5241	0	74759
Quadratic Discriminant	30	5211	348	74411
Logistic Regression	0	5241	0	74759
SVM, Linear	0	5241	0	74759
SVM, Quadratic	0	5241	0	74759
SVM, Cubic	0	5241	1	74758
SVM, Fine Gaussian	0	5241	0	74759
KNN, Fine	166	5075	1979	72780
KNN, Medium	0	5241	0	74759
KNN, Coarse	0	5241	0	74759
KNN, Cosine	0	5241	3	74756
KNN, Cubic	0	5241	0	74759
KNN, Weighted	0	5241	0	74759

Table 5.1 Continued

	Thermal Failure		Capacity Failure	
Classification Method	True Positive	False Negative	False Positive	True Negative
Ensemble, Boosted Trees	0	5241	0	74759
Ensemble, Bagged Trees	309	4932	244	74515
Ensemble, Subspace Discriminant	0	5241	0	74759
Ensemble, Subspace KNN	4	5237	0	74759
Ensemble, RUS Boosted Trees	1737	3504	15720	59039

Multiple classification methods reports equal accuracy, but almost all thermal failures are misclassified to capacity failure.

Table 5.2 Feature Extracted, Charge and Discharge Resistance Removed

	Thermal Failure		Capacity Failure	
Classification Method	True Positive	False Negative	False Positive	True Negative
Tree, Fine	228	5013	281	74478
Tree, Median	53	5188	55	74704

Table 5.2 Continued

Tree, Coarse	11	5230	22	74737
Linear Discriminant	0	5241	0	74759
Quadratic Discriminant	106	5135	1197	73562
Logistic Regression	0	5241	0	74759
SVM, Linear	0	5241	0	74759
SVM, Quadratic	0	5241	0	74759
SVM, Cubic	4	5237	28	74731
SVM, Fine Gaussian	0	5241	0	74759
SVM, Medium Gaussian	0	5241	0	74759
SVM, Coarse Gaussian	0	5241	0	74759
KNN, Fine	164	5077	1676	73083
KNN, Medium	0	5241	0	74759
KNN, Coarse	0	5241	0	74759
KNN, Cosine	2	5239	8	74751
KNN, Cubic	0	5241	0	74759
KNN, Weighted	0	5241	0	74759
Ensemble, Boosted Trees	0	5241	0	74759

Table 5.2 Continued

	Thermal Failure		Capacity Failure	
Classification Method	True Positive	False Negative	False Positive	True Negative
KNN, Cubic	0	5241	0	74759
KNN, Weighted	0	5241	0	74759
Ensemble, Boosted Trees	0	5241	0	74759
Ensemble, Bagged Trees	373	4868	292	74467
Ensemble, Subspace Discriminant	0	5241	0	74759
Ensemble, Subspace KNN	3	5238	4	74755

As an example, the confusion matrix is shown in the figure above. A total number of 80,000 banks are generated and classified using Ensemble Bagged Tree method. It can be seen from the confusion matrix among, the total accuracy is 93.55%. However only 373 of a total number of 5,241 thermal failure are correctly reported, the rest are classified as false negative. This is completely unacceptable as false negative on thermal failure can cause great loss, where false positive on thermal failure can be more thoroughly investigated. This concept is shown in the Figure 5.6.

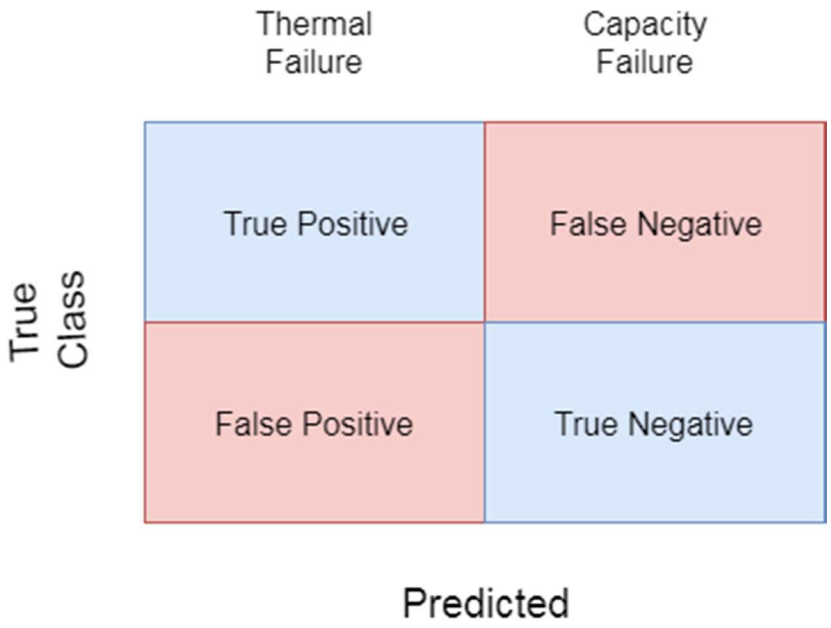

Figure 5.6 Confusion Matrix Concepts

Augmented data with banks with thermal failure added is used for more accurate classification result. The result is shown in Table 5.3. A total number of 134,045 banks are used with a total number of 46,160 thermal failures.

Table 5.3 Augmented Data Classification

	Thermal Failure		Capacity Failure	
Classification Method	True Positive	False Negative	False Positive	True Negative
Tree, Fine	15136	31024	7270	80623
Tree, Median	14670	31490	8927	78966
Tree, Coarse	11564	34596	7409	80484
Linear Discriminant	44	46116	2	87891

Table 5.3 Continued

	Thermal Failure		Capacity Failure	
Classification Method	True Positive	False Negative	False Positive	True Negative
Quadratic Discriminant	40528	5632	12371	75522
SVM, Linear	0	46160	0	87893
SVM, Quadratic	38172	7988	10224	77669
SVM, Cubic	35246	10914	8897	78966
SVM, Fine Gaussian	70	46090	1	87892
SVM, Medium Gaussian	39254	6906	10915	76978
SVM, Coarse Gaussian	37814	8346	9790	78103
KNN, Fine	2015	44145	2297	85596
KNN, Medium	0	46160	0	87893
KNN, Coarse	0	46160	0	87893
KNN, Cosine	13842	32318	4322	83571
KNN, Cubic	0	46160	0	87893
KNN, Weighted	121	46039	2	87891
Ensemble, Boosted Trees	11052	35108	1120	86773

Table 5.3 Continued

	Thermal Failure		Capacity Failure	
Classification Method	True Positive	False Negative	False Positive	True Negative
Ensemble, Bagged Trees	36964	9196	9645	78248
Ensemble, Subspace Discriminant	0	46160	0	87893
Ensemble, Subspace KNN	1543	44617	2350	85543

In Table 5.4 below, feature extraction is performed on the data generated. In this feature extraction process, different combinations of battery parameters are removed for quicker convergence and better accuracy.

Table 5.4 Augmented Data, Feature Extracted, Z-score Normalized

	Thermal Failure		Capacity Failure	
Classification Method	True Positive	False Negative	False Positive	True Negative
Tree, Fine	NA	NA	NA	NA
Tree, Median	NA	NA	NA	NA
Tree, Coarse	NA	NA	NA	NA
Linear Discriminant	37	46123	2	87891

Table 5.4 Continued

	Thermal Failure		Capacity Failure	
Classification Method	True Positive	False Negative	False Positive	True Negative
Quadratic Discriminant	40519	5641	12368	75525
Logistic Regression	NA	NA	NA	NA
SVM, Linear	0	46160	0	87893
SVM, Quadratic	38169	7991	10243	77650
SVM, Cubic	35271	10889	8939	78954
SVM, Fine Gaussian	64	46096	1	87892
SVM, Medium Gaussian	39266	6894	10926	76967
SVM, Coarse Gaussian	37778	8382	9767	78126
KNN, Fine	1963	44197	2313	85580
KNN, Medium	0	46160	0	87893
KNN, Coarse	0	46160	0	87893
KNN, Cosine	13812	32348	4292	83601
KNN, Cubic	0	46160	0	87893
KNN, Weighted	106	46054	1	87892

Table 5.4 Continued

	Thermal Failure		Capacity Failure	
Classification Method	True Positive	False Negative	False Positive	True Negative
Ensemble, Boosted Trees	NA	NA	NA	NA
Ensemble, Bagged Trees	NA	NA	NA	NA
Ensemble, Subspace Discriminant	279	45881	13	87880
Ensemble, Subspace KNN	0	46160	0	87893
Ensemble, RUS Boosted Trees	NA	NA	NA	NA

5.3. Artificial Neural Network Classification

Artificial neural network based classification differs from the aforementioned deterministic method in the sense that the initial division of samples used for classification and validation has great effect on the result. Although these can all be considered brutal force methods are an extensive amount of calculation is needed to reach satisfactory result. Error entropy is calculated for the specific network after each iteration, and alteration to the weights in the network are based on gradient descend. The

end of search condition can either be defined as a minimum gradient or max number of iterations is reached.

One can be seen from Figure 5.7 below, artificial neural network employs a layered structure.

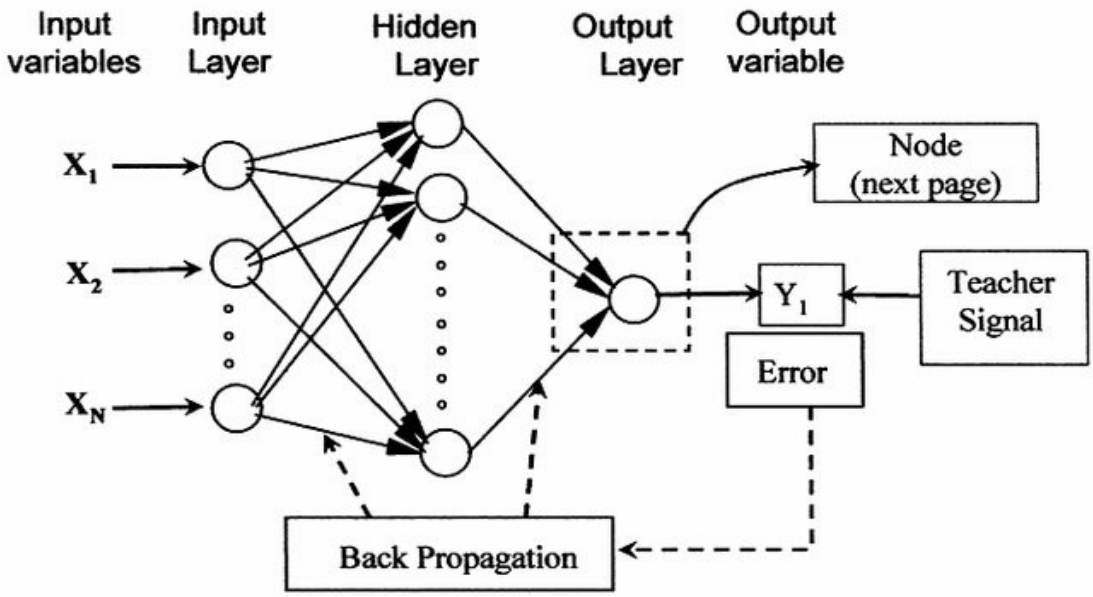

Figure 5.7 Typical Structure of Neural Network. Reprinted from [67]**.**

The number of hidden layers, number of neurons in each hidden layer and weights of each path are design parameters of the network. In this case battery bank case, input variables are parameters of the batteries in the bank; teacher signal, which can be considered as reference, is the failure mode data collected. The choice of weights is usually automated as the number of weights is quite substantial even for a simple network. Different number of hidden layers are tested in Matlab neural network toolbox, shown in Figure 5.8. Multiple iterations are tested on each specific network for the aforementioned reason. Note the input the networks are the data with charge and

discharge resistance removed as such procedure greatly reduced the time require for training while achieve very comparable accuracy.

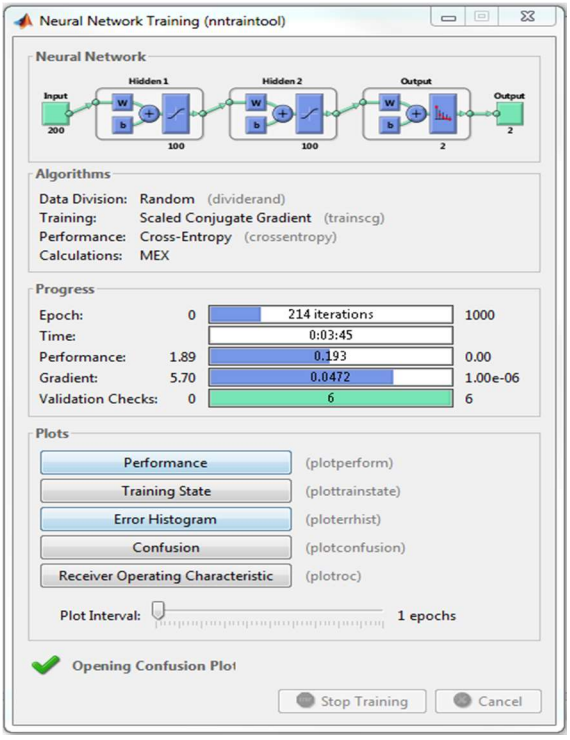

Figure 5.8 Matlab Neural Network Toolbox

The result of employing 3 hidden layers with 1000, 1000 and 100 neurons in each layer respectively is tested on augmented data. The corresponding confusion matrices are shown in Figure 5.9. Data is randomly divided into 3 categories, used separately for training, validation and test per the first 3 matrices. The last matrix is the combined result. Class 1 is capacity failure, class 2 is thermal failure. The same rules apply to all the result included in this work.

The result of employing 2 hidden layers with 1000 and 100 neurons in each layer respectively is tested on augmented data. The corresponding confusion matrices are shown in Figure 5.10.

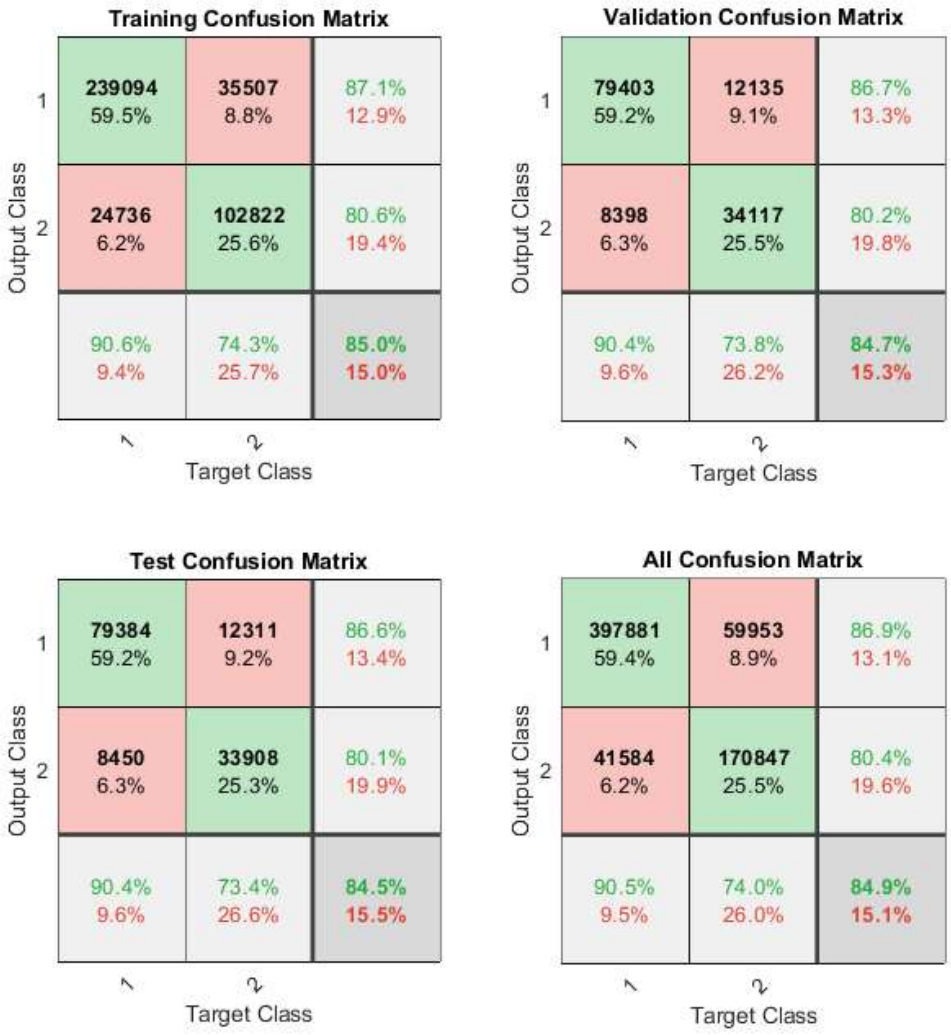

Figure 5.9 Confusion Matrices for Network with Three Hidden Layers with 1000, 1000 and100 Neurons with Augmented Data.

Figure 5.10 Confusion Matrices of Neural Network with Two Hidden Layers with 1000 and 100 Neurons with Normalized Data

In these confusion matrices, the data point of greatest interest is the one on the last column of second row in the combined all confusion matrix, as this shows the accuracy of failure prediction on thermal failure. The accuracy achieved in the figure above of

81.2%. The reason of such low accuracy cannot be exactly specified. The hypothesis we propose here is because the spatial relationship between the batteries in the bank is not past to the neural network as usual information. We think this is also the same reason that limits the accuracy of deterministic methods.

5.4. Chapter Conclusion

In this chapter, a viable path for battery bank failure prediction is developed. The path is shown in the figure below. Improvements need to be made on prediction accuracy.

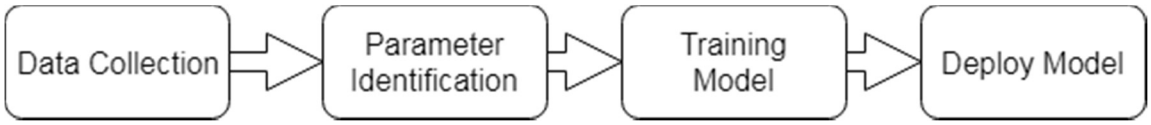

Figure 5.11 Path for Failure Prediction

6. CONCLUSION

The major findings of this research is follows:

The different factors in battery bank and their effect on battery bank failure is thoroughly investigated. Float charge has been clearly identified as leading cause for catastrophic failures.

An improved topology is proposed that meets the requirement of long float charge period and shows robustness to single point step failure.

A viable path for battery bank failure prediction based on machine learning is developed.

Future work that this research can be extended to:

Extend the same methodology to battery banks of other chemistry, i.e. lithium ion battery.

Development of algorithm that can handle generalized structured data for classification purpose.

REFERENCE

[1] H. O. F. Batteries, D. E. Library, and T. M. Companies, *Handbook of batteries*. 2004.

[2] D. A. J. Rand, J. Garche, P. T. Moseley, and C. D. Parker, *Valve-Regulated Lead-Acid Batteries*. 2004.

[3] "VARTA." [Online]. Available: http://www.varta.com/. [Accessed: 04-Apr-2019].

[4] "Car and Deep Cycle Battery Frequently Asked Questions (FAQ) Section 2." [Online]. Available: http://jgdarden.com/batteryfaq/carfaq2.htm. [Accessed: 04-Apr-2019].

[5] P. T. Moseley, R. F. Nelson, and A. F. Hollenkamp, "The role of carbon in valve-regulated lead–acid battery technology," *J. Power Sources*, vol. 157, no. 1, pp. 3–10, Jun. 2006.

[6] D. (Dietrich) Berndt, *Maintenance-free batteries : lead-acid, nickel/cadmium, nickel/metal hydride : a handbook of battery technology*. Research Studies Press, 1997.

[7] Eaton, "The UPS Battery Handbook," vol. BAT11LTA, p. 16, 2012.

[8] "Separators." [Online]. Available: http://evbatterymonitoring.com/batterybook2/Battery_Book_2.htm#Paste_for_Engine_Starting_Batteries.htm.

[9] K. Pan *et al.*, "The performance of a silica-based mixed gel electrolyte in lead acid batteries," *J. Power Sources*, vol. 209, pp. 262–268, Jul. 2012.

[10] D. Pavlov, "Lead-acid batteries : science and technology : a handbook of lead-acid battery technology and its influence on the product." pp. 12–13, 2011.

[11] "Production cycle of a sealed lead-acid battery - 15 November 2017 - Forbatt SA - Dataweek." [Online]. Available: http://www.dataweek.co.za/58744n. [Accessed: 05-Apr-2019].

[12] D. M. Ludlum, "Lead Acid Battery Manufacture Background Information for Proposed Standards," 1979.

[13] "Know About the Steps of Battery Manufacturing Process." [Online]. Available: https://www.watelectrical.com/know-about-the-steps-of-battery-manufacturing-process/. [Accessed: 30-Sep-2019].

[14] H. a. Kiehne, *Battery Technology Handbook*. 2003.

[15] V. A. M. J. D. Cox, D. D. Wagman, "Key Values for Thermodynamics," *Berichte der Bunsengesellschaft für Phys. Chemie*, vol. 94, no. 1, pp. 93–93, Jan. 1989.

[16] Thi Minh Phuong Nguyen, "LEAD ACID BATTERIES IN EXTREME CONDITIONS : ACCELERATED CHARGE , MAINTAINING THE CHARGE WITH IMPOSED LOW CURRENT , POLARITY INVERSIONS INTRODUCING NON-CONVENTIONAL CHARGE METHODS," 2009.

[17] K. R. Bullock, "The electromotive force of the lead-acid cell and its half-cell potentials," *J. Power Sources*, vol. 35, no. 3, pp. 197–223, Oct. 1991.

[18] E. U. Franck, "Electrolyte Solutions, von R. A. Robinson und R. H. Stokes. — The Measurement and Interpretation of Conductance, Chemical Potential and Diffusion in Solutions of Simple Electrolytes. Butterworths Scientific Publication, London 1959. 2. Aufl., XV, 559 S., geb. £ 3.5.0," *Angew. Chemie*, vol. 72, no. 12, pp. 426–426, Jun. 1960.

[19] C. Kirstein, "The difference between Failure Modes and Failure Mechanisms," pp. 6–8, 2017.

[20] C. (Carl S. Carlson, *Effective FMEAs : achieving safe, reliable, and economical products and processes using failure mode and effects analysis*. John Wiley & Sons, 2012.

[21] Y. Shi, "modeling, real-time degradation identification, and remediation of lead-acid battries." 2013.

[22] M. Cugnet *et al.*, "A Mathematical Model for the Simulation of New and Aged Automotive Lead-Acid Batteries," *J. Electrochem. Soc.*, vol. 156, no. 12, p. A974, Dec. 2009.

[23] IEEE-SA-Standards-Board, *IEEE Guide for Selecting, Charging, Testing, and Evaluating Lead-Acid Batteries Used in Stand-Alone Photovoltaic (PV) Systems*,

vol. 2014. 2014.

[24] J. Kang, A. T. Conlisk, and G. Rizzoni, “Integration of capacity fading in an electrochemical model of Li-ion batteries,” *J. Solid State Electrochem.*, vol. 18, no. 9, pp. 2425–2434, 2014.

[25] R. Deshpande, M. Verbrugge, Y.-T. Cheng, J. Wang, and P. Liu, “Battery Cycle Life Prediction with Coupled Chemical Degradation and Fatigue Mechanics,” *J. Electrochem. Soc.*, vol. 159, no. 10, pp. A1730–A1738, 2012.

[26] J. A. Byrne and J. Estes, “What can be learned from visual inspections of stationary lead-acid batteries ? Real world examples . Abstract Introduction,” pp. 1–12, 2014.

[27] D. Pavlov, “Suppression of premature capacity loss by methods based on the gel—crystal concept of the PbO2 electrode,” *J. Power Sources*, vol. 46, no. 2–3, pp. 171–190, Oct. 1993.

[28] P. Ruetschi, “Aging mechanisms and service life of lead-acid batteries,” in *Journal of Power Sources*, 2004, vol. 127, no. 1–2, pp. 33–44.

[29] M. L. Gopikanth and S. Sathyanarayana, “Impedance parameters and the state-of-charge. II. Lead-acid battery,” *J. Appl. Electrochem.*, vol. 9, no. 3, pp. 369–379, 1979.

[30] H. A. Catherino, F. F. Feres, and F. Trinidad, “Sulfation in lead-acid batteries,” in *Journal of Power Sources*, 2004, vol. 129, no. 1 SPEC. ISS., pp. 113–120.

[31] P. E. Pascoe and A. H. Anbuky, “A VRLA battery simulation model,” *Energy Convers. Manag.*, vol. 45, no. 7–8, pp. 1015–1041, May 2004.

[32] J. Newman and W. Tiedemann, “Temperature Rise in a Battery Module with Constant Heat Generation,” *J. Electrochem. Soc.*, vol. 142, no. 4, p. 1054, 1995.

[33] D. Pavlov, “Energy balance of the closed oxygen cycle and processes causing thermal runaway in valve-regulated lead/acid batteries,” *J. Power Sources*, vol. 64, no. 1–2, pp. 131–137, Jan. 1997.

[34] L. T. Lam, N. P. Haigh, C. G. Phyland, and A. J. Urban, “Failure mode of valve-regulated lead-acid batteries under high-rate partial-state-of-charge operation,” *J.*

Power Sources, vol. 133, no. 1, pp. 126–134, 2004.

[35] A. Millner, "Modeling lithium ion battery degradation in electric vehicles," in *2010 IEEE Conference on Innovative Technologies for an Efficient and Reliable Electricity Supply, CITRES 2010*, 2010, pp. 349–356.

[36] H. A. Catherino, "Secondary Batteries: Lead Acid Battery Thermal Runaway Encyclopedia of Electrochemical Power Sources."

[37] G. Papazov, T. Rogatchev, D. Pavlov, J. Garche, and K. Wiesener, "Influence of the lead dioxide active mass on the corrosion rate of the spines of positive lead—acid battery plates," *J. Power Sources*, vol. 6, no. 1, pp. 15–24, Jan. 1981.

[38] T. Tsujikawa, T. Matsushima, K. Yabuta, and T. Matsushita, "Estimation of the lifetimes of valve-regulated lead-acid batteries," *J. Power Sources*, vol. 187, no. 2, pp. 613–619, Feb. 2009.

[39] C. Zhang, K. Li, S. McLoone, and Z. Yang, "Battery modelling methods for electric vehicles - A review," *2014 Eur. Control Conf. ECC 2014*, pp. 2673–2678, 2014.

[40] P. H. . Bergveld, H.J., Kruijt, W.S., Notten, H. J. Bergveld, W. S. Kruijt, and P. H. L. Notten, *Battery Management Systems - Design by Modelling*. 2002.

[41] G. Piłatowicz, A. Marongiu, J. Drillkens, P. Sinhuber, and D. U. Sauer, "A critical overview of definitions and determination techniques of the internal resistance using lithium-ion, lead-acid, nickel metal-hydride batteries and electrochemical double-layer capacitors as examples," *J. Power Sources*, vol. 296, pp. 365–376, 2015.

[42] C. M. Shepherd, "Design of Primary and Secondary Cells," *J. Electrochem. Soc.*, vol. 112, no. 7, p. 657, Jul. 1965.

[43] V. Boovaragavan, R. N. Methakar, V. Ramadesigan, and V. R. Subramanian, "A Mathematical Model of the Lead-Acid Battery to Address the Effect of Corrosion," *J. Electrochem. Soc.*, vol. 156, no. 11, p. A854, 2009.

[44] M. Mastali, J. Vazquez-Arenas, R. Fraser, M. Fowler, S. Afshar, and M. Stevens, "Battery state of the charge estimation using Kalman filtering," *J. Power Sources*,

vol. 239, pp. 294–307, Oct. 2013.

[45] V. Pop, H. J. Bergveld, P. H. L. Notten, and P. P. L. Regtien, “State-of-the-art of battery state-of-charge determination,” *Meas. Sci. Technol.*, vol. 16, no. 12, 2005.

[46] J. Unger, M. Quasthoff, and S. Jakubek, “Battery management,” in *SpringerBriefs in Applied Sciences and Technology*, no. 9783319297958, Elsevier, 2016, pp. 11–41.

[47] C&D technologies, “Impedance and conductance testing.” .

[48] C. M. Hoff, “NEW INSIGHTS INTO THERMAL RUNAWAY OF VALVE REGULATED LEAD-ACID BATTERIES.” pp. 1–10.

[49] “Thermal Runaway Model of Lead-Acid Battery (Part 2) | Math Encounters Blog.” [Online]. Available: http://mathscinotes.com/2010/12/thermal-runaway-model-of-lead-acid-battery-part-2/. [Accessed: 24-Apr-2019].

[50] D. Berndt, “Valve regulated lead acid batteries-gas and heat management,” in *10th International Telecommunications Energy Conference*, pp. 89–96.

[51] F. Yang, Y. Xing, D. Wang, and K.-L. Tsui, “A comparative study of three model-based algorithms for estimating state-of-charge of lithium-ion batteries under a new combined dynamic loading profile,” *Appl. Energy*, vol. 164, pp. 387–399, Feb. 2016.

[52] “Emissivity Table.” [Online]. Available: https://www.thermoworks.com/emissivity_table. [Accessed: 24-Apr-2019].

[53] “Convective Heat Transfer Coefficients Table Chart | Engineers Edge | www.engineersedge.com.” [Online]. Available: https://www.engineersedge.com/heat_transfer/convective_heat_transfer_coefficients__13378.htm. [Accessed: 24-Apr-2019].

[54] J. J. Lander, “Anodic Corrosion of Lead in H[sub 2]SO[sub 4] Solutions,” *J. Electrochem. Soc.*, vol. 98, no. 6, p. 213, Jun. 1951.

[55] J. J. Lander, “Effect of Corrosion and Growth on the Life of Positive Grids in the Lead-Acid Cell,” *J. Electrochem. Soc.*, vol. 99, no. 11, p. 467, Nov. 1952.

[56] J. J. Lander, “Some Preliminary Studies of Positive Grid Corrosion in the Lead-

Acid Cell," *J. Electrochem. Soc.*, vol. 98, no. 6, p. 220, Jun. 1951.

[57] J. J. Lander, "Further Studies on the Anodic Corrosion of Lead in H[sub 2]SO[sub 4] Solutions," *J. Electrochem. Soc.*, vol. 103, no. 1, p. 1, Jan. 1956.

[58] J. J. Lander, "Silver, Cobalt, and Positive-Grid Corrosion in the Lead-Acid Battery."

[59] J. Schiffer, D. U. Sauer, H. Bindner, T. Cronin, P. Lundsager, and R. Kaiser, "Model prediction for ranking lead-acid batteries according to expected lifetime in renewable energy systems and autonomous power-supply systems," *J. Power Sources*, vol. 168, no. 1 SPEC. ISS., pp. 66–78, May 2007.

[60] H. Bindner, T. Cronin, P. Lundsager, J. F. Manwell, U. Abdulwahid, and I. Baring-gould, *Lifetime Modelling of Lead Acid Batteries*, vol. 1515, no. April. 2005.

[61] T. Nguyen, G. Dillenseger, and C. Glaize, "Traditional float charges: are they suited to stationary antimony-free lead acid batteries?," *Cdn.Intechweb.Org*, pp. 1–10, Mar. 2010.

[62] A. Doucet and A. M. Johansen, "A Tutorial on Particle Filtering and Smoothing: Fifteen years later."

[63] D. Andre, C. Appel, T. Soczka-Guth, and D. U. Sauer, "Advanced mathematical methods of SOC and SOH estimation for lithium-ion batteries," *J. Power Sources*, vol. 224, pp. 20–27, Feb. 2013.

[64] K. Uosaki and T. Hatanaka, "NONLINEAR STATE ESTIMATION BY EVOLUTION STRATEGIES BASED PARTICLE FILTERS," *IFAC Proc. Vol.*, vol. 38, no. 1, pp. 994–999, Jan. 2005.

[65] S. Chattaraj and A. Mukherjee, "Efficient In-flight Transfer Alignment Using Evolutionary Strategy Based Particle Filter Algorithm," in *11th International Conference on Informatics in Control, Automation and Robotics*, 2014, pp. 5–13.

[66] P. Taylor, P. Butler, and W. Nerbun, "Lead/acid batteries in systems to improve power quality," *J. Power Sources*, vol. 67, no. 1–2, pp. 187–191, 1997.

[67] K. Pasupa and W. Sunhem, "A comparison between shallow and deep

architecture classifiers on small dataset," in *Proceedings of 2016 8th International Conference on Information Technology and Electrical Engineering: Empowering Technology for Better Future, ICITEE 2016*, 2017, pp. 1–6.